

Connecting mean-field theory with dynamo simulations

Petri J. Käpylä

Received: date / Accepted: date

Abstract Mean-field dynamo theory, describing the evolution of large-scale magnetic fields, has been the mainstay of theoretical interpretation of magnetism in astrophysical objects such as the Sun for several decades. More recently, three-dimensional magnetohydrodynamic simulations have reached a level of fidelity where they capture dynamo action self-consistently on local and global scales without resorting to parametrization of unresolved scales. Recent global simulations also capture many of the observed characteristics of solar and stellar large-scale magnetic fields and cycles. Successful explanation of the results of such simulations with corresponding mean-field models is a crucial validation step for mean-field dynamo theory. Here the connections between mean-field theory and current dynamo simulations are reviewed. These connections range from the numerical computation of turbulent transport coefficients to mean-field models of simulations, and their relevance to the solar dynamo. Finally, the most notable successes and current challenges in mean-field theoretical interpretations of simulations are summarized.

Keywords Dynamo · Turbulence · Numerical simulations

Petri J. Käpylä
Institute for Solar Physics (KIS)
Georges-Köhler-Allee 401a
D-79110 Freiburg im Breisgau, Germany
Tel.: +49-761-3198229
E-mail: pkapyla@leibniz-kis.de
ORCID: 0000-0001-9619-0053

Contents

1	Introduction and scope of the review	3
2	Brief overview of relevant solar observations	5
2.1	Large-scale magnetism of the Sun	5
2.2	Sunspots	6
2.3	Differential rotation and meridional circulation in the Sun	7
3	Self-consistent three-dimensional dynamo simulations	8
3.1	Equations of magnetohydrodynamics (MHD)	9
3.1.1	Microphysics	10
3.1.2	Dimensionless parameters	11
3.1.3	Boundary conditions	12
3.2	Classification of dynamo simulations	13
3.2.1	Dynamos in simulations with forced flows (Class 1)	15
3.2.2	Local simulations of dynamos due to convection (Class 2)	16
3.2.3	Representative global solar and stellar dynamo simulations (Class 3)	17
4	Mean-field dynamo theory	20
4.1	Analytic methods to compute turbulent transport coefficients	22
4.1.1	First order smoothing approximation (FOSA)	23
4.1.2	Minimal tau approximation (MTA)	23
4.1.3	Lagrangian methods for vanishing diffusivity	24
4.2	Nonlinearity due to direct magnetic back-reaction	25
4.3	Magnetic helicity conservation	26
5	Prerequisites for accurate mean-field modeling	28
6	Methods to compute turbulent transport coefficients from simulations	29
6.1	Imposed field method	29
6.2	Multidimensional regression methods	31
6.2.1	Moments method of Brandenburg and Sokoloff (2002)	31
6.2.2	Singular value decomposition (SVD)	33
6.3	Test field methods	35
6.3.1	Quasi-kinematic test field method	35
6.3.2	Nonlinear test field methods	40
7	Comparisons of 3D dynamo simulations with mean-field theory and models	43
7.1	Forced turbulence simulations with and without shear (Class 1)	43
7.1.1	Helically forced turbulence without shear (α^2 dynamo)	43
7.1.2	Helically forced turbulence with shear ($\alpha\Omega$ dynamo)	45
7.1.3	Nonhelically forced turbulence with shear	46
7.2	Convective dynamos in local boxes (Class 2)	47
7.3	Global simulations of convection in spherical shells (Class 3)	50
7.3.1	Interpretation in terms of $\alpha\Omega$ dynamos	50
7.3.2	Magnetic driving of dynamos?	52
7.3.3	Relative strength of dynamo effects as function of rotation	53
7.3.4	Mean-field modeling	53
7.4	Magnetic helicity conservation and saturation of large-scale dynamos	57
7.5	Active region formation via negative effective magnetic pressure	58
8	Outstanding issues	61
8.1	Self-consistent inclusion of large-scale flows	61
8.2	Nonlinearity and non-locality	62
9	Conclusions and outlook	62
	References	63

1 Introduction and scope of the review

Development of dynamo theory has its motivation in solar observations starting from Schwabe’s realization of cyclicity of sunspots (Schwabe 1844) and Hale’s discovery of magnetic fields (Hale 1908) and polarity reversals (Hale et al. 1919) of sunspots. Now we know that the solar magnetic field shows relatively coherent quasi-cyclic behavior with a 22-year period with superimposed longer term variations and extended minima such as the Maunder minimum (e.g. Hathaway 2015). Direct observations of the sunspot cycle extend over more than four centuries (e.g. Arlt and Vaquero 2020) whereas the activity of the Sun can be followed over a much longer period using cosmogenic isotopes gathered from ice cores and tree rings (e.g. Solanki et al. 2004; Usoskin 2017). The apparent regularity of the solar cycle is remarkable considering the underlying highly turbulent and chaotic dynamics of the solar plasma (e.g. Miesch and Toomre 2009; Schumacher and Sreenivasan 2020).

The efforts to explain solar magnetism go back to the seminal work of Larmor (1919) who proposed that rotation of sunspots maintains the observed magnetic fields. This road led to an impasse with Cowling’s anti-dynamo theorem (Cowling 1933), stating that a purely axisymmetric magnetic field cannot be maintained by dynamo action. The first successful solar dynamo model was presented by Parker (1955a) who considered the combined action of helical convection cells and differential rotation, ideas which are still central concepts in current efforts to explain solar and stellar dynamos (e.g. Charbonneau 2020; Brandenburg et al. 2023, and references therein). These same ideas were incorporated in the mathematically rigorous mean-field dynamo theory that was developed independently in the former German Democratic Republic under the leadership of Max Steenbeck (e.g. Steenbeck et al. 1966; Krause and Steenbeck 1967; Krause and Rädler 1980). This theory is based on the idea that turbulent motions do not only diffuse but also generate large-scale magnetic fields, with differential rotation and meridional flows contributing to the process. The advent of mean-field dynamo theory led to a proliferation of dynamo models of the Sun, planets, and of stars other than the Sun (e.g. Steenbeck and Krause 1969a,b; Stix 1971; Moss and Brandenburg 1995; Pipin 2017).

The main difficulty with mean-field dynamo models is that the turbulent electromotive force $\mathcal{E} = \overline{\mathbf{u} \times \mathbf{b}}$, where the overbars denote suitably chosen averages, and where \mathbf{u} and \mathbf{b} are the turbulent (small-scale) velocities and magnetic fields, needs to be known. This information is not available observationally from the interiors astrophysical objects such as the Sun. Analytic studies face the turbulence closure problem (e.g. Speziale 1991) and have to resort to approximations that typically cannot be rigorously justified in astrophysically relevant parameter regimes (e.g. Rädler and Rheinhardt 2007). Mean-field models are therefore susceptible to ad hoc modifications and simplifications, and very different physical ingredients can be used to construct models that reproduce, for example, the salient features of the solar cycle (e.g. Charbonneau 2020, and references therein).

Numerical simulations solving the equations of magnetohydrodynamics (MHD) self-consistently in spherical shells have been around since the 1980s with pioneering works of [Gilman and Miller \(1981\)](#), [Gilman \(1983\)](#), and [Glatzmaier \(1985\)](#). While these simulations produced differential rotation reminiscent of the Sun with a fast equator and slower poles, the magnetic field solutions were distinctly non-solar such that either no cycles were detected ([Gilman and Miller 1981](#)) or the *dynamo waves* propagated toward the poles instead of the equator as in the Sun ([Gilman 1983](#)). The steady increase of computing power has enabled more comprehensive parameter studies and changed the picture to the extent that *ab initio* simulations produce solutions that are in many respects similar to the Sun within a limited range of parameters. For example, solar-like large-scale differential rotation (e.g. [Brun et al. 2004](#); [Käpylä et al. 2014](#); [Hotta et al. 2015](#)) and cyclic equatorward propagating magnetic fields (e.g. [Ghizaru et al. 2010](#); [Käpylä et al. 2012b](#); [Augustson et al. 2015](#); [Strugarek et al. 2017](#); [Brun et al. 2022](#)) emerge routinely in such models. Nevertheless, the mechanism producing the solar-like dynamo solutions in many of these simulations is unlikely to be the same as in the Sun ([Warnecke et al. 2014](#), see also Section 7.3).

Furthermore, the parameter regimes of even the most recent state-of-the-art simulations are still far removed from the Sun (e.g. [Ossendrijver 2003](#); [Käpylä et al. 2023](#)) and it is questionable whether these simulations have reached an asymptotic regime where diffusion at small scales no longer affects the results at large scales (e.g. [Käpylä et al. 2017a](#); [Hotta et al. 2022](#); [Guerrero et al. 2022](#)). Even though the computing power a modern astrophysicist has access to is rapidly increasing, the immense disparity of spatial and temporal scales in the convection zones of the Sun and stars means that direct simulations of solar and stellar dynamos are still far beyond the reach of any current or foreseeable supercomputers (e.g. [Kupka and Muthsam 2017](#); [Käpylä et al. 2023](#)). Finally, even in the case that fully realistic simulations of the Sun were available, it is more than likely that we would not be able to understand them without resorting to simpler theoretical models that capture the essential physics. Thus there is still a great demand for mean-field models that faithfully capture the relevant dynamics of complex 3D systems.

From the point of view of mean-field dynamo theory, 3D simulations offer a great advantage over observations of astrophysical objects in that the full information about the flows, magnetic fields, and the electromotive force is readily at hand. Thus it is much easier to construct mean-field models of simulations than of the Sun where the detailed information of flows and magnetic fields is missing and therefore subject to speculation. Furthermore, such comparisons can be viewed as an essential validation step of the mean-field dynamo theory itself. That is, if mean-field models can accurately capture the physics of 3D simulations, there is hope to do the same with more complex systems such as the Sun. However, starting such detailed comparisons with mean-field theory from simulations of solar and stellar dynamos is likely to be complicated and the results are not necessarily easy to interpret. Thus it is often more fruitful for physical understanding to study systems that are con-

siderably simpler and which isolate one or a few of the physical effects that are present in the highly non-linear, strongly stratified, and rotating convection zone of the Sun. Such simpler setups will also be the starting point of the comparisons between simulations and mean-field theory in this review, with systems of increasing complexity following from there.

The outline of the review is as follows: since the mean-field models and simulations often seek to capture some physical system such as the Sun, a brief overview of the relevant observations is therefore warranted. This is presented in Sect. 2 with emphasis on the salient solar observations. Section 3 summarizes different types of 3D dynamo simulations, what they try to accomplish, their usefulness with respect to comparisons to mean-field theory, and their relation to the Sun and stars. A brief outline of mean-field dynamo theory is presented in Sect. 4. The necessary prerequisites for comparing simulations with corresponding mean-field theory are discussed in Sect. 5. Methods for extracting turbulent transport coefficients from simulations and results obtained with such methods are discussed in Sect. 6. Finally, comparisons of various kinds between simulations and mean-field models are discussed in Sect. 7. Finally, outstanding issues are discussed in Sect. 8, and Sect. 9 sums up the current state of affairs.

2 Brief overview of relevant solar observations

The ultimate aim of 3D dynamo simulations and mean-field models is to address parts or the totality of the dynamo in some real system. Therefore it is in order to briefly summarize the pertinent observations that the models seek to capture. Here the discussion is limited to solar global magnetism and large-scale flows that are an essential ingredient in the dynamo process.

2.1 Large-scale magnetism of the Sun

The observational knowledge of the Sun both in terms of quality and quantity far exceeds that of any other star. Therefore it is logical that efforts at dynamo modeling have to a large extent targeted the Sun (cf. [Charbonneau and Sokoloff 2023](#)). More than four centuries of systematic observations has revealed the approximately 11-year sunspot cycle and a century of magnetic field observations the 22-year magnetic cycle. Furthermore, sunspots appear on a latitude strip $\pm 40^\circ$, appearing progressively closer to the equator as the cycle advances. The surface magnetic fields consists largely of bipolar regions with opposite polarities at different hemispheres. A poleward branch, believed to be caused by turbulent diffusion and advection by the meridional flow (see [Jiang et al. 2014](#), and references therein), is also present at high latitudes; see Fig. 1. The polar field changes sign at sunspot maximum and the radial and longitudinal fields are thought to be in anticorrelation ([Stix 1976](#)). The spatiotemporal behavior of the large-scale magnetic fields of the Sun captured in

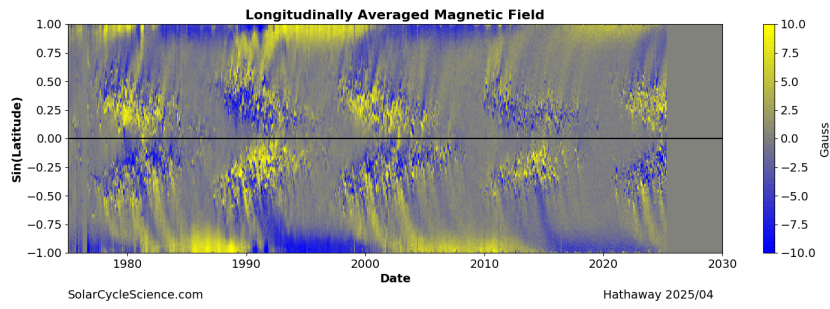


Fig. 1 Time-latitude or butterfly diagram of the longitudinally averaged radial magnetic field at the solar surface. The color scale is clipped at ± 10 G to highlight the weak fields on high latitudes. Courtesy of David Hathaway (<http://solarcyclescience.com>).

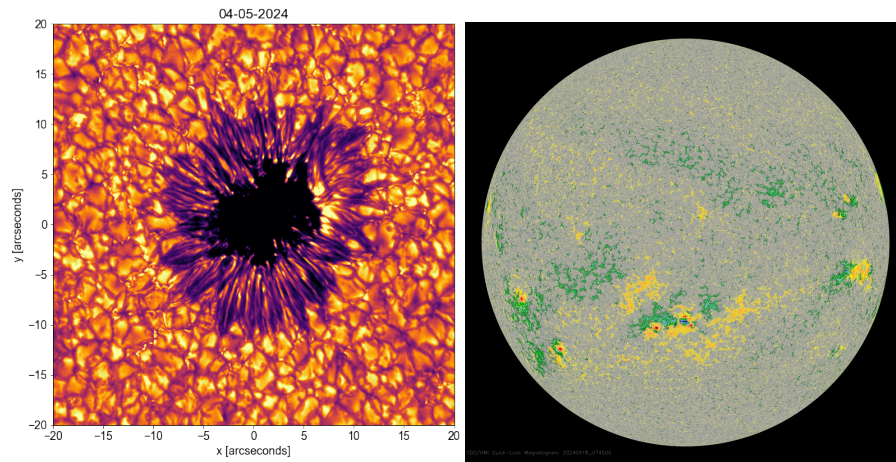


Fig. 2 Left: Sunspot from the GREGOR solar telescope, courtesy of Rolf Schlichenmaier and Nazaret Bello González, Institute for Solar Physics (KIS). Right: magnetogram of the solar surface on 18th September 2024 from the Solar Dynamics Observatory.

this figure is the primary observable that 3D simulations and mean-field models seek to reproduce. The reader is referred to other reviews in this series for the details of the solar cycle and its long-term variations; see, e.g., Hathaway (2015), Usoskin (2017), and Karak (2023).

2.2 Sunspots

The visible manifestation of large-scale magnetism in the Sun are sunspots which are concentrations of kilogauss strength magnetic fields at the surface of the Sun (e.g. Solanki 2003; Berdyugina 2005); see also the left panel of Fig. 2. Although the visible spots on the solar surface are highly concentrated, corresponding magnetograms indicate that the spots are associated with larger

scale magnetism beneath; see the right panel of Fig. 2. Detecting magnetic fields in subsurface layers of the Sun is very challenging and typically relies on indirect methods. One such method is to follow the rise of active regions in the Sun and in corresponding numerical simulations of surface convection where magnetic flux tubes are advected through the bottom boundary (e.g. Birch et al. 2016). This study suggest that the rise speeds of active regions are too low for them to originate in the tachocline at the base of the convection zone. A possible explanation is that active regions form close to the surface (e.g. Brandenburg 2005a).

This idea arises from the observation that the rotation rate of sunspots depends systematically on their age: the youngest spots have a rotation rate that matches that of the base of the near-surface shear layer (NSSL; see Sect. 2.3) at $r = 0.95R_{\odot}$, whereas the oldest ones are more in line with the surface rotation rate (e.g. Pulkkinen and Tuominen 1998). This can be interpreted as spots being anchored at different depths, and that even the youngest spots would be a shallow phenomenon. Another hint toward this direction is the strengthening of the surface f mode of the Sun prior to active region emergence (e.g. Singh et al. 2016; Waidele et al. 2023), which can be seen up to 48 hours before any magnetic fields are detected at the surface. The effect of subsurface magnetic fields on the f mode has been studied using idealised numerical simulations (Singh et al. 2014, 2015, 2020), where strengthening was found for spatially concentrated fields near the surface. Nevertheless, the formation mechanism of sunspots is currently unknown but a successful solar and stellar dynamo theory has to incorporate this.

2.3 Differential rotation and meridional circulation in the Sun

Another remarkably well-known characteristic of the Sun is its interior differential rotation (e.g. Schou et al. 1998; Howe 2009); see the left panel of Fig. 3. The interior rotation in the bulk of the convection zone is roughly constant on radial lines whereas the boundary layers near the surface (i.e., the NSSL) and at the base of the convection zone (tachocline) are characterized by strong radial shear. The radiative interior of the Sun is nearly rigidly rotating. Solar differential rotation is thought to be driven by the interaction of convective turbulence and rotation (e.g. Rüdiger 1989; Kitchatinov and Rüdiger 1995), although recent simulations suggest that magnetic fields can also be important (e.g. Hotta and Kusano 2021; Hotta et al. 2022; Käpylä 2023; Hotta 2025). In the NSSL the gradients of velocity and density are large and the convective timescale is much shorter than the solar rotation period. Therefore the NSSL is challenging to reproduce in global 3D simulations and can be incorporated self-consistently only at high resolutions (Hotta et al. 2015; Matilsky et al. 2019; Hotta 2025). The transition to rigid rotation in the radiative core is thought to be mediated by magnetic fields, either of fossil (e.g. Rüdiger and Kitchatinov 1997; Gough and McIntyre 1998) or dynamo origin (e.g. Forgács-Dajka and Petrovay 2001; Matilsky et al. 2022).

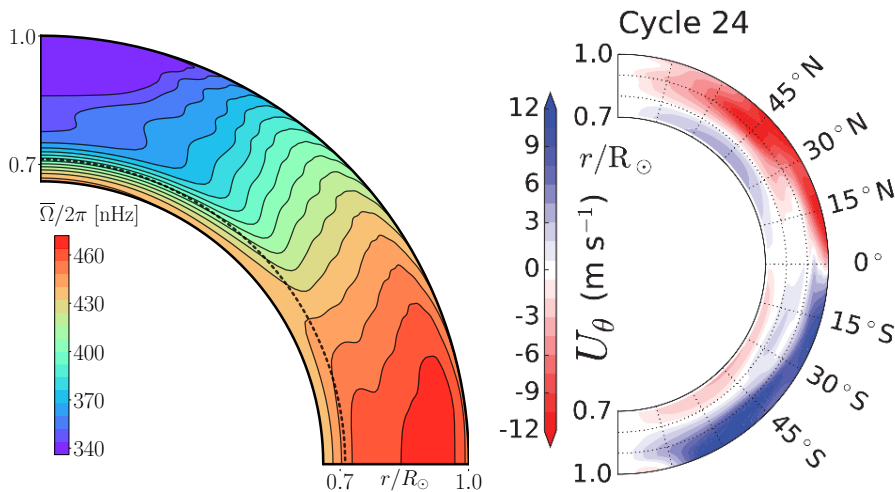


Fig. 3 Left: mean angular velocity in the solar interior from global helioseismology using data from Larson and Schou (2018). The dashed line at $r/R_\odot = 0.71$ indicates the base of the convection zone. Right: latitudinal component of the solar meridional circulation from helioseismology from Gizon et al. (2020).

A significantly less well constrained part of solar interior large-scale flows is the meridional circulation (e.g. Hanasoge 2022). Whereas the poleward flow near the surface is well-established, the deep subsurface structure and speed of the meridional flow is still under debate: helioseismic inversions have yielded both single (e.g. Gizon et al. 2020) and multiple cell (e.g. Schad et al. 2013; Zhao et al. 2013) structures in radius depending on the methods used. The results from solar cycle 24 from Gizon et al. (2020) is shown in the right panel of Fig. 3. Numerical 3D simulations consistently produce multiple meridional circulation cells per hemisphere in cases with solar-like differential rotation profile (e.g. Käpylä et al. 2014; Passos et al. 2015; Brun et al. 2017). In dynamo theory these large-scale flows contribute to the generation of global magnetism: differential rotation winds up poloidal fields to produce the toroidal field (Ω effect) and meridional flows are crucially important in a class of mean-field models known as flux-transport or advection dominated dynamos (e.g. Dikpati and Charbonneau 1999; Chatterjee et al. 2004).

3 Self-consistent three-dimensional dynamo simulations

Before delving into the details of the various kinds of dynamo simulations at large, it is necessary to clarify what is meant by a self-consistent dynamo simulation. In what follows this is taken to encompass the simultaneous solution of (at least) the induction and Navies–Stokes equations in three dimensions without further approximations, and where dynamo action is due to the resolved

dynamics. These models can be considered as “direct numerical simulations” (DNS) of systems where most dimensionless parameters, such as Reynolds and Prandtl numbers, are unrealistically small in comparison to the Sun and stars (see, e.g. Kupka and Muthsam 2017; Käpylä et al. 2023). Alternatively we may consider them as “large-eddy simulations” (LES) that seek to capture the large-scale phenomena (possibly of a real system) down to the grid scale directly, while modeling the subgrid-scale dynamics typically by highly enhanced diffusion coefficients. This is in contrast to mean-field models where typically all but the largest scales are parameterized.

3.1 Equations of magnetohydrodynamics (MHD)

A non-relativistic charge neutral gas that is sufficiently collisional that it can be described as a single fluid can be described by the standard set of MHD equations (see, e.g. Davidson 2001). For the fully compressible case in a rotating frame these are given by:

$$\frac{\partial \mathbf{B}}{\partial t} = \nabla \times (\mathbf{U} \times \mathbf{B} - \eta \mu_0 \mathbf{J}), \quad (1)$$

$$\frac{\partial \rho}{\partial t} = -\nabla \cdot (\rho \mathbf{U}), \quad (2)$$

$$\rho \frac{\partial \mathbf{U}}{\partial t} = -\rho \mathbf{U} \cdot \nabla \mathbf{U} + \rho \mathbf{g} - \nabla p - 2\rho \boldsymbol{\Omega} \times \mathbf{U} + \mathbf{J} \times \mathbf{B} + \nabla \cdot (2\rho \nu \mathbf{S}) + \mathbf{f}, \quad (3)$$

$$\rho T \frac{\partial s}{\partial t} = -\rho T \mathbf{U} \cdot \nabla s + \nabla \cdot \mathcal{F} + \eta \mu_0 \mathbf{J}^2 + 2\nu \rho \mathbf{S}^2 + \mathcal{H}, \quad (4)$$

where \mathbf{B} is the magnetic field, \mathbf{U} is the velocity, η is the magnetic diffusivity, μ_0 is the permeability of vacuum, $\mathbf{J} = \nabla \times \mathbf{B} / \mu_0$ is the current density, ρ is the density, ν is the kinematic viscosity, \mathbf{S} is the traceless rate-of-strain tensor, $\mathbf{g} = -\nabla \phi_g$ is the acceleration due to gravity, where ϕ_g is the gravitational potential, p is the pressure, $\boldsymbol{\Omega}$ is the rotation vector, \mathbf{f} describes additional body forces, T is the temperature, s is the specific entropy, $\mathcal{F} = \mathcal{F}_{\text{rad}} + \mathcal{F}_{\text{SGS}}$ is a flux which often contains radiative ($\mathcal{F}_{\text{rad}} = -K \nabla T$) and subgrid-scale (SGS) (e.g., $\mathcal{F}_{\text{SGS}} = -\chi_t \rho \nabla s$)¹ contributions, where K is the heat conductivity and χ_t describes SGS entropy diffusion (Braginsky and Roberts 1995; Rogachevskii and Kleorin 2015; Käpylä 2023). Finally, \mathcal{H} describes additional heating and cooling from, e.g., from nuclear reactions. To close the system, an equation of state $p = p(\rho, T)$ relating pressure to the other thermodynamic quantities is needed. The mean molecular weight $\mu = \mu(\rho, T)$ enters the equation of state and depends on the ionization state of the matter. Very often the equation of state is for simplicity taken to be that of a monoatomic ideal gas, $p = \mathcal{R} \rho T$,

¹ Sometimes the SGS flux is defined with an additional T factor via $\mathcal{F}_{\text{SGS}} = -\chi_t \rho T \nabla s$ (e.g. Brun et al. 2004; Jones and Kuzanyan 2009; Käpylä et al. 2013b; Orvedahl et al. 2018). Rogachevskii and Kleorin (2015) point out that this is formally correct if the internal energy equation is solved instead of the entropy equation.

where $\mathcal{R} = c_P - c_V$ is the universal gas constant, and c_P and c_V are the heat capacities at constant pressure and volume with $\gamma = c_P/c_V = 5/3$.

However, in many dynamo simulations a reduced set of equations is considered. For example, the flow can be assumed incompressible or anelastic in which cases Eq. (2) is replaced by $\nabla \cdot \mathbf{U} = 0$ or by $\nabla \cdot (\rho \mathbf{U}) = 0$, respectively. In fully compressible simulations of convection the timestep constraint due to the low Mach number in the deep convection zone is sometimes alleviated by reducing the sound speed artificially by multiplying the rhs of Eq. (2) by a factor $\xi^{-2} < 1$ (e.g. Rempel 2005; Hotta et al. 2012). Often idealized simulations are done assuming an isothermal equation of state $p = \rho c_s^2$, in which case the energy equation drops out. These models also often neglect density stratification and rotation, and flows and helicity are injected through an external force \mathbf{f} at a pre-defined forcing scale k_f .

3.1.1 Microphysics

In addition to the equation of state, microphysics enter at least in principle also through the diffusion coefficients ν and η , and via the gas opacity κ that goes into the description of radiation. The dependence of the fluid viscosity and magnetic diffusivity on the ambient thermodynamic state can be computed using Spitzer formulas (Spitzer 1962) with $\nu \propto \rho^{-1} T^{5/2}$ and $\eta \propto T^{-3/2}$. These have been used to compute the microscopic diffusion coefficients for various astrophysical objects; see Brandenburg and Subramanian (2005a), Schumacher and Sreenivasan (2020), and Jermyn et al. (2022). However, the Spitzer formulae are almost never used in numerical dynamo simulations because in practically all cases of astrophysical interest the resulting diffusion coefficients either vary too much within the computational domain and/or are too small to be used in computationally affordable simulations; see discussions about convection and global dynamo simulations in, e.g., Kupka and Muthsam (2017) and Käpylä et al. (2023). Furthermore, the thermal Prandtl number $\text{Pr} = \nu/\chi$, where $\chi = K/c_P\rho$, and the corresponding magnetic Prandtl number $\text{Pr}_M = \nu/\eta$ are in reality very small in stars such as the Sun (e.g. Schumacher and Sreenivasan 2020). Therefore 3D dynamo simulations most often use either constant or spatially varying prescribed diffusivities that are much larger than the corresponding Spitzer equivalents or seek to minimize the effective diffusion by the use of implicit or explicit SGS modeling (see, e.g. Miesch et al. 2015). Values of the thermal and magnetic Prandtl numbers of the order of unity are used out of numerical necessity.

A similar situation occurs with the opacity of the gas. Most often the gas is assumed optically thick in which case \mathbf{F}^{rad} can be written in terms of the diffusion approximation

$$\mathbf{F}^{\text{rad}} = -K \nabla T, \quad (5)$$

where K is the heat conductivity given by

$$K = \frac{16\sigma_{\text{SB}}T^3}{3\kappa\rho}, \quad (6)$$

where σ_{SB} is the Stefan–Boltzmann constant. The opacity of the gas depends in a complex way on thermodynamics and chemical composition. In stellar surface convection simulations the opacity is often taken from tabulated values (e.g. [Rempel et al. 2009b](#)), but this approach is typically not used in most 3D large-scale dynamo simulations. Instead, global simulations often adopt profiles of K from 1D solar/stellar models (e.g. [Brun et al. 2004, 2022](#)) or coarser approximations such as the Kramers law (e.g. [Käpylä et al. 2019, 2020b](#); [Viviani and Käpylä 2021](#)), or simply assume either constant or fixed spatial profiles for K (e.g. [Käpylä et al. 2012b](#); [Mabuchi et al. 2015](#); [Simatev et al. 2015](#)). The effects of these different choices for the dynamo solutions can only be indirect, e.g., that the vigour and form of the flows and the thermodynamic structure of the dynamo region are altered. A prominent example is the weakly stably stratified deep parts of convection zones that have been detected in simulations where the heat conductivity K connects smoothly from the convective to radiative zones (e.g. [Roxburgh and Simmons 1993](#); [Tremblay et al. 2015](#); [Hotta 2017](#); [Käpylä et al. 2017b](#)).

Finally, the additional heating and cooling terms are often used in models to either mimic radiative cooling near the surface or heating due to nuclear reactions in the core (e.g. [Dobler et al. 2006](#); [Käpylä 2021](#); [Hidalgo et al. 2024](#)). Sometimes the effects of radiation are also parameterized in terms of a heating/cooling term that makes no recourse to heat conductivity or opacities and is therefore included in \mathcal{H} (e.g. [Ghizaru et al. 2010](#); [Guerrero et al. 2016](#); [Matilsky and Toomre 2020](#); [Hotta et al. 2022](#)).

3.1.2 Dimensionless parameters

The solutions of MHD equations are characterized by dimensionless parameters that define the system that arise upon non-dimensionalization. These include thermal and magnetic Prandtl numbers, the Taylor number, and in the case of convection the Rayleigh number:

$$\text{Pr} = \frac{\nu}{\chi}, \quad \text{Pr}_M = \frac{\nu}{\eta}, \quad \text{Ta} = \frac{4\Omega_0 d^4}{\nu^2}, \quad \text{Ra} = \frac{gd^4}{\nu\chi} \left(-\frac{1}{c_P} \frac{ds}{dr} \right), \quad (7)$$

d is a system-scale length scale, e.g., the depth of the convection zone. The Taylor number is related to the Ekman number $\text{Ek} = \nu/\Omega_0 d^2$ via $\text{Ta} = 4\text{Ek}^{-2}$. In stars such as the Sun, where the luminosity L is practically constant on timescales relevant for the dynamo, it is convenient to use a flux-based Rayleigh number

$$\text{Ra}_F = \frac{gd^4 F_{\text{tot}}}{c_P \rho T \nu \chi^2}, \quad (8)$$

where $F_{\text{tot}} = L/4\pi r^2$ is the total flux. The Prandtl, Taylor, and flux-based Rayleigh number can be combined to a diffusion-free modified Rayleigh number (e.g. [Christensen 2002](#); [Christensen and Aubert 2006](#))

$$\text{Ra}_F^* = \frac{gF_{\text{tot}}}{8c_P \rho T \Omega^3 d^2}. \quad (9)$$

This is the only system parameter that 3D simulations of the solar dynamo can reproduce. Choosing the length scale as $d = c_p T/g \equiv H$, $\text{Ra}_F^* = \text{Co}_F^{-3}$, where $\text{Co}_F = 2\Omega H(F_{\text{tot}}/\rho)^{-1/3}$ is a flux-based Coriolis number (Käpylä 2023, 2024).

Further dimensionless numbers describing the system are diagnostics that are available *a posteriori*. These include the fluid and magnetic Reynolds numbers and the Péclet number

$$\text{Re} = \frac{u\ell}{\nu}, \quad \text{Re}_M = \frac{u\ell}{\eta}, \quad \text{Pe} = \frac{u\ell}{\chi}, \quad (10)$$

where u and ℓ are typical velocity amplitude and length scale. The importance of rotation is given by the Coriolis number

$$\text{Co} = \frac{2\Omega_0\ell}{u} = 2\text{Ro}^{-1}, \quad (11)$$

where Ro is the Rossby number. In a density-stratified system such as the solar interior all of the numbers listed above are functions of radius and can vary several order of magnitude between the base and the surface of the convection zone. In simulations this needs to be avoided for numerical reasons (Käpylä et al. 2023).

3.1.3 Boundary conditions

An important but often overlooked aspect of numerical modeling are the boundary conditions that invariably need to be imposed. Most commonly dynamo models, be it mean-field or 3D, adopt simplified expressions such as setting the magnetic field parallel or normal to the boundary. The former corresponds to a perfect conductor and the magnetic field is confined into the simulation domain, while the latter allows field lines to cross the boundary. Another condition similar to the normal field condition is to assume a potential field outside of the domain. The choice of boundary conditions seems innocuous but can in fact have far-reaching consequences. First, the allowed modes and symmetries of magnetic fields depend on the boundary conditions and can lead to qualitatively different results (e.g. Cole et al. 2016; Brandenburg 2017, 2018b). Furthermore, magnetic boundary conditions have a crucial importance for magnetic helicity conservation: if magnetic field lines cannot cross the boundary of the domain, magnetic helicity cannot escape which can lead to resistively slow growth of magnetic field and saturation of the dynamo; see Sect. 4.3.

Numerical simulations of the Sun and stars would in principle also need to include the surface where the density is decreasing very rapidly and the gas becomes optically thin. Global dynamo simulations either do not include the full stratification of the Sun or only model the star until a manageable outer radius which is smaller than the actual stellar radius. Yet another approach is to embed the star into a cube where no explicit boundary condition is

imposed at the surface (e.g. [Dobler et al. 2006](#); [Masada et al. 2022](#); [Ortiz-Rodríguez et al. 2023](#)). However, in such cases the surface of the star is typically determined by spatially fixed profiles of cooling and the transition between the stellar interior and exterior is much smoother than in reality. However, there is some evidence to the effect that including layers outside the star lead to qualitatively different outcomes (e.g. [Warnecke et al. 2016](#); [Käpylä 2022](#)).

3.2 Classification of dynamo simulations

The design of dynamo simulations depends to a great extent on the goal: to study a particular dynamo effect in isolation calls for models where only the necessary ingredients are retained in a simple geometry, while study of global dynamos, such as the solar dynamo, requires spherical geometry and the interplay of convection, rotation, stratification, and non-linearity due to magnetism. A great variety of models fits in the spectrum between these extremes. As a general rule the amount of control of the simulation decreases with increasing complexity and physical ingredients. At the same time, the complexity of the corresponding mean-field models increases due to the larger number and higher dimensionality of turbulent transport coefficients and mean fields. Dynamo simulations can be categorized in roughly three classes:

1. *Class 1: Forced turbulence simulations* where the geometry of the system is simplified and where flows are driven by external forcing instead of a natural instability. This class corresponds to, for example, fully periodic Cartesian forced turbulence simulations of helical (e.g. [Meneguzzi et al. 1981](#); [Brandenburg 2001](#); [Candelaresi and Brandenburg 2013](#); [Subramanian and Brandenburg 2014](#)) and non-helical (e.g. [Iskakov et al. 2007](#); [Warnecke et al. 2023](#)) dynamos where imposed uniform large-scale shear can be further included (e.g. [Yousef et al. 2008b](#); [Käpylä and Brandenburg 2009](#); [Teed and Proctor 2016](#)). However, also systems where physical parameters such as the imposed kinetic helicity or large-scale flows have systematic spatial variations (e.g. [Mitra et al. 2010a](#); [Tobias and Cattaneo 2013](#); [Rincon 2021](#)) or more realistic geometry (e.g. [Mitra et al. 2009b, 2010b](#); [Jabbari et al. 2015](#)) belong to this class. Furthermore, simulations where kinetic helicity is not necessarily due to forcing but due to the combined effects of density stratification and rotation (e.g. [Brandenburg et al. 2012b, 2013a](#)) belong to Class 1. Such simulations are typically used to study isolated aspects of the dynamo problem such as predictions of mean-field theory or the non-linear saturation of dynamos. The simplified geometry and idealized physics mean that mean-field theoretic interpretation of Class 1 simulations is the most straightforward of all models although still not necessarily easy.
2. *Class 2: Local instability-driven simulations* where the geometry is still simple, for example, a Cartesian portion of a star, accretion disk, or a Galaxy, where flows are driven by physical instabilities such as convection (e.g. [Käpylä et al. 2008](#); [Hughes and Proctor 2009](#); [Masada and Sano 2014](#)), magnetorotational instability (e.g. [Brandenburg et al. 1995](#); [Gressel 2010](#)),

Table 1 Classification of dynamo simulations. The abbreviations denote: for = forcing, sc = self-consistent, loc = local, typically Cartesian, and glo = global, typically spherical.

Class	Forcing	Helicity	Shear	Geometry
1	External	for/sc	for	loc/glo
2	Instability	sc	for/sc	loc/glo
3	Instability	sc	sc	glo

or supernovae (e.g. [Gressel et al. 2008](#); [Gent et al. 2013](#); [Bendre et al. 2015](#)). In comparison to simulations in Class 1, Class 2 models are more physically consistent in that flows and their statistical properties such as turbulence and kinetic helicity are not put in by hand via forcing but emerge self-consistently as solutions of the MHD equations. A major advantage in this type of models is that the mean-field theoretic interpretation of the results remains tractable, especially if planar averages are a good representation of the mean fields (e.g. [Käpylä et al. 2009a,b](#); [Masada and Sano 2014](#)). In simulations of Class 1 and 2 the large-scale flows are typically either absent or externally imposed and therefore a mean-field treatment of the Navier-Stokes equations does not need to be considered.

3. *Class 3: Semi-global and global simulations* are similar to the local instability-driven models in terms of physics with the distinction that a realistic geometry is assumed. Thus comparisons with actual astrophysical objects such as the Sun and stars are at least in principle possible. In Class 3 simulations the large-scale flows are outcomes of the models and in the general case they also would need to be subject to mean-field treatment (e.g. [Rüdiger 1989](#)). This increases the complexity of the mean-field description considerably and typically this task is omitted in comparisons of 3D simulations with mean-fields models which is also the path taken in the current review. Most relevant examples for the current topic of Class 3 models are simulations of solar and stellar dynamos (e.g. [Ghizaru et al. 2010](#); [Käpylä et al. 2012b](#); [Augustson et al. 2015](#); [Mabuchi et al. 2015](#); [Warnecke et al. 2021](#); [Brun et al. 2022](#); [Warnecke et al. 2025](#)). In these cases the mean fields can be considered as averages over the longitude, leading to 2D mean-field description with a corresponding (r, θ) -dependence of the turbulent transport coefficients.

The boundaries between the different categories are somewhat fluid but the big picture is accurate enough. The different classes are summarized in [Table 1](#). Classes 1 and 2 are useful when studying individual dynamo effects and have the most straightforward theoretical interpretation. Simulations of Class 3 are, at least in theory, the most realistic but also the most challenging to deal with mean-field theory. The discussion in the current review concentrates on simulations that are *successful large-scale dynamos*, that is, they produce an identifiable large-scale magnetic field which is interpreted to be due to dynamo action. While simulations leading to small-scale dynamos are mentioned where

relevant, especially when co-existing with a large-scale dynamo, the reader is referred to, for example, [Rempel et al. \(2023\)](#) for an in depth review of this topic. The following sections summarize examples of each class of simulations relevant to solar and stellar dynamos.

3.2.1 *Dynamos in simulations with forced flows (Class 1)*

The history of 3D dynamo simulations can be considered to start from the seminal study of [Meneguzzi et al. \(1981\)](#) who used forced turbulence in a fully periodic cube to study dynamos in helical and non-helical cases, and who were the first to show large-scale magnetic field growth by helical turbulence by means of a 3D numerical simulation. This can be considered as the first demonstration of an α^2 dynamo in the mean-field sense using direct solutions of the MHD equations. However, computational constraints were still holding back the simulators: [Meneguzzi et al. \(1981\)](#) had to use hyperdiffusivity to resolve the helical case and to run the simulations in the National Center for Atmospheric Research (NCAR) Cray-1 – the most powerful supercomputer in the world at the time. A proliferation of modeling efforts of this kind started in earnest only much later when the required computational power became more accessible (cf. [Balsara and Pouquet 1999](#); [Brandenburg 2001](#)). A landmark in this respect is the study of [Brandenburg \(2001\)](#) where the importance of magnetic helicity conservation in the non-linear phase of large-scale dynamo action was demonstrated. Many aspects of the helically forced, or α^2 dynamo, have hence been studied by means of 3D simulations: for example, [Candelaresi and Brandenburg \(2013\)](#) studied the minimum helicity to drive large-scale dynamo action, [Brandenburg and Dobler \(2001\)](#) and [Brandenburg et al. \(2002\)](#) investigated the effects of magnetic helicity losses through boundaries, [Brandenburg et al. \(2008b\)](#) simulated simultaneous small-scale and large-scale dynamos to measure the quenching of turbulent transport coefficients, and [Subramanian and Brandenburg \(2014\)](#) disentangled the growth rates of small-scale and large-scale fields.

Another set of models that are conceptually very similar to those discussed above have the kinetic helicity vary spatially such that it has a sign change or an “equator” ([Mitra et al. 2010b,a](#); [Rincon 2021](#)). These simulations represent another incarnation of an α^2 dynamo but unlike in the case where the kinetic helicity is constant, these setups lead to oscillatory solutions where the dynamo wave propagates toward the equator reminiscent of the Sun (e.g. [Baryshnikova and Shukurov 1987](#); [Rädler and Bräuer 1987](#)).

The addition of imposed large-scale shear flow on top of helical turbulence arising from the forcing fulfills the minimal requirements for a classical $\alpha\Omega$ dynamo (e.g. [Parker 1955a](#); [Steenbeck and Krause 1969a](#)). Such systems very often lead to cyclic solutions (e.g. [Käpylä and Brandenburg 2009](#); [Hubbard et al. 2011](#); [Tobias and Cattaneo 2013](#); [Pongkitiwanchakul et al. 2016](#)), see also Fig. 4; that can indeed be interpreted in terms of $\alpha\Omega$ dynamos. A more recent discovery is that also shearing *non-helical* turbulence can maintain large-scale magnetic fields (e.g. [Yousef et al. 2008b,a](#); [Brandenburg et al.](#)

2008a; Squire and Bhattacharjee 2015a; Teed and Proctor 2016). In such cases, the α effect vanishes on average and straightforward explanation of the origin of the dynamo in terms of mean-field theory is not possible. Theoretical interpretation of shearing non-helical dynamos has turned out to be challenging and it is still under debate in the community; see more details in Sect. 7.1.3.

The discussion has so far concentrated on simulations where the flow is driven by an external force in the Navier–Stokes equation leading to a turbulent solution. For completeness, we mention that there are also flows that are less complex, but contain the necessary ingredients for dynamo action such as kinetic helicity. Two prominent examples include the Roberts flows (e.g. Roberts 1972) and the Galloway–Proctor flow (Galloway and Proctor 1992). Often the Navier–Stokes equations are not solved in such cases. In some cases these flows allow analytic calculation of mean-field transport coefficients due to which these flows have been used extensively to compare with mean-field dynamo theory (e.g. Rädler and Brandenburg 2009; Courvoisier et al. 2010; Rheinhardt et al. 2014).

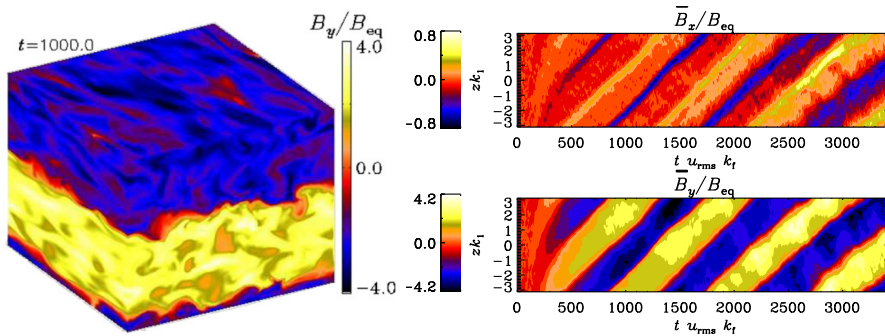


Fig. 4 Left: Instantaneous stream-wise magnetic field B_y in a simulation with forced helical turbulence and imposed linear shear flow $\bar{\mathbf{U}} = (0, xS, 0)$ with $\text{Re}_M = 209$, $\text{Pr}_M = 10$, and $\text{Sh} = S/(u_{\text{rms}}k_f) = -0.18$, where u_{rms} is the turbulent rms-velocity and k_f is the wavenumber corresponding to the forcing scale. Right: space-time diagrams of the horizontally averaged horizontal magnetic fields $\bar{B}_x(z, t)$ and $\bar{B}_y(z, t)$ from the same simulation. Adapted from Käpylä and Brandenburg (2009).

3.2.2 Local simulations of dynamos due to convection (Class 2)

Replacing externally driven flows by ones that are produced by instabilities occurring in nature while retaining the simplified geometry is the next step in complexity. Dynamos driven by convection is naturally the most interesting case for solar and stellar applications. While small-scale dynamos were reported from local convection simulations starting in the late 1980s (Meneguzzi and Pouquet 1989; Nordlund et al. 1992; Brandenburg et al. 1996; Cattaneo 1999), exciting a dynamo that produces appreciable large-scale magnetic fields

in such simulations turned out to be significantly more challenging. Rigidly rotating stratified or inhomogeneous convection produces kinetic helicity and has therefore all the ingredients of an α^2 dynamo. However, simulations often still fail to produce appreciable large-scale magnetic fields (e.g. Cattaneo and Hughes 2006; Hughes and Cattaneo 2008; Favier and Bushby 2012). Large-scale dynamos were obtained only when rapid rotation was considered (e.g. Käpylä et al. 2009b, 2013a; Masada and Sano 2014; Guervilly et al. 2015; Masada and Sano 2016; Guervilly et al. 2017; Bushby et al. 2018). Often these dynamos are associated with hydrodynamic states that are dominated by large-scale vortices (e.g. Chan 2007; Käpylä et al. 2011; Chan and Mayr 2013; Guervilly et al. 2014) that are possibly due to two-dimensionalization of turbulent flows in the rapid rotation regime. Simulations including large-scale shear lead to successful large-scale dynamos much more easily (e.g. Käpylä et al. 2008, 2010b, 2013a; Hughes and Proctor 2009, 2013).

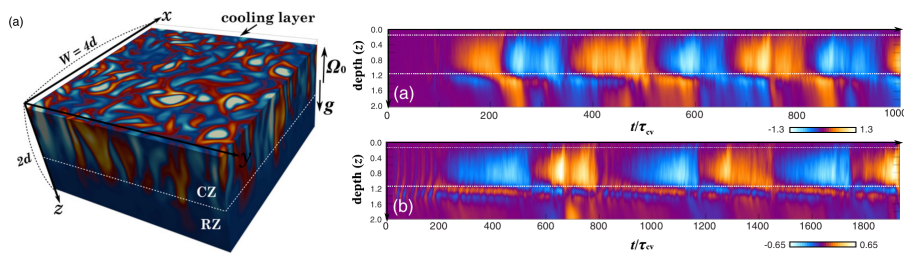


Fig. 5 Left: Instantaneous vertical velocity U_z in a simulation of rigidly rotating density-stratified convection in a Cartesian slab. Right: time-depth diagrams of the horizontally averaged magnetic field $\overline{B}_x(z, t)$ from simulations with $\text{Pr}_M = 2$ (top) and $\text{Pr}_M = 8$ (bottom). Adapted from Masada and Sano (2014).

3.2.3 Representative global solar and stellar dynamo simulations (Class 3)

Global convective dynamo simulations have been around since the early 1980s when the first large-scale dynamos were obtained from such models (Gilman and Miller 1981; Gilman 1983). Initial simulations were made using the Boussinesq approximation but anelastic models enabling density stratification were soon also deployed (Glatzmaier 1984, 1985). The initial enthusiasm regarding global simulations waned after the early simulations constantly yielded solutions where the dynamo wave propagated poleward in contradiction to the Sun. A renaissance of global modeling started with the creation of the ASH (anelastic spherical harmonic) code in the late 90s and early 2000s (e.g. Miesch et al. 2000; Elliott et al. 2000; Brun and Toomre 2002). Since then several methods have been developed to model solar and stellar convection and dynamos either in spherical shells (e.g. Ghizaru et al. 2010; Fan and Fang 2014; Simitev et al. 2015; Strugarek et al. 2017; Guerrero et al. 2019; Matilsky and Toomre 2020; Hotta and Kusano 2021; Brun et al. 2022; Hotta et al. 2022)

and wedges (e.g. Käpylä et al. 2010c, 2012b; Mabuchi et al. 2015; Käpylä et al. 2019), or in a star-in-a-box setup where a spherical star is embedded into a Cartesian cube (e.g. Dorch 2004; Dobler et al. 2006; Käpylä 2021, 2022; Masada et al. 2022; Ortiz-Rodríguez et al. 2023; Hidalgo et al. 2024).

To capture global phenomena such as solar and stellar magnetic cycles on the scale of the convection zone, simulations in global spherical geometry are required. This inevitably means that the effective resolution in such models is severely reduced compared to local models discussed above. Considering the Sun and other late-type stars, the challenge is exacerbated by the immense density stratification of the convection zone (more than 20 pressure scale heights), time scales ranging from 12 days at the base of the convection zone to 5 minutes near the surface, high fluid and magnetic Reynolds numbers (10^{12} and 10^9 , respectively), low Prandtl numbers ($\text{Pr} = 10^{-7}$ and $\text{Pr}_M = 10^{-3}$), and the strong variation of the Mach number between the base of the convection zone and the surface ($\text{Ma} \approx 10^{-4}$ in deep convection zone, transonic near the surface) (e.g. Kupka and Muthsam 2017; Schumacher and Sreenivasan 2020; Jermyn et al. 2022). None of these characteristics can be fully reproduced in current global simulations: the Reynolds numbers are typically of the order of a few hundred and Prandtl numbers of the order of unity. The only characteristic that can be accurately modeled is the rotational influence on the flows, measured by Ra_F^* or the flux Coriolis number Co_F (e.g. Käpylä 2024). Furthermore, helioseismic and solar surface observations suggest that the velocity amplitudes at large horizontal length scales are much lower in the Sun in comparison to simulations (e.g. Hanasoge et al. 2012, 2020; Proxauf 2021; Birch et al. 2024). This is commonly referred to as the convective conundrum (O’Mara et al. 2016) which is most likely the key reason why there is no global simulation to date that captures the solar dynamo and interior differential rotation fully self-consistently. Comparison of observations with global simulations is a vibrant current topic and the reader is referred to Hotta et al. (2023) and Käpylä et al. (2023) for more thorough discussions of the current status of global numerical simulations targeting solar differential rotation and solar and stellar dynamos, respectively.

Nevertheless, there have been many studies of convective dynamos as a function of rotation which have revealed that cyclic solutions, akin to those in the Sun, appear on a relatively narrow range of Coriolis numbers (e.g. Viviani et al. 2018; Brun et al. 2022). For slow rotation – roughly corresponding to $\text{Co} \lesssim 1$ – the large-scale magnetic fields tend to be predominantly axisymmetric and quasi-steady (e.g. Käpylä et al. 2017a; Strugarek et al. 2018). This coincides with *anti-solar* differential rotation: the rotation rate at the equator is slower than at the poles. A transition to a solar-like differential rotation occurs around $\text{Co} \approx 1$ (e.g. Gastine et al. 2014; Käpylä et al. 2014). The large-scale magnetic fields in such simulations tend to be still predominantly axisymmetric but the dominant dynamo mode is oscillatory (e.g. Ghizaru et al. 2010; Simatev et al. 2015; Strugarek et al. 2017, 2018; Viviani et al. 2018; Bice and Toomre 2023). A number of simulations have appeared where a solar-like dynamo with equatorward migration is found (e.g. Käpylä et al. 2012b;

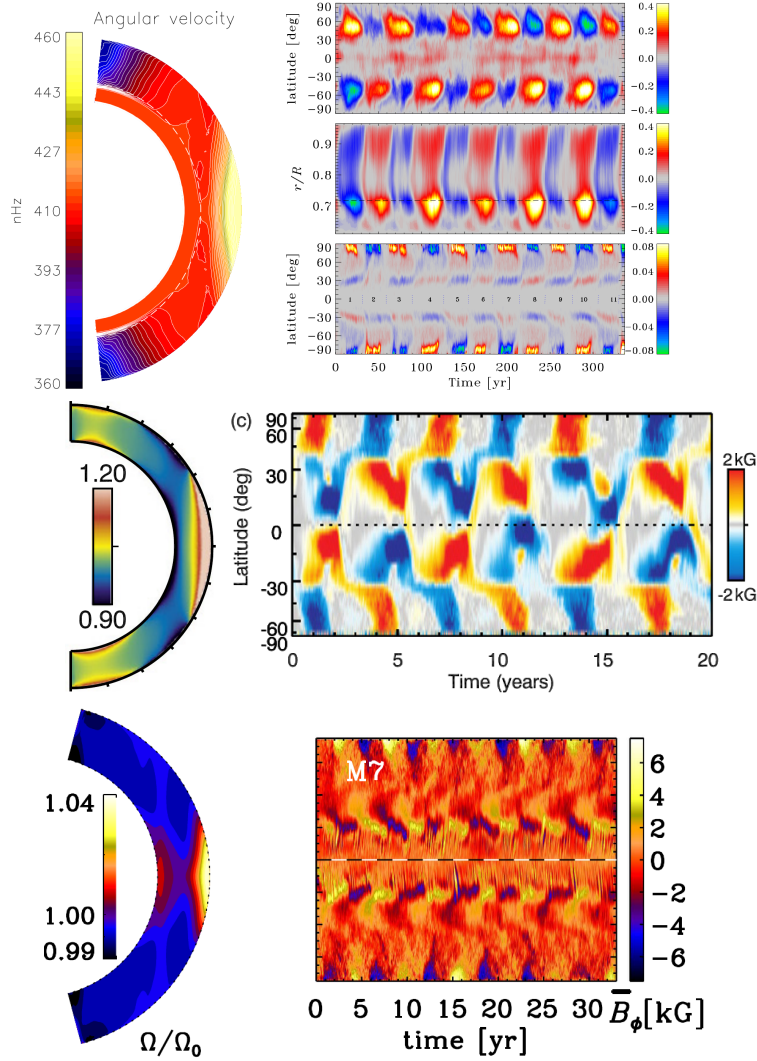


Fig. 6 Left: Azimuthally and temporally averaged mean angular velocity from global dynamo simulations of Ghizaru et al. (2010), here adapted from Racine et al. (2011) (top), Augustson et al. (2015) (middle), and (Warnecke 2018) (bottom). Right: corresponding time-latitude diagrams of the azimuthally averaged magnetic field $\overline{B}_\phi(\theta, t)$, except in the top panel where $\overline{B}_\phi(r, t)$ and $\overline{B}_r(\theta, t)$ are also shown.

Augustson et al. 2015; Strugarek et al. 2018; Warnecke 2018; Matilsky and Toomre 2020; Käpylä 2022; Brun et al. 2022). Representative examples of such solar-like solution are shown in Fig. 6. Comparisons of global convection-driven dynamos with mean-field theory has concentrated on this particular type of simulations which will be discussed in detail in Section 7.3.

4 Mean-field dynamo theory

The large-scale spatiotemporal coherence of the solar magnetic field is suggestive that perhaps its evolution can be explained by a model that has far fewer degrees of freedom than the full 3D magnetohydrodynamic (MHD) problem where all scales down to the dissipation scales are solved. The latter is, and will likely remain, numerically infeasible for the foreseeable future (e.g. [Kupka and Muthsam 2017](#); [Käpylä et al. 2023](#)). The premise behind mean-field theory is to solve only for the large scales while the small-scale (turbulent) effects are parameterized by tensorial transport coefficients. There are several textbooks (e.g. [Moffatt 1978](#); [Parker 1979](#); [Krause and Rädler 1980](#); [Zeldovich et al. 1983](#); [Rüdiger and Hollerbach 2004](#); [Rüdiger et al. 2013](#); [Moffatt and Dormy 2019](#)) and review articles (e.g. [Brandenburg and Subramanian 2005a](#); [Rincon 2019](#); [Tobias 2021](#); [Brandenburg et al. 2023](#)) where mean-field dynamo theory is covered in great detail. Therefore only the most relevant parts of this theory will be briefly repeated here.

The starting point of mean-field dynamo theory is the induction equation which describes the evolution of the magnetic field:

$$\frac{\partial \mathbf{B}}{\partial t} = \nabla \times (\mathbf{U} \times \mathbf{B} - \eta \mu_0 \mathbf{J}). \quad (12)$$

Inspection of Eq. (12) shows that a necessary requirement for the maintenance of magnetic fields is that $\mathbf{U} \neq 0$ and that the induction term $\mathbf{U} \times \mathbf{B}$ needs to overcome magnetic diffusion. Therefore the magnetic Reynolds number

$$\text{Re}_M = \frac{u\ell}{\eta}, \quad (13)$$

where u and ℓ are typical velocity and length scales, has to exceed a critical value which depends on the the properties of the flow and the geometry of the system. The velocity and magnetic fields \mathbf{U} and \mathbf{B} must also be sufficiently complex: for example, Cowling's anti-dynamo theorem states that an axisymmetric field cannot be sustained by a dynamo ([Cowling 1933](#))². Furthermore, the Zeldovich theorem states that a planar flow cannot sustain a dynamo ([Zeldovich 1957](#)).

In mean-field theory the idea is to follow the evolution of the large-scale (mean) fields in detail whereas the small-scale (turbulent) contributions are described via turbulent transport coefficients. To obtain closed equations for the large scale quantities the mean and fluctuations need to be separated. This is done using the Reynolds decomposition:

$$\mathbf{B} = \overline{\mathbf{B}} + \mathbf{b}, \quad \mathbf{U} = \overline{\mathbf{U}} + \mathbf{u}, \quad (14)$$

where $\overline{\mathbf{B}}$ and $\overline{\mathbf{U}}$ are suitably averaged mean fields and flows, and \mathbf{b} and \mathbf{u} are the fluctuations. Azimuthal averaging is most often used in the case of solar

² However, [Plunian and Alboussière \(2020\)](#) demonstrated recently that axisymmetric flow can sustain a dynamo provided that the electrical conductivity is non-axisymmetric.

and stellar dynamos whereas planar averages are often used in simulations of Classes 1 and 2. These averages obey the Reynolds rules:

$$\overline{\overline{\mathbf{B}}} = \overline{\mathbf{B}}, \quad \overline{\overline{\mathbf{B}_1 + \mathbf{B}_2}} = \overline{\mathbf{B}_1} + \overline{\mathbf{B}_2}, \quad \overline{\overline{\mathbf{b}}} = 0, \quad (15)$$

$$\overline{\overline{\mathbf{B}_1 \mathbf{B}_2}} = \overline{\mathbf{B}_1} \overline{\mathbf{B}_2} + \overline{\mathbf{b}_1 \mathbf{b}_2}, \quad \frac{\partial \overline{\mathbf{B}_i}}{\partial x_j} = \frac{\partial \overline{\mathbf{B}_i}}{\partial x_j}, \quad \frac{\partial \overline{\mathbf{B}_i}}{\partial t} = \frac{\partial \overline{\mathbf{B}_i}}{\partial t}. \quad (16)$$

The last relation containing the time derivative is exact for ensemble averaging while the accuracy of spatial averaging improves the longer the averaging time is. Using the Reynolds decomposition in Eq. (12) yields the mean-field induction equation

$$\frac{\partial \overline{\mathbf{B}}}{\partial t} = \nabla \times (\overline{\mathbf{U}} \times \overline{\mathbf{B}} + \overline{\boldsymbol{\mathcal{E}}} - \eta \mu_0 \overline{\mathbf{J}}). \quad (17)$$

The additional term that appears in the mean-field induction equation is the electromotive force (EMF):

$$\overline{\boldsymbol{\mathcal{E}}} = \overline{\mathbf{u} \times \mathbf{b}}, \quad (18)$$

which describes the correlations of small-scale velocities and magnetic fields. Solving Eq. (17) thus requires that the EMF is known. It is customary to represent $\overline{\boldsymbol{\mathcal{E}}}$ in terms of the mean magnetic field and its gradients

$$\overline{\boldsymbol{\mathcal{E}}}_i = \overline{\boldsymbol{\mathcal{E}}}_i^{(0)} + a_{ij} \overline{B}_j + b_{ijk} \frac{\partial \overline{B}_j}{\partial x_k} + \dots, \quad (19)$$

where $\overline{\boldsymbol{\mathcal{E}}}_i^{(0)}$ is a contribution that can appear in the absence of a mean field, a_{ij} and b_{ijk} are tensorial coefficients, and where the dots indicate possible higher order derivatives (e.g. Krause and Rädler 1980). Equation (19) is an approximation that is valid if the mean fields vary slowly in space and time in comparison to the integral scale and turbulent time, respectively. In other words, Eq. (19) assumes that the connection between $\overline{\boldsymbol{\mathcal{E}}}$ and $\overline{\mathbf{B}}$ is local and instantaneous.

However, in the general case the effects of non-locality cannot be neglected. In this case the EMF can be formally written as (Rädler 2014)

$$\begin{aligned} \overline{\boldsymbol{\mathcal{E}}}_i(\mathbf{x}, t) = & \overline{\boldsymbol{\mathcal{E}}}_i^{(0)} + \int_0^\infty \int_\infty^\infty (\mathcal{A}_{ij}(\mathbf{x}, t; \boldsymbol{\xi}, \tau) \overline{B}_j(\mathbf{x} + \boldsymbol{\xi}, t - \tau) \\ & + \mathcal{B}_{ij}(\mathbf{x}, t; \boldsymbol{\xi}, \tau) \frac{\partial \overline{B}_j(\mathbf{x} + \boldsymbol{\xi}, t - \tau)}{\partial x_k}) d^3 \xi d\tau, \quad (20) \end{aligned}$$

where \mathcal{A}_{ij} and \mathcal{B}_{ij} are tensorial kernels which, in the kinematic case, depend on \mathbf{U} and η , and where the integrals run over all space and past time. In practice, the contributions from sufficiently large $\boldsymbol{\xi}$ and τ become negligible and real flows fall somewhere between the two extremes Eqs. (19) and (20). Issues related to non-locality will be revisited in later sections.

Equation (19) is not particularly informative about the physical effects that contribute to the EMF via the coefficients a_{ij} and b_{ijk} . An equivalent way of writing the $\overline{\boldsymbol{\mathcal{E}}}$ in the absence of $\overline{\boldsymbol{\mathcal{E}}}_i^{(0)}$ is (e.g. Rädler 1980)

$$\overline{\boldsymbol{\mathcal{E}}} = \boldsymbol{\alpha} \cdot \overline{\mathbf{B}} + \boldsymbol{\gamma} \times \overline{\mathbf{B}} - \boldsymbol{\beta} \cdot (\nabla \times \overline{\mathbf{B}}) - \boldsymbol{\delta} \times (\nabla \times \overline{\mathbf{B}}) - \boldsymbol{\kappa} \cdot (\nabla \overline{\mathbf{B}})^{(s)}, \quad (21)$$

where α is the symmetric part of a_{ij} and describes the generation of magnetic fields through the α effect which is related to kinetic helicity of the flow (Steenbeck et al. 1966). The anti-symmetric part of a_{ij} gives rise to magnetic pumping, $\gamma_i = -\epsilon_{ijk}a_{jk}/2$, which describes an advection-like effect. β is a second rank tensor describing turbulent diffusion, and δ is a vector describing the Rädler or $\overline{\boldsymbol{\Omega}} \times \overline{\boldsymbol{J}}$ effect (Rädler 1969) that can also lead to dynamo action. Finally, κ is a third-rank tensor acting on the symmetric part of the mean magnetic field gradient tensor. The physical interpretation of κ is currently unclear. Another contribution to δ includes the shear-current or $\overline{\boldsymbol{W}} \times \overline{\boldsymbol{J}}$ effect, where $\overline{\boldsymbol{W}} = \nabla \times \overline{\boldsymbol{U}}$ (Rogachevskii and Kleeorin 2003, 2004). This effect is postulated to occur in shearing nonhelical turbulence and which enters through an off-diagonal component of the magnetic diffusivity tensor. Also a magnetic variant of the shear-current effect has been proposed (Rogachevskii and Kleeorin 2004; Squire and Bhattacharjee 2015b, 2016) which is conjectured to occur if the small-scale magnetic fields due to a small-scale dynamo are sufficiently strong. Furthermore, fluctuations of kinetic helicity and α effect have also been shown to support dynamos if large-scale shear is also present in cases where the mean helicity and α effect vanish (e.g. Vishniac and Brandenburg 1997; Sokolov 1997; Proctor 2007; Kleeorin and Rogachevskii 2008; Sridhar and Singh 2010; Jingade and Singh 2021).

Lastly, there is the $\overline{\boldsymbol{\mathcal{E}}}^{(0)}$ term which occurs in the absence of $\overline{\boldsymbol{B}}$. This term can be thought to encompass battery terms such as the Biermann battery (Biermann 1950) which are needed to seed the magnetic field in the absence of magnetic monopoles when $\boldsymbol{B} = 0$ initially. However, there are other possible contributions to $\overline{\boldsymbol{\mathcal{E}}}^{(0)}$ that can occur if there is a pre-existing magnetic turbulence (e.g. Rädler 1976), i.e., a small-scale dynamo where $\boldsymbol{b} \neq 0$ with $\overline{\boldsymbol{B}} = 0$, or when a mean flow and cross-helicity $\boldsymbol{u} \cdot \overline{\boldsymbol{b}}$ are present (e.g. Yoshizawa 1990; Yoshizawa and Yokoi 1993; Brandenburg and Rädler 2013).

4.1 Analytic methods to compute turbulent transport coefficients

The main difficulty in mean-field dynamo theory lies in computation of the turbulent transport coefficients such as those in Eq. (21). In the kinematic case, where \boldsymbol{U} is assumed given, it suffices to solve for the fluctuating magnetic field \boldsymbol{b} which is given by

$$\frac{\partial \boldsymbol{b}}{\partial t} = \nabla \times (\overline{\boldsymbol{U}} \times \boldsymbol{b} + \boldsymbol{u} \times \overline{\boldsymbol{B}} + \boldsymbol{\mathcal{G}}) + \eta \nabla^2 \boldsymbol{b}, \quad (22)$$

where $\boldsymbol{\mathcal{G}} = \boldsymbol{u} \times \boldsymbol{b} - \overline{\boldsymbol{u} \times \boldsymbol{b}}$, is the nonlinear term. It is possible to derive an exact equation for $\boldsymbol{\mathcal{G}}$ but this leads to an infinite chain of equations for increasingly higher order correlations of \boldsymbol{u} and \boldsymbol{b} . To avoid this, analytic methods truncate the series of equations with typically computationally convenient rather than physically justified approximations. The kinematic case considered above is practically never the case in observed astrophysical systems and the magnetic backreaction on the flow cannot be omitted. In that case also the momentum

equation needs to be taken into account. A few of the analytic methods used in mean-field theory are described below; the reader is referred to Rogachevskii (2021) for a more thorough discourse.

4.1.1 First order smoothing approximation (FOSA)

In FOSA, \mathcal{G} is neglected altogether (e.g. Moffatt 1978; Krause and Rädler 1980). This approximation is valid in cases when either

$$\text{Re}_M \ll 1, \quad \text{or} \quad \text{St} = \frac{\tau_c u}{\ell} \ll 1, \quad (23)$$

where St is the Strouhal number and where τ_c is the correlation time of the flow. In astrophysical systems $\text{Re}_M \gg 1$ practically always (e.g. Ossendrijver 2003; Brandenburg and Subramanian 2005a). On the other hand, often in numerical simulations $\text{St} \approx 1$ (e.g. Brandenburg and Subramanian 2005b), and similar estimates can be obtained, e.g., for the solar granulation. Therefore many simulations as well as the Sun fall outside the validity range of FOSA. Nevertheless, the rigorous results obtained using FOSA are very useful as benchmarks for methods that seek to determine turbulent transport coefficients. The validity of FOSA estimates of turbulent transport coefficients is discussed in more detail in Sect. 6.

In the high conductivity limit, where $\text{Re}_M \gg 1$ and $\text{St} \ll 1$, FOSA yields in the case of isotropic and homogeneous turbulence

$$\overline{\mathcal{E}} = \alpha \overline{\mathbf{B}} - \eta_t \mu_0 \overline{\mathbf{J}}, \quad (24)$$

where the scalar α effect and turbulent diffusivity are given by

$$\alpha = -\frac{1}{3} \tau_c \overline{\boldsymbol{\omega} \cdot \mathbf{u}} \quad \text{and} \quad \eta_t = \frac{1}{3} \tau_c \overline{\mathbf{u}^2}, \quad (25)$$

where $\boldsymbol{\omega} = \nabla \times \mathbf{u}$ is the vorticity and $\overline{\boldsymbol{\omega} \cdot \mathbf{u}}$ is the kinetic helicity. In the general anisotropic and inhomogeneous cases the transport coefficients are tensors but they are also in principle tractable under FOSA (see, e.g. Rädler 1980). FOSA is also often referred to as the second-order correlation approximation (SOCA).

4.1.2 Minimal tau approximation (MTA)

Another approximation that gained popularity in the early 2000s is the minimal τ approximation (MTA) (e.g. Kleorin et al. 1990; Blackman and Field 2002; Rogachevskii and Kleorin 2003). In this method time evolution equation of $\overline{\mathcal{E}}$ is derived:

$$\frac{\partial \overline{\mathcal{E}}}{\partial t} = \overline{\dot{\mathbf{u}} \times \mathbf{b}} + \overline{\mathbf{u} \times \dot{\mathbf{b}}}, \quad (26)$$

where the dots indicate time derivatives. In the case of isotropic and homogeneous turbulence the evolution equation for $\overline{\mathcal{E}}$ is given by

$$\frac{\partial \overline{\mathcal{E}}}{\partial t} = \tilde{\alpha} \overline{\mathbf{B}} - \tilde{\eta}_t \mu_0 \overline{\mathbf{J}} + \overline{\mathbf{T}}, \quad (27)$$

where $\overline{\mathbf{T}}$ contains triple correlations and where

$$\tilde{\alpha} = -\frac{1}{3} (\overline{\boldsymbol{\omega} \cdot \mathbf{u}} - \rho^{-1} \overline{\mathbf{j} \cdot \mathbf{b}}) \quad \text{and} \quad \tilde{\eta}_t = \frac{1}{3} \overline{\mathbf{u}^2}. \quad (28)$$

Relating the triple correlations to second correlations via $\overline{\mathbf{T}} = -\overline{\boldsymbol{\mathcal{E}}}/\tau$, where τ is a relaxation time, and assuming stationarity yields the same expression for $\overline{\boldsymbol{\mathcal{E}}}$ as in Eq. (24). There is, however, a significant difference which is the appearance of the magnetic contribution to α via the current helicity $\overline{\mathbf{j} \cdot \mathbf{b}}$ (Pouquet et al. 1976):

$$\alpha = -\frac{1}{3}\tau (\overline{\boldsymbol{\omega} \cdot \mathbf{u}} - \rho^{-1} \overline{\mathbf{j} \cdot \mathbf{b}}) \equiv \alpha_K + \alpha_M \quad \text{and} \quad \eta_t = \frac{1}{3}\tau \overline{\mathbf{u}^2}. \quad (29)$$

The minimal τ approximation appears superior to FOSA in that it takes into account the dynamical velocity through the Navier–Stokes equation due to which there is the magnetic correction to the α effect. The latter can be interpreted to be a consequence of magnetic helicity conservation (see Sect. 4.3). Furthermore, higher than second order correlations are to some degree retained through $\overline{\mathbf{T}}$. However, the drawback is that there is no rigorously defined validity range for MTA; see the discussion in Rädler and Rheinhardt (2007).

4.1.3 Lagrangian methods for vanishing diffusivity

Another way to circumvent the issues related to FOSA is to consider a Lagrangian solution of the dissipationless induction equation, i.e.,

$$B_i(\mathbf{x}, t) = B_j(\mathbf{a}, 0) \frac{\partial x_i}{\partial a_j}, \quad (30)$$

where \mathbf{a} corresponds to the initial position of a particle. Such approach was taken by, e.g., Parker (1971), Moffatt (1974), and Kraichnan (1976), which yields the EMF as:

$$\overline{\mathcal{E}}_i(\mathbf{x}, t) = \langle \mathbf{u} \times \mathbf{b} \rangle_i = \langle \mathbf{u} \times \mathbf{B} \rangle_i = \epsilon_{ijk} \langle u_j^L(\mathbf{a}, t) B_l(a, 0) \frac{\partial x_k}{\partial a_l} \rangle, \quad (31)$$

where \mathbf{u}^L corresponds to the Lagrangian velocity $\mathbf{u}^L(\mathbf{a}, t) = (\partial \mathbf{x} / \partial t)_{\mathbf{a}} = \mathbf{u}(\mathbf{x}, t)$, and where the averages denoted by angular brackets are taken over an ensemble of trajectories. In the homogeneous isotropic case discussed above this leads to

$$\alpha(t) = \frac{1}{3} \alpha_{ii}(t) = -\frac{1}{3} \int_0^t \langle \mathbf{u}^L(\mathbf{a}, t) \cdot \nabla_{\mathbf{a}} \times \mathbf{u}^L(\mathbf{a}, \tau) \rangle d\tau, \quad (32)$$

and

$$\begin{aligned} \beta(t) &= \frac{1}{6} \epsilon_{ijk} \beta_{ijk} = \frac{1}{3} \int_0^t \langle \mathbf{u}^L(t) \cdot \mathbf{u}^L(\tau) \rangle d\tau + \int_0^t \alpha(\tau) d\tau \\ &+ \frac{1}{6} \int_0^t \int_0^t \langle \mathbf{u}^L(t) \cdot \mathbf{u}^L(\tau') \nabla_{\mathbf{a}} \cdot \mathbf{u}^L(\tau) - \mathbf{u}^L(t) \cdot \nabla_{\mathbf{a}} \mathbf{u}^L(\tau) \cdot \mathbf{u}^L(\tau') \rangle d\tau d\tau'. \end{aligned} \quad (33)$$

While Eq. (32) closely resembles the FOSA expression, the Lagrangian result for β is quite different from η_t in Eq. (25). The first term on the rhs of Eq. (33)

corresponds to turbulent diffusion of a scalar which was originally derived by Taylor (1922). The second term describes the effects of fluctuations of α , which can theoretically lead to reduced turbulent diffusion resulting enhanced growth of the magnetic field (e.g. Kraichnan 1976). The remaining terms in Eq. (33) involve triple correlations whose physical interpretation is not as straightforward.

4.2 Nonlinearity due to direct magnetic back-reaction

The expression Eq. (19) is linear in $\overline{\mathbf{B}}$ and therefore applicable in the case where the mean magnetic field is weak. When the mean field is non-negligible the turbulent transport coefficients need to be reinterpreted as $a_{ij} = a_{ij}(\mathbf{B})$ and $b_{ijk} = b_{ijk}(\mathbf{B})$. Arguably the simplest way of incorporating the nonlinearity is to assume that the mean magnetic fields affect the velocity field \mathbf{U} . A common way to deal with the nonlinearity is to assume that the backreaction ensues when the magnetic energy is comparable to equipartition with kinetic energy via an algebraic quenching formula:

$$\alpha = \frac{\alpha_0}{1 + (\overline{\mathbf{B}}/B_{\text{eq}})^2}, \quad (34)$$

where $B_{\text{eq}} = \sqrt{\mu_0 \rho \mathbf{U}^2}$ and α_0 is the kinematic value of α . This can be understood as the back-reaction of the large-scale field on the small-scale flow \mathbf{u} . Another form of α quenching includes a factor containing the magnetic Reynolds number

$$\alpha = \frac{\alpha_0}{1 + \text{Re}_M (\overline{\mathbf{B}}/B_{\text{eq}})^2}, \quad (35)$$

and leads to a negligibly small α even for very weak fields if astrophysically relevant values of Re_M are used. This is known as *catastrophic quenching* in the original sense (Cattaneo and Vainshtein 1991; Vainshtein and Cattaneo 1992; Gruzinov and Diamond 1994, 1995; Bhattacharjee and Yuan 1995; Cattaneo and Hughes 1996). This is now understood in terms of magnetic helicity conservation in fully periodic or closed systems; see Sect. 4.3. The Sun and other astrophysical objects are not fully closed such that magnetic helicity can be shed by various kinds of magnetic helicity fluxes. The preceding discussion has concentrated solely on the nonlinearity of α , but in general all of the turbulent transport coefficients feel the effects of dynamo-generated magnetic fields (e.g. Kitchatinov et al. 1994; Pipin 2008; Karak et al. 2014; Rogachevskii and Kleeorin 2024).

Models with just α quenching can still be considered partly kinematic because the large-scale flow $\overline{\mathbf{U}}$ remains unaffected. Another type of nonlinearity deals with the impact of large-scale magnetic field on the large-scale flows such as the differential rotation via the Lorentz force (Malkus and Proctor 1975)

$$\dot{\overline{\mathbf{U}}} = \dots + \frac{1}{\rho} \overline{\mathbf{J}} \times \overline{\mathbf{B}}, \quad (36)$$

which quenches the large-scale flows taking part in the dynamo process. An analogous contribution arises from turbulent Maxwell stress $\mathcal{M}_{ij} = \overline{b_i b_j} / \mu_0 \bar{\rho}$. The small-scale Maxwell stress is often the dominant magnetic effect affecting the large-scale flows in 3D simulations (e.g. Käpylä et al. 2017a; Hotta et al. 2022; Warnecke et al. 2025; Hotta 2025). However, a mean-field theory for the turbulent Maxwell stress in rotating turbulence has yet to be developed and it is not included in mean-field modeling.

In the preceding discussion the backreaction was considered to be due only to the large-scale field $\overline{\mathbf{B}}$. In astrophysical systems the magnetic Reynolds numbers are so large that a small-scale dynamo is very likely to be operating (e.g. Warnecke et al. 2023; Rempel et al. 2023). The backreaction of \mathbf{b} on the turbulent transport coefficients is much harder to quantify rigorously. First, this involves magnetic helicity conservation which is discussed below. Second, the \mathbf{b} due to a small-scale dynamo can also influence \mathbf{u} directly without a recourse to magnetic helicity arguments. Developments in this direction are discussed in Sect. 6.3.2. Concrete evidence of nonlinear effects due to small-scale dynamos in numerical simulations are still quite sparse and sometimes conflicting. Hotta et al. (2016) found non-monotonic behavior of the energy of the mean magnetic fields as a function of effective Re_M and argued that a small-scale dynamo aids the large-scale field generation at sufficiently high effective Re_M , whereas Käpylä et al. (2017a) found a monotonic increase of $\overline{\mathbf{B}}^2$ as a function of Re_M . On the other hand, Cattaneo and Tobias (2014) suggested that large-scale dynamo action is facilitated by suppression of the small-scale magnetism. This issue is still open and awaits for further systematic theoretical and numerical studies.

4.3 Magnetic helicity conservation

In ideal MHD, an important conserved quantity is the magnetic helicity

$$\mathcal{H}_M \equiv \int \mathbf{A} \cdot \mathbf{B} \, dV, \quad (37)$$

where \mathbf{A} is the magnetic vector potential with $\mathbf{B} = \nabla \times \mathbf{A}$. This can be seen from the evolution equation of \mathcal{H}_M :

$$\frac{\partial \mathcal{H}_M}{\partial t} = -2 \int_V \mathbf{E} \cdot \mathbf{B} \, dV - \int_S (\phi \mathbf{B} + \mathbf{A} \times \mathbf{E}) \cdot \hat{\mathbf{n}} \, dS. \quad (38)$$

where $\mathbf{E} = -\nabla \phi - \partial \mathbf{A} / \partial t$ is the electric field and ϕ is a scalar potential (e.g. Brandenburg and Subramanian 2005a). In a fully periodic or fully closed system the surface integral vanishes. Substituting Ohm's law $\mathbf{E} = \mu_0 \eta \mathbf{J} - \mathbf{U} \times \mathbf{B}$ yields

$$\frac{\partial \mathcal{H}_M}{\partial t} = -2\eta\mu_0 \int_V \mathbf{J} \cdot \mathbf{B} \, dV \equiv -2\mu_0\eta C, \quad (39)$$

where $C = \int_V \mathbf{J} \cdot \mathbf{B} dV$ is the current helicity. Thus, magnetic helicity can change only because of *molecular* magnetic diffusivity, implying that large-scale fields can only saturate on a diffusive timescale (e.g. Brandenburg 2001). Astrophysical dynamos practically always have $\text{Re}_M \gg 1$ such that \mathcal{H}_M can be considered to be very nearly conserved (e.g. Brandenburg and Subramanian 2005a).

Magnetic helicity conservation has important consequences for non-linear dynamos. Let us again consider isotropic and homogeneous helical turbulence in a fully periodic system where $\mathcal{E} = \alpha \bar{\mathbf{B}} - \eta_t \mu_0 \bar{\mathbf{J}}$, where α and η_t are scalars. The magnetic helicity density can be separated the mean and small-scale parts as $\overline{\mathbf{A} \cdot \mathbf{B}} = \overline{\mathbf{A}} \cdot \overline{\mathbf{B}} + \overline{\mathbf{a} \cdot \mathbf{b}}$. In the isotropic case, small-scale magnetic and current helicities are related via $\overline{\mathbf{a} \cdot \mathbf{b}} \approx \mu_0 \overline{\mathbf{j} \cdot \mathbf{b}}/k_f^2$ where k_f is the typical scale of turbulent eddies. With this information, an evolution equation for the total α effect, $\alpha = \alpha_K + \alpha_M$, can be written as (e.g. Brandenburg and Dobler 2002)

$$\frac{\partial \alpha}{\partial t} = -2\eta_t k_f^2 \left(\frac{\alpha \bar{\mathbf{B}}^2 - \eta_t \mu_0 \bar{\mathbf{J}} \cdot \bar{\mathbf{B}}}{B_{\text{eq}}^2} + \frac{\alpha - \alpha_K}{\text{Rm}} \right), \quad (40)$$

where $\text{Rm} = \eta_t/\eta$ is proportional to Re_M . Equation (40) is a dynamical α quenching formula which takes into account magnetic helicity conservation in the absence of magnetic helicity fluxes. Allowing for such fluxes, the dynamical equation for α reads:

$$\frac{\partial \alpha}{\partial t} = -2\eta_t k_f^2 \left(\frac{\alpha \bar{\mathbf{B}}^2 - \eta_t \mu_0 \bar{\mathbf{J}} \cdot \bar{\mathbf{B}}}{B_{\text{eq}}^2} + \frac{\alpha - \alpha_K}{\text{Rm}} \right) - \nabla \cdot \mathcal{F}^{\alpha_M}. \quad (41)$$

An equivalent representation is (e.g. Brandenburg 2008, 2018a)

$$\alpha(\bar{\mathbf{B}}) = \frac{\alpha_K + \text{Rm}[\eta_t \mu_0 \bar{\mathbf{J}} \cdot \bar{\mathbf{B}}/B_{\text{eq}}^2] - \nabla \cdot \mathcal{F}^{\alpha_M}/(2k_f^2 B_{\text{eq}}^2) - (\partial \alpha / \partial t)/(2\eta_t k_f^2)}{1 + \text{Rm}(\bar{\mathbf{B}}/B_{\text{eq}})^2}. \quad (42)$$

This equation reduces to the catastrophic quenching formula in Eq. (35) if the terms proportional to Rm in the numerator vanish. However, this is valid only in the stationary case under the assumption of uniform magnetic fields and vanishing magnetic helicity fluxes. None of these conditions are expected to be valid in real astrophysical systems. There are several potential sources of magnetic helicity fluxes (e.g. Blackman and Field 2000; Kleeorin et al. 2000; Vishniac and Cho 2001; Vishniac and Shapovalov 2014; Kleeorin and Rogachevskii 2022; Gopalakrishnan and Subramanian 2023). The most commonly invoked fluxes include

$$\mathcal{F}^{\alpha_M} = \frac{\eta_t k_f^2}{B_{\text{eq}}^2} (-\kappa_\alpha \nabla \alpha_M - \bar{\mathbf{U}} \alpha_M + \bar{\mathbf{F}}^f). \quad (43)$$

where the first two terms of the rhs correspond to turbulent diffusion (e.g. Covas et al. 1998; Mitra et al. 2010a) and large-scale advection (e.g. Sur et al. 2007) of α_M , whereas the term $\bar{\mathbf{F}}^f$ encompasses additional contributions that

can be independent of the large-scale magnetic field (see [Gopalakrishnan and Subramanian 2023](#), and references therein). The latter can in principle also lead to dynamo action in the absence of kinetic helicity (e.g. [Brandenburg and Subramanian 2005c](#); [Vishniac and Shapovalov 2014](#)).

5 Prerequisites for accurate mean-field modeling

Before diving into the wealth of comparisons between 3D simulations and mean-field theory, some statements regarding the procedure and depth of the comparisons are needed. Roughly three levels of comparisons between simulations mean-field theory can be readily distinguished:

1. Estimates and measurements of inductive and diffusive effects from simulations without necessarily trying to use the results to explain any specific dynamo simulation.
2. The use of measured or inferred mean-field transport coefficients to interpret the simulation results *qualitatively* in terms of mean-field concepts.
3. Detailed extraction and parametrization of the transport coefficients from 3D simulations and their use in corresponding *quantitative* mean-field modeling.

The first kind typically yields only limited insight into the actual dynamo process in the simulations, whereas the second kind is possibly useful in characterizing the dynamo in mean-field-theoretic terms. However, only the most ambitious comparisons of the third kind can give exhaustive knowledge about the dynamo mechanisms at play. To make such comparisons, the following questions need to be addressed:

1. How to reliably measure turbulent transport coefficients such that they faithfully reproduce the EMF of the 3D simulation?
2. Do mean-field models using these parametrization reproduce the dynamo of the original simulations?
3. What is the uncertainty of the results obtained?

The first question can be reformulated such that it is a necessary requirement that the reconstructed $\overline{\mathcal{E}}$ is the same (or sufficiently similar) as that in the original 3D simulation. The second point addresses the requirement that the derived turbulent transport coefficients, when used in a mean-field model, must reproduce the large-scale fields of the 3D simulation. Only if both of these conditions are met, can it be relatively confidently stated that the mean-model captures the behavior of the 3D simulation. However, this is an ambitious goal and typically such accuracy is difficult to obtain. The third question refers mostly to *systematic* uncertainties and is crucial for the assessment of the reliability of the comparisons. This includes the methods of computation of the transport coefficients and the assumptions that enter the ansatz used for the EMF such as the treatment of nonlinearity and nonlocality.

6 Methods to compute turbulent transport coefficients from simulations

A major technical challenge is to compute all of the tensorial coefficients appearing in the EMF ansatz such as Eq. (21). In 3D simulations the three components of $\overline{\mathcal{E}}$ are readily available, but typically a much greater number of tensorial components appear on the rhs of Eq. (21). Often this is not even attempted and only a subset of the coefficients are retrieved. This is achieved via *ad hoc* simplifications of the EMF ansatz Eq. (21), for instance, by neglecting terms proportional to derivatives of $\overline{\mathbf{B}}$. The most common methods to compute the turbulent transport coefficients from simulations along with representative results and issues are discussed next.

6.1 Imposed field method

Arguably the simplest approach to compute the transport coefficients is to impose a mean magnetic field $\overline{\mathbf{B}} = \overline{\mathbf{B}}^{(\text{imp})}$ on the solution and measure the induced $\overline{\mathcal{E}}$ (see e.g. Brandenburg et al. 1990b; Cattaneo and Hughes 1996; Ossendrijver et al. 2001, 2002; Cattaneo and Hughes 2006; Käpylä et al. 2006a). In principle it is possible to choose sufficiently many linearly independent imposed fields such that all of the turbulent transport coefficients in an ansatz such as Eq. (21) can be extracted. However, this is cumbersome because a separate numerical experiment is needed for each $\overline{\mathbf{B}}^{(\text{imp})}$, and great care has to be taken to ensure that the additional mean fields $\overline{\mathbf{B}}(\mathbf{x}, t)$ possibly generated in the simulation remain small compared to $\overline{\mathbf{B}}^{(\text{imp})}$. Therefore the imposed field studies have almost solely been done with uniform fields to study the α effect (see, however Brandenburg et al. 1990a). Assuming that $\overline{\mathbf{B}}^{(\text{imp})} \approx \overline{\mathbf{B}}$, Eq. (21) reduces to

$$\overline{\mathcal{E}} = \boldsymbol{\alpha} \cdot \overline{\mathbf{B}}^{(\text{imp})} + \boldsymbol{\gamma} \times \overline{\mathbf{B}}^{(\text{imp})}, \quad (44)$$

where the latter term is analogous to $\overline{\mathbf{U}} \times \overline{\mathbf{B}}$, and where three experiments suffice to compute all of the components of a_{ij} . The imposed field method was first used to determine the α effect from simulations of rotating stratified convection (e.g. Brandenburg et al. 1990b; Ossendrijver et al. 2001). These studies showed that the horizontal and vertical components of α had opposite signs reflecting the underlying anisotropy of convective flows. Later these studies have been expanded to map a_{ij} as a function of latitude and rotation from simulations of mildly turbulent convection by, for example, Ossendrijver et al. (2002) and Käpylä et al. (2006a). The former found that for moderate rotation ($\text{Co} \approx 1$) the α effect is roughly proportional to $\cos \theta$ which is also the lowest order expectation from mean-field theory; see Fig. 7. Simulations probing cases corresponding to the base of the solar convection zone with $\text{Co} \approx 10$ suggest increasing anisotropy and a latitudinal maximum of the horizontal α effect around latitude 30° (Käpylä et al. 2006a).

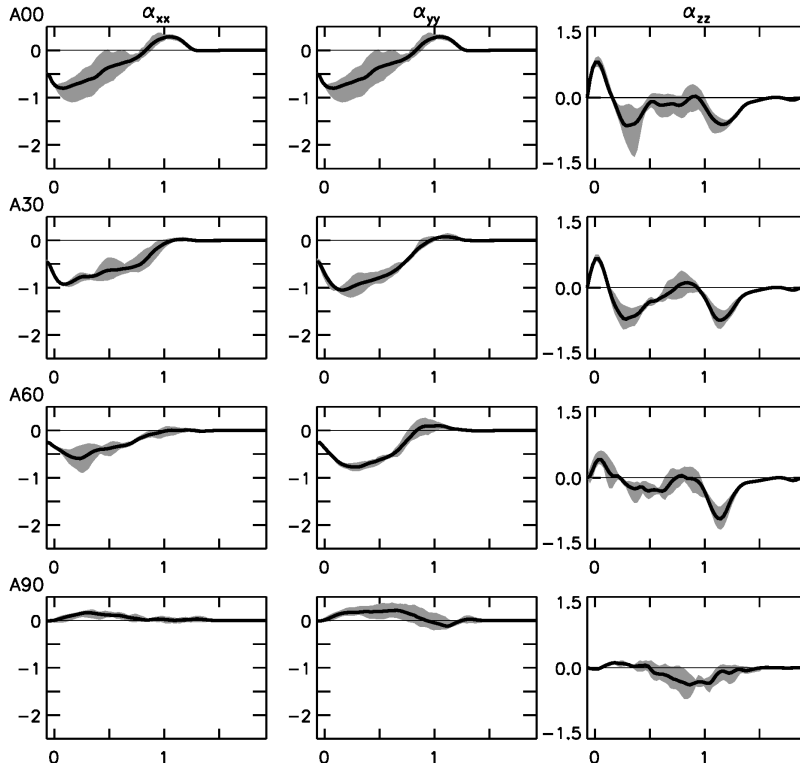


Fig. 7 Diagonal components of α_{ij} in units of $10^{-2}\sqrt{dg}$, where d is the depth of the convection zone and g is the acceleration due to gravity, as functions of height and latitude from Cartesian convection simulations of [Ossendrijver et al. \(2002\)](#) with $Co = 2.4$, $Re = Re_M = 260$ that are based on the system scale. The different panels correspond to latitude $\theta = 0$ (north pole, top row), 30° , 60° , and 90° (equator, bottom row). The horizontal axis shows the vertical coordinate z in units of d . The convection zone spans the range $0 < z/d < 1$.

The simulations of [Ossendrijver et al. \(2002\)](#) and [Käpylä et al. \(2006a\)](#) also extracted the turbulent pumping effect γ . Downward pumping of magnetic fields was already demonstrated by earlier numerical studies (e.g. [Nordlund et al. 1992](#); [Brandenburg et al. 1996](#); [Tobias et al. 1998, 2001](#); [Dorch and Nordlund 2001](#)). [Ossendrijver et al. \(2002\)](#) showed that the vertical pumping of large-scale fields to be dominated by the diamagnetic effect, and that with sufficiently rapid rotation, horizontal components of γ are non-negligible (e.g. [Kichatinov 1991](#)). The latitudinal pumping was found to be predominantly equatorward and the azimuthal pumping retrograde in [Ossendrijver et al. \(2002\)](#), both of which can potentially aid in obtaining equatorward propagation of activity belts. This was confirmed by mean-field models in [Käpylä et al. \(2006b\)](#), where physically plausible turbulent diffusivity η_t and meridional circulation of the Sun along with α and γ coefficients from simulations of [Käpylä et al. \(2006a\)](#) were used.

The main caveat of the imposed field method is that $\overline{\mathbf{B}}^{(\text{imp})}$ is a part of the solution, and that in general $\overline{\mathbf{B}}^{(\text{imp})} \neq \overline{\mathbf{B}}$. This is often the case even if there is no dynamo in the system, for example, due to inhomogeneity because of boundaries (e.g. Käpylä et al. 2010b). This is also related to the choice of averages: even in fully periodic cases with dynamos, for which the volume averaged $\overline{\mathbf{J}}$ vanishes, the relevant mean fields are Beltrami fields with some scale k_m (e.g. Brandenburg 2001). These issues can lead to erroneous estimates of the turbulent transport coefficients. This can be seen by considering the steady state solution of Eq. (17): $\overline{\mathcal{E}} - \mu_0 \eta \overline{\mathbf{J}} = 0$. If $\overline{\mathbf{B}}$ is indeed uniform, then $\overline{\mathbf{J}} = 0$, further implying that $\overline{\mathcal{E}}$ must also vanish if Eq. (44) is assumed. In general $\overline{\mathbf{B}} \neq \overline{\mathbf{B}}^{(\text{imp})}$ in the steady state implying $\overline{\mathbf{J}} \neq 0$, and therefore the more general expression Eq. (24) needs to be used. Furthermore, by order of magnitude the steady state solution and Eq. (44) yield $\alpha B \approx \eta B / \ell$, and lead to a normalized amplitude of $\tilde{\alpha} = \alpha / u = \eta / u \ell = \text{Re}_M^{-1}$, where u is a typical velocity amplitude. Thus in this procedure α appears to be catastrophically quenched proportional to Re_M^{-1} even in the kinematic regime (Cattaneo and Hughes 2006). However, this is a misconception arising from the application of the method outside of its range of validity.

Therefore the imposed field method as described by Eq. (44) is reliable only if the actual mean field does not deviate greatly from the imposed field, that is $\overline{\mathbf{B}} \approx \overline{\mathbf{B}}^{(\text{imp})}$. This is satisfied in 2D where the method is exact and can therefore provide an important benchmark for other methods. To ensure that $\overline{\mathbf{B}} \approx \overline{\mathbf{B}}^{(\text{imp})}$ in 3D often involves resetting of the magnetic field periodically before a steady state is reached (e.g. Ossendrijver et al. 2002; Käpylä et al. 2006a; Hubbard et al. 2009).

6.2 Multidimensional regression methods

6.2.1 Moments method of Brandenburg and Sokoloff (2002)

Another way to get around the problem of underdetermination is to consider a temporally varying MHD solution and exploiting the fact that $\overline{\mathcal{E}}$ and $\overline{\mathbf{B}}$ point to different directions at different times. Using a sufficiently large set of realizations of $\overline{\mathcal{E}}$ and $\overline{\mathbf{B}}$, it is possible to turn an underdetermined problem to an overdetermined one, where the transport coefficients can be obtained by fitting (Brandenburg and Sokoloff 2002). The potential benefit of this method is that the transport coefficients can be obtained from the same calculation without resorting to additional runs with imposed fields. Assuming local and instantaneous relation between $\overline{\mathbf{B}}$ and $\overline{\mathcal{E}}$ and that the mean fields depend only on one coordinate (z), Eq. (19) reduces to:

$$\overline{\mathcal{E}}_i = \alpha_{ij} \overline{B}_j + \eta_{ijz} \partial_z \overline{B}_j, \quad (45)$$

with eight unknowns α_{ij} and η_{ijz} . In Brandenburg and Sokoloff (2002) this was circumvented by forming moments of Eq. (45) with \overline{B}_i and $\partial_z \overline{B}_i$. The

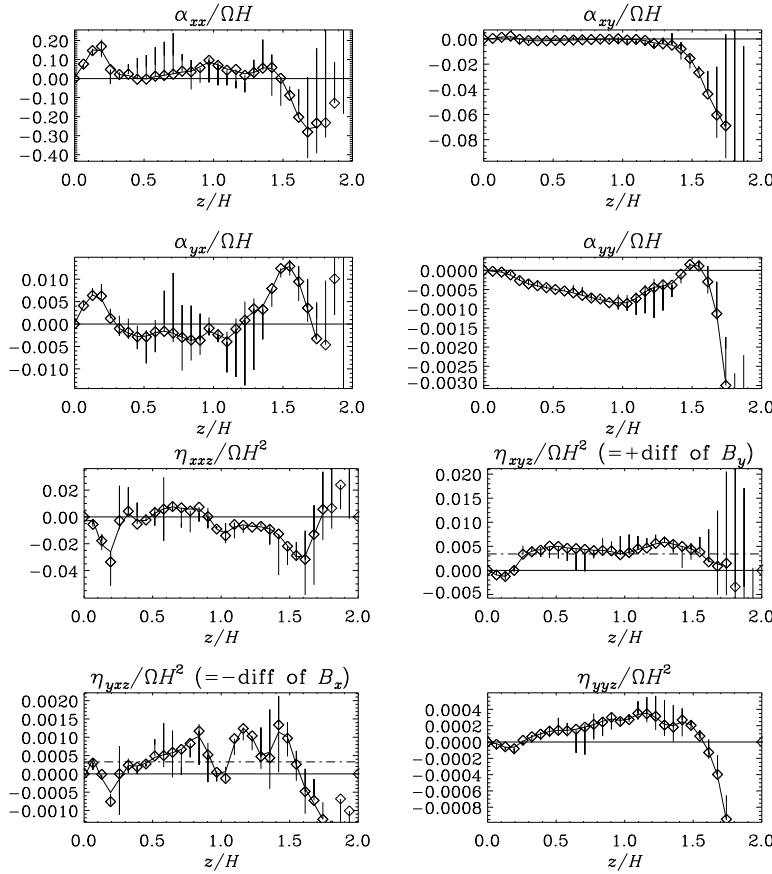


Fig. 8 Upper four panels: α_{ij} from inverting Eq. (46) from a shearing box simulation of the magnetorotational instability (Brandenburg and Sokoloff 2002). Lower four panels: η_{ijk} from Eq. (46) from the same simulation.

resulting eight equations are time averaged and the solution is given by two matrix equations

$$\mathbf{E}^{(i)}(z) = \mathbf{C}^{(i)}(z)\mathbf{M}(z), \text{ for } i = x, y. \quad (46)$$

The matrices $\mathbf{E}^{(i)}$ and $\mathbf{M}^{(i)}$ contain the moments of mean fields and their gradients with \mathcal{E} , and with $\bar{\mathbf{B}}$ and $\partial_z \bar{\mathbf{B}}$ themselves, respectively, whereas $\mathbf{C}^{(i)}$ contains the time-averaged transport coefficients. Figure 8 shows the results from a density-stratified simulation of the magnetorotational instability (MRI) from Brandenburg and Sokoloff (2002). It is not a priori known how α_{ij} or η_{ijk} should look like in this case. However, $-\eta_{yxz}$ is responsible for diffusing the \bar{B}_x component of the mean field. This component is predominantly positive, implying anti-diffusion which is considered unphysical. Further experiments by Brandenburg and Sokoloff (2002) suggest that assuming η_{ijk} to be diagonal

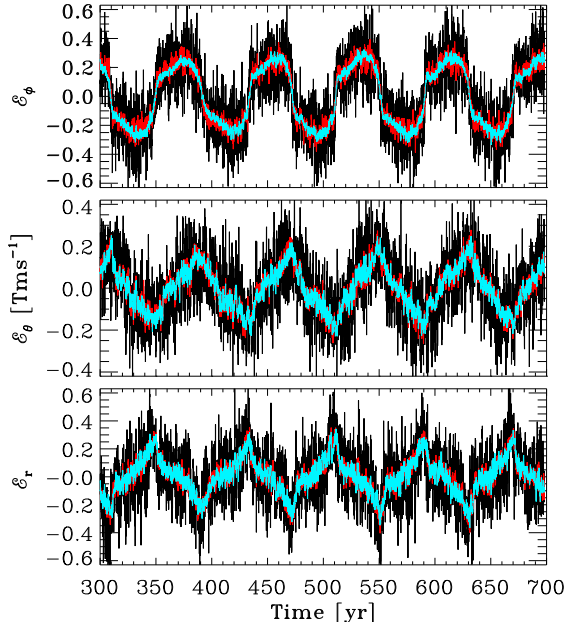


Fig. 9 Components of the EMF (black lines) and fits to it using only the α tensor and α (magenta) and β (red). Adapted from Simard et al. (2016).

removes the problem with anti-diffusion, but there is no physical justification to do this. They also concluded that non-local effects may play a role in that negative diffusion at large scales can be compensated by positive one at higher wavenumbers.

6.2.2 Singular value decomposition (SVD)

The SVD method is similar to the moments method described above and relies on the availability of data to overcome the problem of underdetermination of the EMF ansatz. In this method two time-dependent functions

$$y(t) = \bar{\mathcal{E}}_i(t, r, \theta), \quad \text{and} \quad X_k(t) = [\bar{B}_i(t, r, \theta), \partial_r \bar{B}_i(t, r, \theta), \partial_\theta \bar{B}_i(t, r, \theta)] \quad (47)$$

are constructed from the EMF and magnetic field data. The quantity $\phi_k = [a_{ij}(r, \theta), b_{ijr}(r, \theta), b_{ij\theta}(r, \theta)]$ contains the turbulent transport coefficients. The parametrization of the EMF is given by

$$y(t) = \sum_{k=1}^n \phi_k X_k(t), \quad (48)$$

where n depends on the ansatz for the EMF. The coefficients ϕ_k are required to minimize the least squares fit characterized by a standard χ^2 approach.

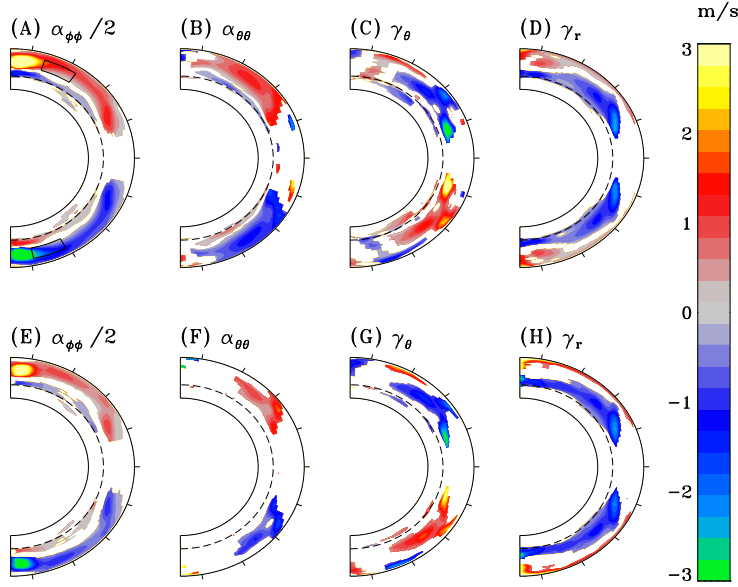


Fig. 10 Top: $\alpha_{\phi\phi}$, $\alpha_{\theta\theta}$, γ_r , and γ_θ extracted from an EULAG simulation where only the α tensor is retained in the SVD analysis. Bottom: same as the top panel but where the β tensor was retained in the fitting. Adapted from Simard et al. (2016).

The SVD method was initially used to extract only the α tensor components from global convection simulations (e.g. Racine et al. 2011; Simard et al. 2013; Nelson et al. 2013; Augustson et al. 2015; Brun et al. 2022; Shimada et al. 2022). In these studies the EMF was assumed to have the form $\mathcal{E} = \alpha \cdot \mathbf{B} + \gamma \times \mathbf{B}$. However, the gradients of \mathbf{B} and the corresponding contributions to the \mathcal{E} cannot in general be dropped, and in a subsequent study, Simard et al. (2016) generalized the EMF to include all of the terms in Eq. (21). Figure 9 illustrates that with the SVD method the reconstructed \mathcal{E} is in very good agreement with the actual EMF in both of the aforementioned cases. The caveat here is that in the SVD method the coefficients are fitting parameters and the method does not guarantee that they are correct or physically realizable.

Nevertheless, the results of Simard et al. (2016) and the earlier studies show that the diagonal components of α are in qualitative agreement with theoretical arguments that $\alpha \propto -\overline{\boldsymbol{\omega} \cdot \mathbf{u}}$, although the magnitude is roughly five times lower than the FOSA estimate irrespective whether the diffusive contribution to the EMF were retained. Similarly the diagonal components of β are predominantly positive where statistically relevant, but again about five times lower than the FOSA estimates. The two experiments discussed above give very similar results for α and γ ; see Fig. 10 and the effects due to the diffusive contributions were therefore found to be small. A (although still not fully conclusive) test of the validity of the coefficients is to use them in a mean-

field model of the same system from which they were extracted. Efforts to this direction are discussed further in Sect. 7.

6.3 Test field methods

6.3.1 Quasi-kinematic test field method

Another way to avoid the issues with imposed fields is to use the test field method (Schrinner et al. 2005, 2007; Brandenburg 2005b), where the imposed fields are replaced by a sufficient number of linearly independent test fields. A separate induction equation for the fluctuating fields is solved for each of the test fields. That is, for each test field $\overline{\mathbf{B}}^{(p)}$,

$$\frac{\partial \mathbf{b}^{(p)}}{\partial t} = \nabla \times \left(\overline{\mathbf{U}} \times \mathbf{b}^{(p)} + \mathbf{u} \times \overline{\mathbf{B}}^{(p)} + \mathcal{G}^{(p)} \right) + \eta \nabla^2 \mathbf{b}^{(p)}, \quad (49)$$

is solved, where the velocity fields $\overline{\mathbf{U}}$ and \mathbf{u} come from the simulation (main run). Neither the test fields $\overline{\mathbf{B}}^{(p)}$ nor the small-scale fields $\mathbf{b}^{(p)}$ react back on the flow. The non-linear term $\mathcal{G}^{(p)} = \mathbf{u} \times \mathbf{b}^{(p)} - \overline{\mathbf{u}} \times \overline{\mathbf{b}}^{(p)}$ is fully retained such that the method is superior to FOSA and MTA. This flavor of the test field method is formally applicable to cases where the small-scale magnetic field \mathbf{b} vanishes when $\overline{\mathbf{B}} \rightarrow 0$, thus excluding cases with \mathbf{b} is due to a small-scale dynamo. On the other hand, the velocity field \mathbf{U} can already be affected by a magnetic field \mathbf{B} in the main run. This is why this flavor is referred to as the quasi-kinematic test field method. Non-linear extensions of the test field method are discussed in Sect. 6.3.2.

In the simplest case the mean fields are assumed to depend only on a single coordinate, here z . The EMF is then

$$\overline{\mathcal{E}}_i = a_{ij} \overline{B}_j - b_{ij} \mu_0 \overline{J}_j, \quad (50)$$

where $b_{i1} = b_{i23}$ and $b_{i2} = -b_{i13}$. The EMF has only x and y components, and a_{ij} and b_{ij} have four components each. A sufficient choice of test fields is

$$\overline{\mathbf{B}}^{1c} = B_0(\cos kz, 0, 0), \quad \overline{\mathbf{B}}^{2c} = B_0(0, \cos kz, 0), \quad (51)$$

$$\overline{\mathbf{B}}^{1s} = B_0(\sin kz, 0, 0), \quad \overline{\mathbf{B}}^{2s} = B_0(0, \sin kz, 0), \quad (52)$$

where k is a wavenumber. This leads to two linear sets of equations from which a_{ij} and b_{ij} can be solved unambiguously. If harmonic test fields are used, higher order derivatives of $\overline{\mathbf{B}}$ can be considered to have been already included because, for example, $(\partial^n / \partial^n x)(\cos kx) = k^n \cos(kx + \frac{\pi n}{2})$. The coefficients a_{ij} and b_{ij} can be recast as

$$\alpha = \frac{1}{2}(a_{11} + a_{22}), \quad \gamma = \frac{1}{2}(a_{21} - a_{12}), \quad (53)$$

$$\eta_t = \frac{1}{2}(b_{11} + b_{22}), \quad \delta = \frac{1}{2}(b_{12} - b_{21}), \quad (54)$$

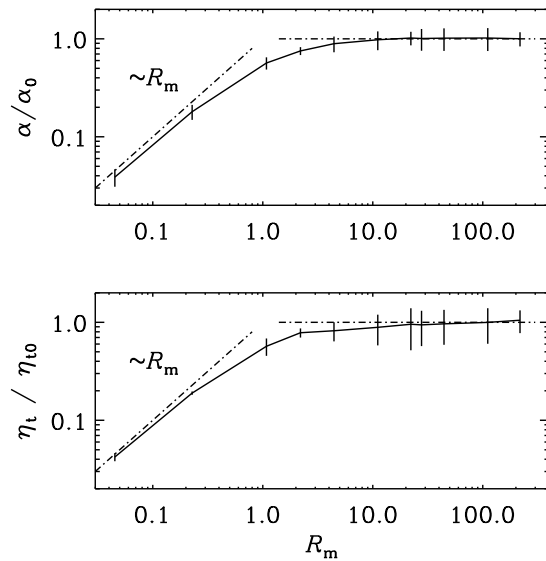


Fig. 11 Top: α normalized by the FOSA estimate α_0 from isotropically forced helical turbulence as a function of the magnetic Reynolds number. Bottom: η_t normalized by the FOSA estimate η_{t0} from the same simulations. Adapted from [Sur et al. \(2008\)](#).

which describe the α effect, turbulent pumping (γ), turbulent magnetic diffusivity (η_t), and the Rädler/shear-current effect (δ), respectively.

Representative results from homogeneous isotropically forced helical turbulence are shown in Fig. 11. Here the measured α effect and η_t turbulent diffusivity are normalized by the FOSA estimates $\alpha_0 = \frac{1}{3}u_{\text{rms}}$, $\eta_{t0} = \frac{1}{3}u_{\text{rms}}k_f^{-1}$, where k_f is the energy-carrying scale of turbulence, and where the former is relevant for fully helical turbulence. Figure 11 shows that both α and η_t are proportional to $\text{Re}_M = u_{\text{rms}}/\eta k_f$ for $\text{Re}_M \lesssim 1$ in accordance with the corresponding FOSA result in the low conductivity limit, see [Krause and Rädler \(1980\)](#). Furthermore, for $\text{Re}_M \gtrsim 10$, α and η_t converge to roughly constant values that agree with within the error estimates with the FOSA estimates. It is remarkable how good the correspondence is given the rather strict validity constraints of FOSA. However, the quasi-kinematic test field method itself is formally valid only when a small-scale dynamo is absent. This is another stringent condition because the critical magnetic Reynolds number is around 30 for $\text{Pr}_M = 1$ (e.g. [Haugen et al. 2004](#)) and increases to a few hundred for $\text{Pr}_M \rightarrow 0$ ([Kleeorin and Rogachevskii 2012](#); [Warnecke et al. 2023](#)).

This method has been used to study the turbulent transport coefficients in shearing turbulence without ([Brandenburg et al. 2008a](#)) and with kinetic helicity ([Mitra et al. 2009a](#)). These studies did not find conclusive evidence for a dynamo effect through the Rädler/shear-current effect in shearing turbulence, which is mediated via off-diagonal components of η_{ij} . Furthermore, [Brandenburg et al. \(2017b\)](#) found a contribution to η_t due to kinetic helicity

from forced turbulence simulations from analysis of test field data. Such contributions go beyond FOSA and arise only when fourth order correlations in the fluctuations are considered in the computation of transport coefficients (e.g. Nicklaus and Stix 1988; Brandenburg et al. 2025; Rogachevskii et al. 2025). A further new aspect discovered with the help of test field calculations is the scaling of the α effect in density-stratified systems (Brandenburg et al. 2013a). While earlier theoretical studies yielded $\alpha \propto \rho^\sigma u_{\text{rms}}$ with $\sigma > 1$ (Rüdiger and Kichatinov 1993), the analytic results by Brandenburg et al. (2013a) suggest that $\sigma = \frac{1}{2}$. Such scaling was also found from forced turbulence and sufficiently stratified turbulent convection simulations for slow rotation ($\text{Co} \lesssim 0.2$) using the test field method in Brandenburg et al. (2013a). Results at more rapid rotation were less coherent but consistently yielded $\sigma < 1$ in contrast to the earlier theoretical predictions.

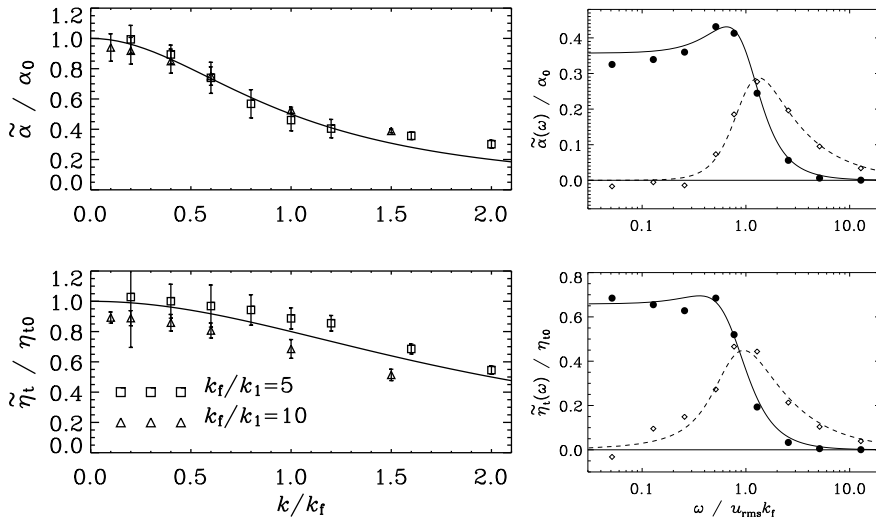


Fig. 12 Left: $\tilde{\alpha}(k)$ (top) and $\tilde{\eta}_t(k)$ (bottom) normalized by the FOSA estimates from isotropically forced helical turbulence as a function of the wavenumber k of the test fields. Adapted from Brandenburg et al. (2008c). Right: $\tilde{\alpha}(\omega)$ (top) and $\tilde{\eta}_t(\omega)$ (bottom) normalized by the FOSA estimates from isotropically forced helical turbulence as a function of the frequency ω of the test fields. Adapted from Hubbard and Brandenburg (2009).

The scale dependence of α and η_t for the Roberts flow and for isotropically forced homogeneous turbulence were studied in Brandenburg et al. (2008c). The dependence of the coefficients on spatial scale was found to be approximately Lorentzian:

$$\tilde{\alpha}(k) = \frac{\alpha_0}{1 + (k/k_f)^2}, \quad \tilde{\eta}_t(k) = \frac{\eta_{t0}}{1 + (k/2k_f)^2}. \quad (55)$$

The results are shown in the left panels of Fig. 12. Such non-local contributions to α and η_t lead to a modification of the growth rate of the dynamo. How-

ever, [Brandenburg et al. \(2008c\)](#) concluded that the non-local effects become important only when the scale of the mean field is comparable to the dominant scale of turbulence. In a subsequent study, [Hubbard and Brandenburg \(2009\)](#) investigated temporal non-locality or memory effects for passive scalar transport and dynamos in Roberts flow and in turbulence. In analogy to the spatial non-locality, they found that memory effects become important when the large-scale field varies on a similar timescale as the flow itself, translating to a Strouhal number of the order of unity or larger; see the right panels of [Fig. 12](#). Finally, [Rheinhardt and Brandenburg \(2012\)](#) considered the case where both spatial and temporal scale separations are poor and suggested to represent the non-local EMF as (see also [Pipin 2023](#))

$$\left(1 + \tau \frac{\partial}{\partial t} - \ell^2 \frac{\partial^2}{\partial z^2}\right) \bar{\mathcal{E}}_i = \alpha_{ij}^{(0)} \bar{B}_j + \eta_{ijk}^{(0)} \bar{B}_{j,k}, \quad (56)$$

where τ and ℓ are a temporal and spatial scale, and where the superscript zero refers to the transport coefficients for $k \rightarrow 0$ and $\omega \rightarrow 0$. [Rheinhardt and Brandenburg \(2012\)](#) admitted that higher order terms are likely needed to fully capture the non-locality but that this expression nevertheless gives a flavor of the issue. A qualitative change of behavior in comparison to the purely local description is that the excitation threshold for the dynamo is lowered if the dynamo is oscillatory (e.g. [Rheinhardt and Brandenburg 2012](#)). A similar conclusion was reached by [Brandenburg and Chatterjee \(2018\)](#) who implemented [Eq. \(56\)](#) in a spherical mean-field dynamo model representative of the Sun. Furthermore, [Rheinhardt et al. \(2014\)](#) showed that the dynamos in two flavors of non-helical Roberts flow ([Roberts 1972](#)) are driven by off-diagonal components of the a_{ij} tensor when memory effects are retained.

Quenching of turbulent transport coefficients was studied by [Karak et al. \(2014\)](#) by means of the test field method from simulations of the Roberts flow, forced turbulence, and convection where a large-scale external field was imposed. Quenching formula proportional to $[1 + p_i (\bar{\mathbf{B}}/B_{\text{eq}})^{q_i}]^{-1}$ was assumed, where p_i and q_i were fit parameters. The quenching exponent q_i depends on the type of the flow and whether B_{eq} is estimated from the unquenched flow or not. In the latter case the exponent q_α for the α effect was 2 for turbulent convection and 3 for isotropically forced homogeneous turbulence whereas the q_{η_t} for the turbulent diffusivity ranged from 1.1 to 1.3. Strongly anisotropic quenching has been assumed in some solar dynamo models in order to assure that turbulent diffusion remains subdominant in determining the cycle period (e.g. [Chatterjee et al. 2004](#); [Karak and Choudhuri 2011](#)). Curiously, [Karak et al. \(2014\)](#) found no evidence of such strong anisotropy even in cases where the large-scale field reached 10^2 times equipartition.

The test field method as presented above can also be applied to inhomogeneous cases such as convection in a Cartesian box. An example is shown in [Figure 13](#) where horizontally averaged kinetic helicity and the coefficients according to [Equations \(53\) and \(54\)](#) are shown from a rotating density stratified convection simulation in Cartesian coordinates ([Käpylä et al. 2009a](#)). The profiles of α and γ are similar to those obtained with the imposed field method

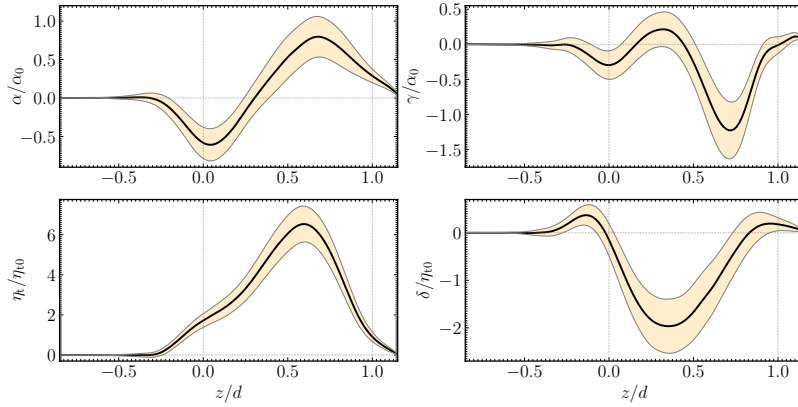


Fig. 13 Turbulent transport coefficients $\alpha(z)$ (top left), $\gamma(z)$ (top right), $\eta_t(z)$ (bottom left), and $\delta(z)$ (bottom right) from Run B of Käpylä et al. (2009a) with $\text{Re} = 35$ and $\text{Co} = 0.36$. The convection zone is situated between $z/d = 0$ and $z/d = 1$.

(Ossendrijver et al. 2001), which also roughly agree with theoretical (FOSA) predictions. The vertical pumping effect γ is downward only in the upper convection zone, whereas η_t is positive everywhere. Stratified convection is highly non-local such that flows can traverse long distances and even penetrate the whole convection zone. Therefore the assumption of a local and instantaneous connection between $\bar{\mathcal{E}}$ and $\bar{\mathbf{B}}$ is *a priori* not well justified. Figure 14 shows the same turbulent transport coefficients as in Fig. 13 but computed with test fields with different vertical wavenumber k ranging between $0 \dots 3$, where $k = 0$ corresponds to an imposed field. These results show that some of the coefficients, such as α and γ can even change sign as a function of spatial scale, whereas the amplitudes of η_t and δ are reduced for higher values of k^3 .

Considering stars such as the Sun, the method has to operate spherical coordinates. Assuming axisymmetry and that non-local effects can be omitted, a total of 27 independent a_{ij} and b_{ijk} coefficients are needed; see Schrunner et al. (2005, 2007). In these, and in subsequent works (e.g. Schrunner 2011; Schrunner et al. 2011, 2012; Schrunner 2013; Warnecke et al. 2018; Viviani et al. 2019), the test fields were chosen to be

$$(\bar{B}_r, \bar{B}_\theta, \bar{B}_\phi) = (1, 1, 1), (\bar{B}_r, \bar{B}_\theta, \bar{B}_\phi) = (r, r, r), (\bar{B}_r, \bar{B}_\theta, \bar{B}_\phi) = (\theta, \theta, \theta). \quad (57)$$

The EMF is given by

$$\bar{\mathcal{E}}_i = \tilde{a}_{ij} \bar{B}_j + \tilde{b}_{ijr} \partial_r \bar{B}_j + \tilde{b}_{ij\theta} \partial_\theta \bar{B}_j, \quad i, j = r, \theta, \phi. \quad (58)$$

The coefficients can be worked out from Eq. (58) using Eq. (21), (see e.g. Appendix A of Viviani et al. 2019). Figure 15 shows representative results for the components of $\boldsymbol{\alpha}$ and $\boldsymbol{\beta}$ from Warnecke et al. (2018). The diagonal components of α_{ij} and the estimate $\alpha_K = -\frac{1}{3} \tau \overline{\boldsymbol{\omega} \cdot \mathbf{u}}$, where $\tau = (u_{\text{rms}} k_1)^{-1}$ is an

³ In Käpylä et al. (2009a) the coefficient δ had a sign error which is corrected in Fig. 14.

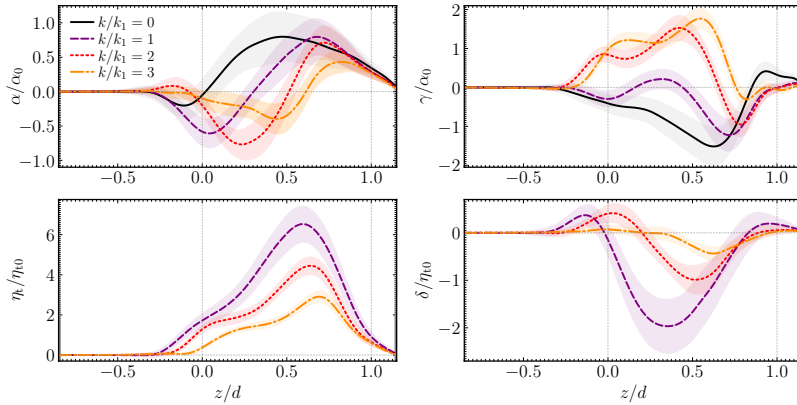


Fig. 14 Effects of non-locality on the turbulent transport coefficients α , γ , η_t , and δ from stratified convection in Cartesian geometry. Data from Runs B11-B14 of Käpylä et al. (2009a). The legend indicates the normalized wavenumber of the test fields.

estimate of the convective turnover time, are in rough qualitative agreement. This entails a positive α effect in the bulk of the convection zone in the northern hemisphere. However, the α effect in density stratified rotating convection is necessarily anisotropic and the α_K estimate cannot be expected to be accurate in detail (e.g. Kleorin and Rogachevskii 2003). Furthermore, the diagonal components of β_{ij} are predominantly positive. Non-positivity of turbulent diffusion is most likely unphysical but it can also be related to insufficient data or non-local effects which were not considered.

A check of the validity of the computed transport coefficients is that they are used to reconstruct the actual EMF of the main run. An example is shown in Fig. 16 for the simulation presented in Viviani et al. (2019). While reasonable qualitative agreement can be found especially at low latitudes, the magnitude of the reconstructed EMF is higher than the actual EMF by a factor of two to three; see Viviani et al. (2019). A possible explanation is that the test fields in Eq. (57), vary on large scales that are comparable to coherent structures in convective flows in which case non-local effects can become important. Therefore the assumption of a local and instantaneous correspondence between $\overline{\mathbf{B}}$ and $\overline{\mathbf{E}}$ can be questioned in the case of convection. On the other hand, correspondence between a DNS and a mean-field model was found to be much better for a forced turbulence simulation with a significantly higher scale separation and $\text{Re}_M \approx 1$ where the effects of non-locality are likely to be less important (Warnecke et al. 2018).

6.3.2 Nonlinear test field methods

The quasi-kinematic test field method is formally applicable to situations where also the small scale fields owe their existence to $\overline{\mathbf{B}}$. This is a rather restrictive condition from astrophysical perspective where small-scale dynamos

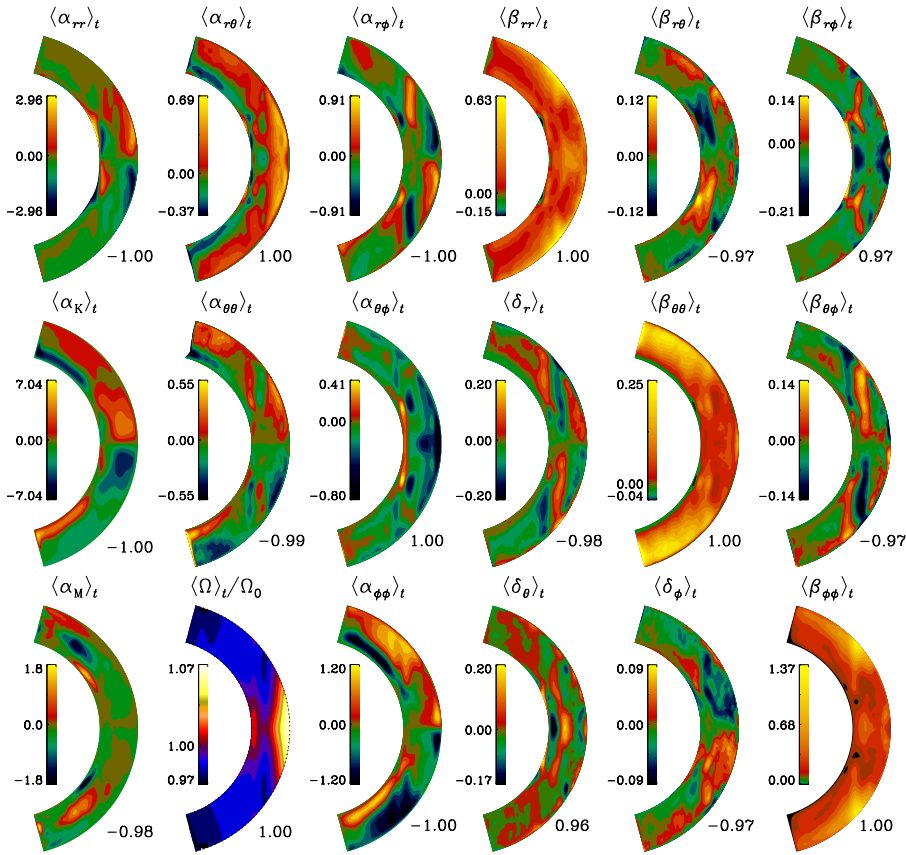


Fig. 15 Nine panels on the left: time averaged components of the α_{ij} tensor, $\alpha_K = -\frac{1}{3}\tau\boldsymbol{\omega}\cdot\mathbf{u}$, $\alpha_M = \frac{1}{3}\tau\mathbf{j}\cdot\mathbf{b}$, and $\bar{\Omega} = \bar{U}_\phi/r\sin\theta + \Omega_0$ from a convection simulation in a spherical wedge (Warnecke et al. 2018). Nine panels on the right: Independent components of β and δ from the same simulation.

are likely ubiquitous (e.g. Rempel et al. 2023). A succession of methods to generalize the quasi-kinematic test field method have been developed to accommodate this (Rheinhardt and Brandenburg 2010; Käpylä et al. 2020a, 2022). These methods have gradually included more of the terms in the Navier-Stokes equation that are now needed for the calculation of the test field $\bar{\mathcal{E}}^{(p)}$. Here only the most general case, the compressible test field method, is discussed (Käpylä et al. 2022). In this method the full set of MHD equations are solved for the main run (mr) where a self-consistent small-scale and large-scale dynamos can operate, a zero run (0) where the mean magnetic field is zero, and for each of the imposed test fields (B). For example, for isotropically forced homogeneous turbulence this corresponds to evolving \mathbf{u} , \mathbf{b} , and $h = c_s^2 \ln \rho$ for each of these cases. A full mean-field representation of this system requires

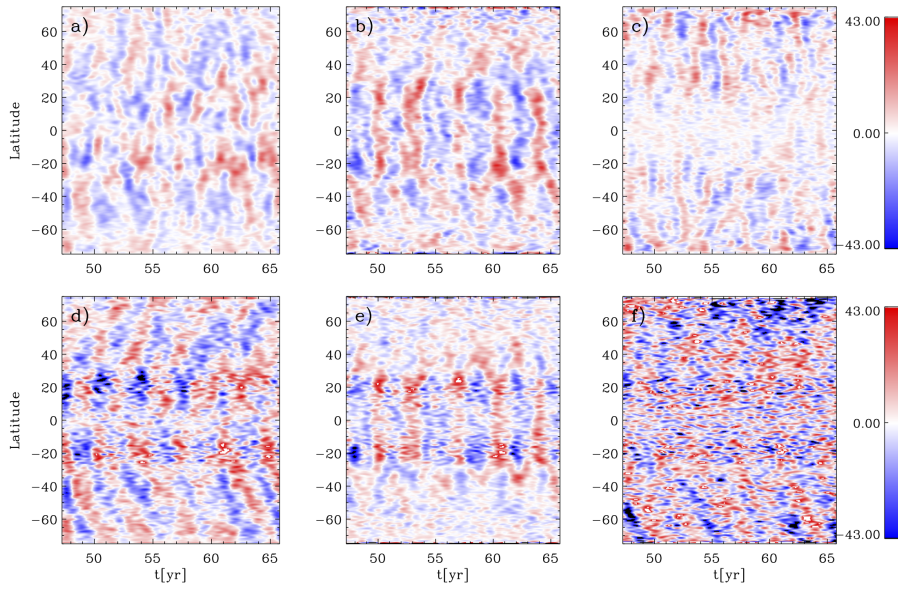


Fig. 16 Top row: The actual radial, latitudinal and longitudinal components of the $\bar{\mathcal{E}}$ from the simulation presented in [Viviani et al. \(2019\)](#). Bottom row: the same quantities but reconstructed using Eq. (21) with the measured turbulent transport coefficients and mean magnetic field $\bar{\mathbf{B}}$ in the same simulation.

that the mean electromotive force $\bar{\mathcal{E}}^{(B)}$, the ponderomotive force

$$\mathcal{F}^{(B)} = \overline{(\mathbf{j} \times \mathbf{b}) / \rho_{\text{ref}} - \mathbf{u} \cdot \nabla \mathbf{u} + 2\nu \mathbf{s} \cdot \nabla \mathbf{h}}^{(B)}, \quad (59)$$

and the mean mass source

$$\mathcal{Q}^{(B)} = -\overline{(\mathbf{u} \cdot \nabla \mathbf{h})}^{(B)}, \quad (60)$$

where ρ_{ref} is a constant reference density and \mathbf{s} is the fluctuating rate-of-strain tensor, are computed. However, all of these correlations contain terms that are ultimately non-linear in $\bar{\mathbf{B}}$. Furthermore, there is no direct connection between the main run and the test field equations. In [Käpylä et al. \(2022\)](#) this is circumvented by assuming that $\mathbf{b}^{(\text{mr})} \approx \mathbf{b} = \mathbf{b}^{(0)} + \mathbf{b}^{(B)}$. This is not fully rigorous but it is assumed to be sufficiently accurate if the actual mean field in the main run and the test fields are similar. This leads to freedom in choosing which combinations of the fluctuating quantities from the main run, zero run, and test field runs are used to construct the turbulent correlations that are non-linear, such as $(\mathbf{u} \times \mathbf{b})^{(B)}$, in the mean field. In the case studied in [Käpylä et al. \(2022\)](#) this leads to a total of 32 possible flavors of the compressible test field method, four of which (see also [Rheinhardt and Brandenburg 2010](#)) were studied in more detail.

So far the compressible test field method has been applied to study the shear dynamo problem along with simpler configurations involving the Roberts

flow. For the shear dynamo the results from compressible test field method are in agreement with those of the quasi-kinematic test field method in that no evidence of a coherent shear-current or Rädler effects were found, even in a regime where a strong small-scale dynamo was present. Currently the usefulness of the compressible test field method is limited to relatively low Re_M because the linear test field solutions are prone to a small-scale dynamo-like instability. This issue is alleviated to some degree by resetting similarly as in the case of the quasi-kinematic test field method (e.g. [Hubbard et al. 2009](#)).

7 Comparisons of 3D dynamo simulations with mean-field theory and models

7.1 Forced turbulence simulations with and without shear (Class 1)

7.1.1 Helically forced turbulence without shear (α^2 dynamo)

Forced turbulence simulations in periodic cubes offer the simplest point of comparison between DNS and mean-field models. The helically forced case with no shear constitutes the minimal ingredients of an α^2 dynamo in the parlance of mean-field theory. The dispersion relation for such a dynamo in the kinematic regime is given by (e.g. [Moffatt 1978](#); [Krause and Rädler 1980](#))

$$\lambda = |\alpha|k - \eta_T k^2, \quad (61)$$

where k is the wavenumber of the magnetic field and $\eta_T = \eta_t + \eta$. The maximum growth rate is obtained at $k_{\max} = |\alpha|/(2\eta_T)$, where k_{\max} is the wavenumber corresponding to the fastest growing mode. Assuming fully helical turbulence forced at wavenumber k_f , such that $\alpha = \frac{1}{3}u_{\text{rms}}$ and $\eta_t = \frac{1}{3}u_{\text{rms}}k_f^{-1}$, the wavenumber of the fastest growing for sufficiently large Re_M with $\eta_t \gg \eta$ is $k_{\max} = \frac{1}{2}k_f$ ([Brandenburg et al. 2002](#)). In the general case the flow is not fully helical and the molecular diffusivity η cannot be neglected. Then, $\alpha = \frac{1}{3}\epsilon_f u_{\text{rms}}$, where $\epsilon_f = \overline{\boldsymbol{\omega} \cdot \mathbf{u}}/(u_{\text{rms}}\omega_{\text{rms}})$ is the fractional helicity, and the expression for the wavenumber of the fastest growing mode is

$$k_{\max} = \frac{\epsilon_f k_f}{2(1 + \text{Re}_M^{-1})}. \quad (62)$$

This expression was obtained by [Brandenburg et al. \(2002\)](#) who also found from simulations that k_{\max} increases for increasing Re_M in accordance with Eq. (62).

The wavenumber of the fastest growing mode corresponds to a maximum growth rate is $\lambda_{\max} = \alpha^2/(4\eta_T)$, suggesting that the growth rate of the magnetic field is quadratic in the kinetic helicity due to $\alpha \propto \overline{\boldsymbol{\omega} \cdot \mathbf{u}}$. Simulations provide support for such scaling; see Fig. 8 of [Subramanian and Brandenburg \(2014\)](#). However, in the same study λ_{\max} was found to be about twice larger than the actual growth rate λ in the 3D simulation. The reason for this discrepancy is currently unclear but it is known that an additional correction to

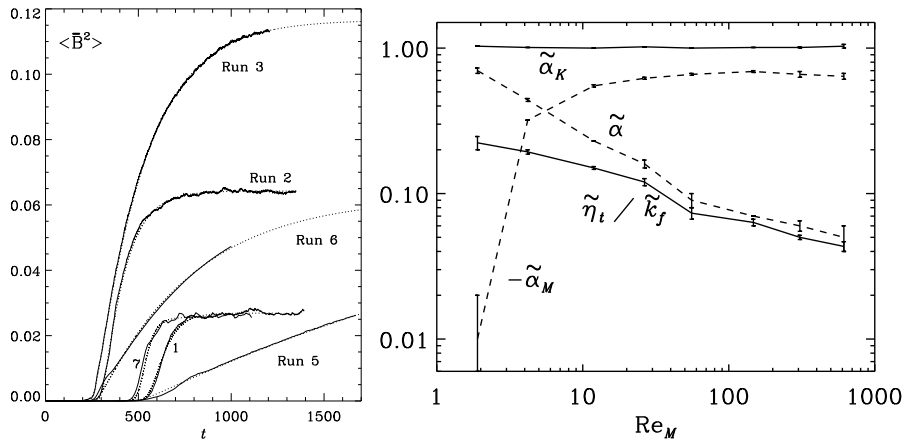


Fig. 17 Left: Average energy of the mean magnetic field as a function of time (solid lines) along with predictions based on magnetic helicity conservation (dotted lines). Adapted from [Brandenburg \(2001\)](#). Right: quenching of α and η_t from dynamo simulations driven by helical turbulence ([Brandenburg et al. 2008b](#))

the dispersion relation arises due to a kinetic helicity dependence of turbulent diffusivity ([Nicklaus and Stix 1988](#); [Mizerski 2023](#); [Rogachevskii et al. 2025](#)) which was reported from simulations by [Brandenburg et al. \(2017b, 2025\)](#). Furthermore, the dispersion relation (61) is also modified if a memory effect, or temporal non-locality, is present such that $\alpha = \alpha(\lambda)$ and $\eta_t = \eta_t(\lambda)$ ([Hubbard and Brandenburg 2009](#)). While this effect was found to be important for the Roberts flow in [Hubbard and Brandenburg \(2009\)](#), it has yet to be demonstrated for turbulence.

The non-linear state of a fully periodic helical dynamo is of mean-field theoretical interest because it can be used to study the effects of magnetic helicity conservation. In this context, [Brandenburg \(2001\)](#) studied the non-linear evolution of large-scale dynamos using helically forced turbulence without shear. Such simulations produce large-scale fields are of Beltrami type for which $\bar{\mathbf{J}} = a\bar{\mathbf{B}}$. Furthermore, the saturation of the mean field in these simulations was found to occur on a resistive timescale in accordance with arguments arising from mean-field theory and magnetic helicity conservation; see the left panel of [Fig. 17](#). Furthermore, quenching of α and η_t as functions of Re_M was studied using the quasi-kinematic test field method in [Brandenburg et al. \(2008b\)](#). The magnetic diffusivity was shown to be decreased by a factor of roughly 5 in the range $Re_M = 2 \dots 600$, while the total α effect defined via [Eq. \(29\)](#) was reduced by a factor of 14; see right panel of [Fig. 17](#). The reduction of α was attributed to be almost solely due to the increasing α_M with Re_M .

7.1.2 Helically forced turbulence with shear ($\alpha\Omega$ dynamo)

Another example of a Class 1 dynamo is the α -shear dynamo, which is driven by imposed shear flow and helical turbulence (e.g. Käpylä and Brandenburg 2009; Hubbard et al. 2011; Tobias and Cattaneo 2013; Cattaneo and Tobias 2014; Pongkitiwanchakul et al. 2016). Such a setup corresponds to classical $\alpha\Omega$ or $\alpha^2\Omega$ dynamos depending on the strength of the shear. In shearing box simulations with uniform imposed shear $\bar{U} = (0, xS, 0)$ this is denoted by the shear number $\text{Sh} = S/(u_{\text{rms}}k_f)$. Such dynamos produce cyclic magnetic fields where the propagation direction is consistent with the Parker-Yoshimura rule (Brandenburg and Käpylä 2007). Furthermore, assuming a stationary saturated state of the dynamo, the cycle frequency ω_{cyc} is given by

$$\omega_{\text{cyc}} = \eta_{\Gamma} k_m^2, \quad (63)$$

where k_m is the wavenumber of the large-scale mean magnetic field. Assuming Eq. (63) to hold also in the nonlinear regime where $\eta_{\Gamma} = \eta_{\Gamma}(\bar{B})$, the relation $\omega_{\text{cyc}}(\bar{B})$ can be interpreted as a proxy of the quenching of the magnetic diffusivity. This was done in Käpylä and Brandenburg (2009); see Fig. 18. The results suggest that quenching becomes significant for $\bar{B}/B_{\text{eq}} \gtrsim 1$ and that the onset of quenching depends on the strength of the shear measured by Sh .

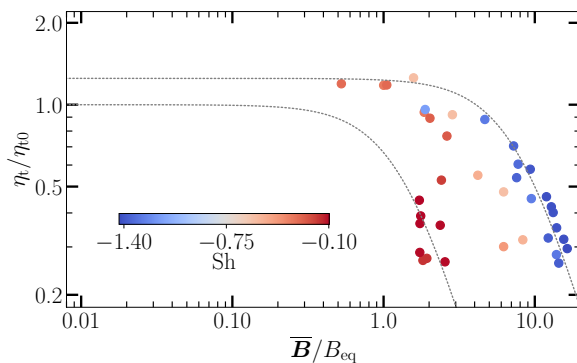


Fig. 18 Normalized turbulent magnetic diffusivity $\tilde{\eta}_t = \eta_t/\eta_{t0}$, where $\eta_{t0} = u_{\text{rms}}/(3k_f)$, where η_t is computed from Eq. (63) as a function of the mean magnetic field in units of B_{eq} . The curves show quenching functions proportional to $\tilde{\eta}_t/[1 + p_{\eta_t}(\bar{B}/B_{\text{eq}})^2]$ with $\tilde{\eta}_t = 1.25$ (1.0) and $p_{\eta_t} = 0.015$ (0.5) for the upper (lower) curve. Based on data from Fig. 10 of Käpylä and Brandenburg (2009).

An important question to consider is the influence of a concurrent small-scale dynamo on the large-scale field generation. This was studied by Karak and Brandenburg (2016) in a series of simulations where the relative importance of the small-scale dynamo was varied. They found that when the small-scale dynamo was absent, the small-scale magnetic fields were positively correlated with the cyclic large-scale field. When the small-scale dynamo was also

excited, two scenarios appeared. First, if the large-scale field was weaker than the equipartition value, the small-scale fields were almost independent of the large-scale field. Second, if the large-scale field was stronger than equipartition, the small-scale field was anti-correlated with the cycle, interpreted as suppression of the SSD. In the Sun the small-scale magnetic fields are independent of – or weakly anticorrelated with – the cycle, suggesting that both a small-scale and a large-scale dynamo are operating. Furthermore, [Karak and Brandenburg \(2016\)](#) found decent agreement between their simulation results and analytic theory of tangling of small-scale fields in the absence of a small-scale dynamo ([Rogachevskii and Kleeorin 2007](#)).

[Hubbard et al. \(2011\)](#) studied helically forced dynamos with shear in a parameter regime where both α^2 and $\alpha^2\Omega$ dynamos were possible. While an oscillatory $\alpha^2\Omega$ mode was found to have the fastest growth rate, it was often overwhelmed by a non-oscillatory α^2 mode in the nonlinear regime. Sometimes such transition was found to occur long after the dynamo had reached a saturated state. This was mentioned as a challenge for mean-field models and calls for methods to extract turbulent transport coefficients in the nonlinear regime. [Hubbard et al. \(2011\)](#) connected these transitions to the Sun and conjectured that a transition between $\alpha^2\Omega$ and α^2 modes could explain, for example, the Maunder minimum. However, [Hubbard et al. \(2011\)](#) found only a unidirectional transition $\alpha^2\Omega \rightarrow \alpha^2$ such that the original oscillatory mode never recovered.

7.1.3 Nonhelically forced turbulence with shear

While the theoretical interpretation of helically forced dynamos with shear is relatively straightforward, the situation is much less obvious when the turbulence is non-helical. Mean-field effects leading to such shear dynamo were derived theoretically much before a numerical demonstration. These include the $\overline{\boldsymbol{\Omega}} \times \overline{\boldsymbol{J}}$ or Rädler effect ([Rädler 1969](#)) and the shear-current effect ([Rogachevskii and Kleeorin 2003, 2004](#)), which rely on the off-diagonal component η_{yx} of the diffusivity tensor for driving the dynamo. More specifically, a necessary condition is that η_{yx} and S have opposite signs (e.g. [Brandenburg and Subramanian 2005a](#)). Shear dynamo action was demonstrated numerically by [Yousef et al. \(2008b,a\)](#), and [Brandenburg et al. \(2008a\)](#), showing that the growth rate of the dynamo is proportional to the shear rate S for weak shear. The large-scale magnetic fields produced by such dynamos tend to be quasi-steady or show random polarity reversals (e.g. [Brandenburg et al. 2008a](#); [Teed and Proctor 2017](#)); see the left panel of [Fig. 19](#).

However, test field simulations of [Brandenburg et al. \(2008a\)](#) yielded a non-zero η_{yx} , but the sign was not conducive to dynamo action. Subsequent studies have either found consistency with zero or the wrong sign for η_{yx} (e.g. [Mitra et al. 2009a](#)). More recently, in a series of papers [Squire & Bhattacharjee](#) introduced a magnetic shear-current effect that is analogous to its kinematic counterpart, but it is driven by small-scale magnetism ([Squire and Bhattacharjee 2015a, 2016](#)). However, results from nonlinear test field method have not

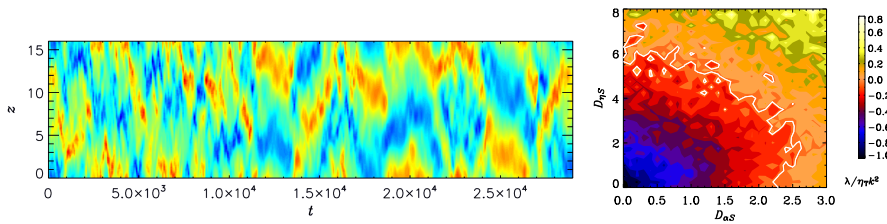


Fig. 19 Left: Horizontally averaged stream-wise magnetic field B_y from a simulation of nonhelical shear dynamo. Adapted from [Teed and Proctor \(2017\)](#). Right: Dynamo growth rate from mean-field models as functions of the strengths of the incoherent α and shear-current effects quantified by the dynamo numbers $D_{\alpha S}$ and $D_{\eta S}$. Adapted from [Brandenburg et al. \(2008a\)](#).

confirmed a sign change between the kinematic and small-scale dynamo cases ([Käpylä et al. 2020a, 2022](#)). Therefore the existence of coherent shear-current effect – in its kinematic and magnetic incarnations – remains inconclusive. The most likely cause for the nonhelical shear dynamo is due to incoherent dynamo effects such as the cumulative effects of fluctuations of the on average zero α effect or kinetic helicity with the shear flow (e.g. [Brandenburg et al. 2008a; Käpylä et al. 2022](#)). This is demonstrated in the right panel of Fig. 19 where the dynamo growth rate is shown as a function of dynamo numbers $D_{\alpha S} = \alpha_{\text{rms}}|S|/(\eta_T^2 k^3)$ and $D_{\eta S} = \eta_{xy}^{\text{rms}}|S|/(\eta_T^2 k^2)$ describing the incoherent α and shear-current effects. The simulations of [Brandenburg et al. \(2008a\)](#) typically had $D_{\alpha S} \approx D_{\eta S} \approx 4$ indicating that the incoherent α effect was the driver of the dynamo whereas even the incoherent shear-current effect was subcritical.

7.2 Convective dynamos in local boxes (Class 2)

A step forward from forced turbulence simulations is to consider thermally driven convection under the influence of rotation and/or shear in Cartesian geometry; see the left panel of Fig. 20. Inhomogeneous convection with rotation and/or shear leads to kinetic helicity production and an α effect (e.g. [Rädler and Stepanov 2006](#)), and the interaction between shear and turbulent flows enables the shear dynamo via the Rädler and incoherent dynamo effects. Furthermore, the magnetorotational instability ([Velikhov 1959; Balbus and Hawley 1991](#)) can also operate given suitable signs of shear and rotation (e.g. [Käpylä et al. 2013a](#)). The mean fields in this type of simulations are one- (e.g. [Käpylä et al. 2008](#)) or two-dimensional (e.g. [Hughes and Proctor 2009; Käpylä et al. 2010a](#)) depending, e.g., on the spatial structure of the imposed shear flow.

The first successful large-scale dynamos were obtained from local convection simulations where a large-scale horizontal shear was additionally imposed ([Käpylä et al. 2008; Hughes and Proctor 2009](#)). These setups include all the ingredients of classical $\alpha\Omega$ dynamo similarly to the α -shear dynamos discussed

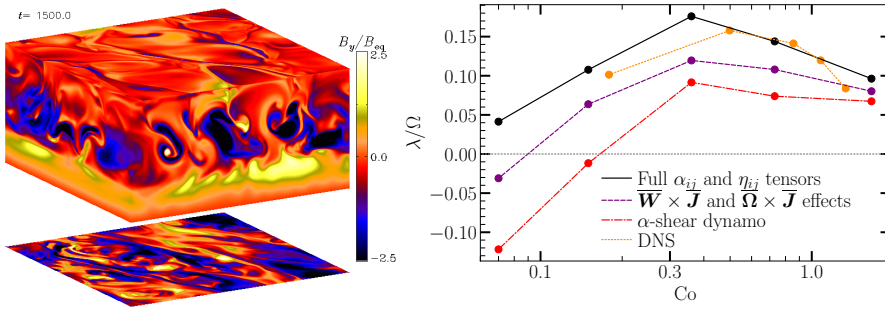


Fig. 20 Left: Stream-wise magnetic field component B_y at the periphery of the simulation domain in a convection simulation with linear shear and rotation from Käpylä et al. (2008). Right: Growth rate λ of the magnetic field, normalized by the rotation rate Ω , from Cartesian DNS (orange dotted line), and one-dimensional mean-field models using the full α_{ij} and η_{ij} tensors (black solid), only the shear-current and Rädler effects (purple dashed), and a pure α -shear dynamo (red dash-dotted). The turbulent transport coefficients were acquired from corresponding DNS using the test field method (Käpylä et al. 2009a).

in Sect. 7.1.2. For weak shear the growth rate λ of the large-scale magnetic field was found to be roughly proportional to the shear rate S in both studies, similarly to the nonhelical shear dynamo simulations of Yousef et al. (2008b). In comparison, in a classical $\alpha\Omega$ dynamo, albeit with spatially uniform α and η_t , the growth rate scales as $S^{1/2}$ (e.g. Brandenburg and Subramanian 2005a). Another difference to classical $\alpha\Omega$ dynamos is that the large-scale fields in this type of simulations are almost always non-oscillatory (see, however Käpylä et al. 2013a). In Käpylä et al. (2009a) the turbulent transport coefficients $\alpha_{ij}(z)$ and $\eta_{ij}(z)$ were computed using the quasi-kinematic test field method for a set of simulations similar to those in Käpylä et al. (2008). Kinematic growth rates realized in the DNS were compared to one-dimensional mean-field models where the test field coefficients from corresponding DNS were used. The results are shown in the right panel of Fig. 20. The growth rates from DNS match well with the mean-field models when all of the components of α_{ij} and η_{ij} were retained. These results also suggest that the Rädler/shear-current effects contribute to the dynamo but that it is subdominant in comparison to the contribution from the α effect. These simulations were made with modest Re_M of around 35, such that no small-scale dynamo was present. Important caveats include the omission of incoherent dynamo effects (e.g. Brandenburg et al. 2008a) and the effects of nonlocality (Käpylä et al. 2009a).

Simulations of rigidly rotating convection without shear flows, which have all the hallmarks of a classical α^2 dynamo, routinely produced dynamos but most often no appreciable large-scale magnetic fields were reported (e.g. Jones and Roberts 2000; Cattaneo and Hughes 2006; Hughes and Cattaneo 2008; Tobias et al. 2008; Käpylä et al. 2008). This happened despite the presence of an α effect in such simulations (e.g. Brandenburg et al. 1990b; Ossendrijver et al. 2001, 2002; Käpylä et al. 2006a). The test field calculations of Käpylä et al. (2009a) showed that the α effect increases and turbulent diffusivity η_t

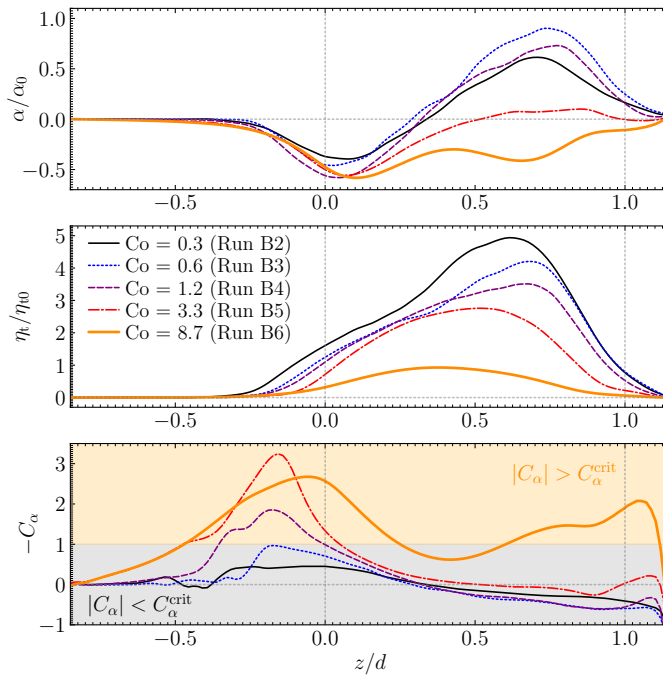


Fig. 21 Top and middle panels: α and η_t , respectively, as functions of height from a set of Cartesian convection simulations from Käpylä et al. (2009b). The Coriolis number is indicated by the legend in the middle panel. Bottom: Dynamo number C_α corresponding to the simulations on the upper panels. Gray (orange) shading indicates $|C_\alpha| < C_\alpha^{\text{crit}}$ ($> C_\alpha^{\text{crit}}$). The dotted vertical lines indicate the extent of the initially convectively unstable layer.

decreases as a function of rotation. For a one-dimensional z -dependent α^2 dynamo, the dynamo number $C_\alpha(z) = \alpha(z)/[\eta_t(z)k_1]$, where $k_1 = 2\pi/L_z$ and L_z is the vertical size of the system, has to exceed the critical value $C_\alpha^{\text{crit}} = 1$ for dynamo action (e.g. Brandenburg and Subramanian 2005a). This condition was fulfilled for sufficiently large Co in Käpylä et al. (2009b); see Fig. 21⁴. This was confirmed by a corresponding dynamo simulations. These results suggest that mean-field theory has predictive power at least in a limited sense considered here. However, in Käpylä et al. (2009b) large-scale dynamo action was obtained only in cases where large-scale hydrodynamic vortices were excited in the kinematic regime of the simulations. The large-scale vorticity generation occurs when Co and Re exceed certain threshold values; see e.g. Chan (2007), Käpylä et al. (2011), and Guervilly et al. (2014). The origin of the vortices is often attributed to two-dimensionalization of turbulence but the observed threshold behavior with respect to Reynolds and Coriolis numbers could also be signs of an instability. Such large-scale vortices aid the dynamo

⁴ In Käpylä et al. (2009b), $c_\alpha = \alpha(z)/(\eta_t(z)k_f)$, where $k_f = 2\pi/d$, where d is the depth of the initially convectively unstable layer, was used to characterize the dynamo. With $d = L_z/2$ and $k_f = 2k_1$, the critical value in terms of c_α corresponds to $|c_\alpha^{\text{crit}}| > 0.5$.

in the kinematic regime, whereas once the magnetic fields become dynamically important, the vortices are quenched (e.g. Käpylä et al. 2013a; Masada and Sano 2014; Guervilly et al. 2015, 2017; Bushby et al. 2018). The non-linear state of such dynamos is cyclic; see an example in Fig. 5. There is considerable uncertainty as to how this dynamo is generated, although an oscillatory α^2 dynamo is a possible candidate (e.g. Baryshnikova and Shukurov 1987; Rädler and Bräuer 1987).

Masada and Sano (2014) made a comparisons of DNS and mean-field models of this type of systems and found that the mean-field model reproduced the cyclic behavior of the mean field of the DNS. Magnetic α effect was invoked as the non-linearity whereas turbulent pumping and diffusivity were assumed to be catastrophically quenched. However, the mean-field models used isotropic FOSA expressions for the kinematic α and η_t . Nevertheless, the correspondence of the DNS and mean-field models is remarkably good; see Fig. 22. A similar analysis was made of simulations with significantly larger density stratification in Masada and Sano (2022), where similar cyclic solutions were found in an earlier study (Masada and Sano 2016).

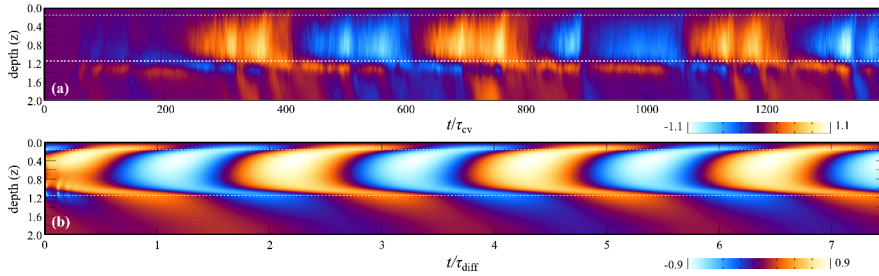


Fig. 22 Time-depth diagram of the horizontally averaged horizontal magnetic field component $\overline{B}_x(z, t)$ from a DNS (upper panel) and from a corresponding mean-field model (lower panel). Adapted from Masada and Sano (2014).

7.3 Global simulations of convection in spherical shells (Class 3)

7.3.1 Interpretation in terms of $\alpha\Omega$ dynamos

Early successful dynamos in global geometry by Gilman (1983) and Glatzmaier (1985) produced cyclic large-scale magnetic fields that migrated poleward. Given that in these simulations $\partial\overline{\Omega}/\partial r > 0$, and $\overline{\boldsymbol{\omega}} \cdot \overline{\boldsymbol{u}} < 0$ in the northern hemisphere, poleward propagation of the dynamo wave is consistent with the Parker-Yoshimura rule (Parker 1955a; Yoshimura 1975). Similar poleward propagating dynamos have been found in numerous other studies in Boussinesq (e.g. Busse and Simitev 2006), anelastic (e.g. Brown et al. 2011; Gastine et al. 2012), as well as fully compressible simulations (e.g. Käpylä et al. 2010c;

Warnecke et al. 2014; Mabuchi et al. 2015), where they have often been interpreted in terms of mean-field $\alpha\Omega$ dynamos. In Warnecke (2018) the cycle frequency was shown to correspond to that obtained from dispersion relation of the $\alpha\Omega$ dynamo

$$\omega_{\text{cyc}} = \left(\frac{\alpha k_\theta}{2} r \cos \theta \frac{\partial \bar{\Omega}}{\partial r} \right)^{1/2}, \quad (64)$$

where k_θ is a latitudinal wavenumber and α corresponds to the isotropic FOSA expression (25). In reality, the periods of dynamo cycles are independent of r and θ and therefore typical values of α and $\partial \bar{\Omega} / \partial r$ from the dynamo region are used in Eq. (64). This relation was found to be consistent with a variety of simulations with different density stratifications and shell thicknesses in Gastine et al. (2012); see Fig. 23. Warnecke (2018) studied the dependence of simulated cycles on rotation. The simulation results were shown to be consistent with Eq. (64) in the cases where clear cycles were present by using simple estimates of α and η_t from Eq. (29). Furthermore, assuming a quasi-stationary saturated state of the dynamo, Eq. (63) can be used to estimate the turbulent diffusivity η_t , which leads to $\eta_t = \Delta r R^2 / (2P_{\text{cyc}})$, where Δr is the depth of the convection zone and $P_{\text{cyc}} = 2\pi / \omega_{\text{cyc}}$ (Roberts and Stix 1972). This was shown to coincide with FOSA estimate, Eq. (25), and the cycle period was interpreted to be controlled by the turbulent diffusivity.

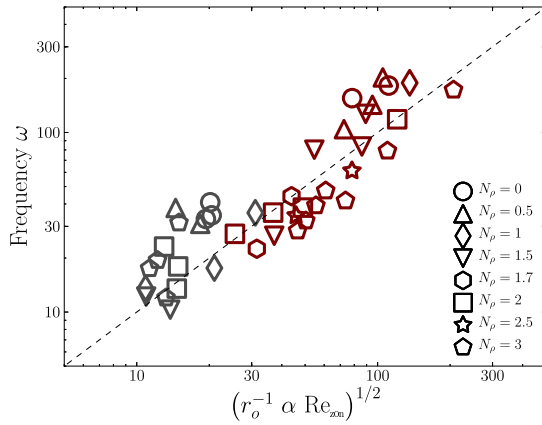


Fig. 23 Frequency of the dynamo wave versus a proxy from mean-field $\alpha\Omega$ theory. In comparison to Eq. (64), $r_o \propto k_y^{-1}$ is the outer radius of the shell and $\text{Re}_{\text{zon}} \propto \partial \bar{\Omega} / \partial r$ is the Reynolds number related to the mean zonal flow. The symbols refer to different density stratifications whereas the red (gray) symbols denote thick (thin) shells. Adapted from Gastine et al. (2012).

As mentioned in Sect. 3 since the pioneering efforts of the 1980s, there have been several simulations that produce solar-like equatorward migration (e.g.

Käpylä et al. 2012b; Augustson et al. 2015; Duarte et al. 2016; Strugarek et al. 2017, 2018; Warnecke 2018; Matilsky and Toomre 2020; Käpylä 2022; Brun et al. 2022). The results of many of these simulations can also be understood in terms of $\alpha\Omega$ dynamos, although with a twist that makes them incompatible with the solar dynamo. This was shown in Warnecke et al. (2014) who studied the cause of equatorward migration of dynamo waves in simulations similar to those presented in Käpylä et al. (2012b) and Käpylä et al. (2013b), again employing the simple FOSA expressions for α and η_t . The main conclusion of this study was that the oscillatory solutions can be qualitatively explained by the Parker-Yoshimura rule and that equatorward migration is due to a mid-latitude minimum in the angular velocity, that leads to a localized region where $\partial\bar{\Omega}/\partial r < 0$. An otherwise similar simulation but where the mid-latitude minimum in the angular velocity is absent shows poleward migration, again in accordance with the Parker-Yoshimura rule. A similar analysis was made in Warnecke et al. (2018), but using turbulent transport coefficients computed using the test field method. Qualitative agreement with the Parker-Yoshimura rule is found also in this case. A similar local mid-latitude minimum of $\bar{\Omega}$ is also present in the equatorward migrating solutions in Augustson et al. (2015).

Another mechanism to achieve equatorward migration was introduced in Duarte et al. (2016) where the sign of the kinetic helicity in much of the convective layer is reversed. This is commonly encountered in the overshoot region below the convection zone but in the simulations of Duarte et al. (2016) the reversal extended to much of the convection zone. It is unclear why exactly the helicity reversal occurs and how robust it is. Duarte et al. (2016) attribute it to a combination of low Pr, weak stratification in the layer with the reversal, distributed internal heat sources, and fixed flux boundary conditions. The helicity reversal leads to a negative α effect in the northern hemisphere and equatorward migration of dynamo waves with a solar-like differential rotation in accordance with the Parker-Yoshimura rule. However, the simulation setup in these models significantly differs from the Sun in that much deeper convective shells were studied and in some cases convection transported only a small fraction of the total flux. Further studies are needed to ascertain if this mechanism can operate in the Sun.

7.3.2 Magnetic driving of dynamos?

The analyses discussed in the previous section have assumed that the non-linear evolution of the large-scale dynamos can be represented in terms of the standard mean-field dynamo theory where the influence of the magnetic field is taken into account in the turbulent transport coefficients. However, it is also possible that MHD instabilities that require a finite-amplitude magnetic field to begin with can drive dynamo action.

For example, Guerrero et al. (2019) analyzed simulations with and without tachoclines employing the isotropic MTA expressions for α and η_t where the magnetic contribution to α was retained; see Eq. (29). Their results suggest that dynamos in their simulations are of $\alpha^2\Omega$ type with the α effect being

dominated by the magnetic contribution in the stably stratified regions below the convection zone. The source of the magnetic α effect in the layers below the convection zone was conjectured to be the buoyancy (Parker 1955b) or Taylor instability (Tayler 1973). The former has been shown to lead to an α effect (e.g. Chatterjee et al. 2011) while the latter has been demonstrated to lead to dynamos recently (e.g. Petitdemange et al. 2023). Furthermore, Strugarek et al. (2018) argued that the cycles in their simulations arise from the non-linear influence the magnetic field exerts on the differential rotation. However, more refined analyses, e.g., with nonlinear test field methods, are required to definitively establish the cause of dynamo action in these cases

7.3.3 Relative strength of dynamo effects as function of rotation

Magnetic activity in stars is a strong function of stellar rotation (e.g. Brun and Browning 2017). Numerical simulations of convection-driven dynamos have been used to study the rotation-activity relation by several groups (e.g. Viviani et al. 2018; Strugarek et al. 2018; Warnecke 2018; Warnecke and Käpylä 2020; Brun et al. 2022). From the dynamo-theoretical point of view the interest lies in the rotation dependence of various dynamo effects. This was studied by Warnecke and Käpylä (2020) who computed the turbulent transport coefficients using the spherical quasi-kinematic test field method from a similar set of dynamo simulations as in Warnecke (2018). The contributions of individual mean-fields effects were compared over a large range of Coriolis numbers. This entails comparing the volume averaged rms values of terms such as $\nabla \times (\boldsymbol{\alpha} \cdot \overline{\mathbf{B}})$, $\nabla \times (\boldsymbol{\beta} \cdot \nabla \times \overline{\mathbf{B}})$, etc., as functions of rotation.

Warnecke and Käpylä (2020) concluded that for slow rotation with strong anti-solar differential rotation the dominant effects besides the differential rotation are the α and Rädler effects. In the intermediate rotation regime where predominantly axisymmetric oscillatory dynamos exist, the α effect contributes both to poloidal and toroidal fields whereas the Ω effect is also important for the latter. Thus these dynamos can be classified to be of $\alpha^2\Omega$ type. In the rapid rotation regime differential rotation is quenched and the highly anisotropic α effect dominates, with these dynamos being classified as α^2 . Brun et al. (2022) concluded that most of their simulations are more likely $\alpha\Omega$ type based on an SVD analysis of the α_{ij} coefficients and the strength of differential rotation.

7.3.4 Mean-field modeling

The most rigorous test of the turbulent transport coefficients extracted from simulations is to use them in a mean-field model corresponding to the simulation where they were extracted from. Several levels of rigor how this is done can be distinguished. In the simplest cases only a fraction of the possible turbulent transport coefficients are extracted while the rest are either omitted, replaced by physically plausible parameterized alternatives, or used as free parameters. Similar arguments apply to the mean flows that go into the mean-field models.

Here the starting point is in cases with most free parameters followed by more constrained and rigorous comparisons.

However, a related complementary approach combines local simulations and global mean-field models (e.g. Käpylä et al. 2006a,b). In Käpylä et al. (2006a), α and γ were computed using the imposed field method from local simulations at different latitudes and Coriolis numbers. The latter was interpreted to correspond to different depths in the solar convection zone where Co ranges between 10^{-4} near the surface to about 10 at the base (e.g. Ossendrijver 2003). The data from 3D simulations was combined to meridional profiles of $\alpha_{ij}(r, \theta)$ and $\gamma_i(r, \theta)$ and used in mean-field dynamo models of the Sun (Käpylä et al. 2006b). Turbulent diffusivity was assumed to be isotropic and uniform with a value of the order of $10^8 \text{ m}^2 \text{ s}^{-1}$. Furthermore, the helioseismic rotation profile of the Sun and a plausible single-cell counterclockwise meridional flow were used. These models yield solar-like equatorward migration especially when equatorward pumping γ_θ and meridional flow were included. The near-surface shear layer also contributes to this but its effect is subdominant. This case is rather more illustrative than predictive but this approach shows some promise in probing turbulent phenomena locally.

One of the first efforts to explain global 3D dynamo simulation with mean-field models was presented by Dubé and Charbonneau (2013), who extracted the differential rotation, and α and η_t using FOSA estimates from a suite of global 3D simulations similar to that of Ghizaru et al. (2010). Meridional flows in the simulations were weak and therefore assumed to vanish in the mean-field models. Despite these simplifications, the mean-field models with these ingredients were able to recover the large-scale magnetic fields of the 3D simulations remarkably well in some cases. The next step in rigor came with the study of Racine et al. (2011), who extracted α from the simulation presented in Ghizaru et al. (2010) using the SVD method; see Sect. 6.2.2. Simard et al. (2013) used these coefficients to drive a kinematic $\alpha\Omega$, α^2 , and $\alpha^2\Omega$ mean-field dynamo models with the rotation profile from a hydrodynamic simulation and a generic single cell per hemisphere meridional flow circulation pattern. The magnetic diffusivity was assumed to be a scalar with uniform value in the convection zone. The best agreement between the simulation of Ghizaru et al. (2010) and the mean-field models was obtained when the full α tensor was included. Despite the differences to the original simulation, remarkably good correspondence between the simulation and the mean-field model was found; see Fig. 24.

In a related study, Simard et al. (2016) used the time series encompassing about 40 magnetic cycles from the simulation of Passos and Charbonneau (2014) to extract the a_{ij} and b_{ijk} coefficients using the SVD method. Mean-field modeling applying these coefficients was done by Beaudoin et al. (2016) with similar simplifications as in Simard et al. (2013). The main motive of Beaudoin et al. (2016) was to study the origin of seemingly two coexisting dynamo modes in the simulation of Passos and Charbonneau (2014) that resemble the quasi-biennial oscillations observed in the Sun. The mean-field models indeed suggest two spatially separated dynamos. However, here the

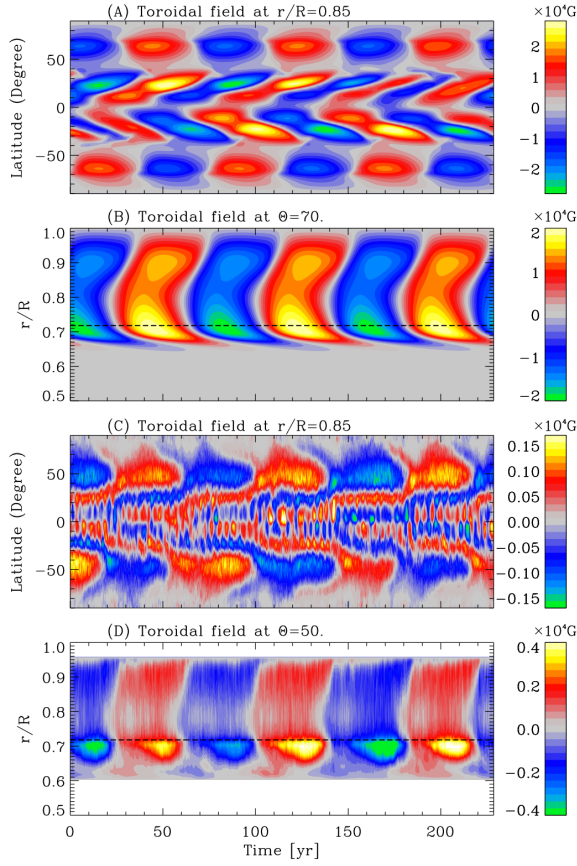


Fig. 24 Top panels: Mean toroidal field $\overline{B}_\phi(\theta, t)$ at the middle of the convection zone at $r/R = 0.85$ and $\overline{B}_\phi(r, t)$ at latitude $\theta = 70^\circ$ in an $\alpha^2\Omega$ mean-field model from Simard et al. (2013). Bottom panels: corresponding azimuthally averaged magnetic fields from the 3D convective dynamo simulation of Ghizaru et al. (2010).

correspondence between the simulation and the mean-field models was significantly worse than in Simard et al. (2013). Finally, Simard and Charbonneau (2020) followed a very similar approach but allowed for a back-reaction of the magnetic field on the differential rotation via the large-scale Lorentz force, and found that this leads to long-term modulation of cycles and Maunder minimum-like events.

The use of isotropic turbulent diffusivity and generic mean flow profiles in mean-field modeling is problematic because these are integral parts of the dynamo solutions of 3D simulations. The first studies that took into account also the tensorial turbulent diffusivity b_{ijk} were done with the test field method by Schirmer et al. (2005, 2007). They computed the turbulent transport coefficients from Boussinesq magnetoconvection and dynamo sim-

ulations in spherical shells. The actual and reconstructed EMFs were compared and mean-field dynamo models of the dynamo simulations were made. The correspondence between the DNS and mean-field models was found to be satisfactory in cases where convection and dynamos were close to marginal and time-independent. Clearer differences appeared more supercritical time-dependent quasi-stationary dynamos. [Schrinner et al. \(2007\)](#) noted that the ansatz Eq. (21) was not sufficient to reproduce the EMF and that either higher order terms in the expansion or the effects of non-locality are a possible causes for this. [Schrinner \(2011\)](#) found that the issues related to poor scale separation could be alleviated by simultaneous spatial and temporal averaging. Nevertheless, although the EMF and the resulting DNS and mean-field solutions differed in details, the large-scale dynamo mode was correctly captured in all of the cases (see also [Schrinner et al. 2011](#)).

Finally, [Warnecke et al. \(2021\)](#) did mean-field modeling using the turbulence transport coefficients measured with the test field method in [Warnecke et al. \(2018\)](#) from a density-stratified simulation of rotating convection in spherical wedge geometry. This simulation was targeted to model stellar dynamos and it includes higher density stratification and it is more supercritical than the earlier models of, for example, [Schrinner \(2011\)](#). In this simulation a solar-like cyclic large-scale magnetic field arises showing a dominant dynamo wave that propagates equatorward (poleward) at low (high) latitudes with a long cycle and a secondary poleward cycle near the equator with a much shorter cycle; see also [Käpylä et al. \(2012b, 2016a\)](#). Time-averaged turbulent transport coefficients and mean flows were extracted and post-processed to remove rapid spatial and temporal variations.

Linear mean-field models were used which is compatible with the fact that the coefficients were obtained from a simulation where the magnetic field is already saturated. The mean-field model reproduces large-scale features such as the cycle period and both the poleward and equatorward migration of the magnetic field in the direct simulation when the magnitude of α tensor was scaled up by a factor that varies between 1.40 and 1.525; see Fig. 25. By systematically turning on and off various effects, [Warnecke et al. \(2021\)](#) concluded that almost all of the turbulent transport coefficients are needed to reproduce the large-scale magnetic field solution, and that the meridional flow has a negligible effect of the solutions in these simulations. The authors further concluded that the dynamo in the simulation in question is of $\alpha^2\Omega$ type and that effects of non-locality are not needed to reproduce the evolution of the large-scale magnetic field. Remarkably also the short secondary cycle is reproduced with the mean-field models and conjectured to be of α^2 type. This can have significance for the interpretation of stellar cycles where co-existing long and short cycles have been pointed out by [Brandenburg et al. \(2017a\)](#) using data from the Mount Wilson Survey.

To conclude, detailed mean-field modeling consistently reproduces the large-scale dynamo mode of the DNS at least qualitatively. This is despite the fact that the reconstructed EMF is typically significantly less well reproduced (e.g. [Viviani et al. 2019](#)), such that the amplitudes of the reconstructed and actual

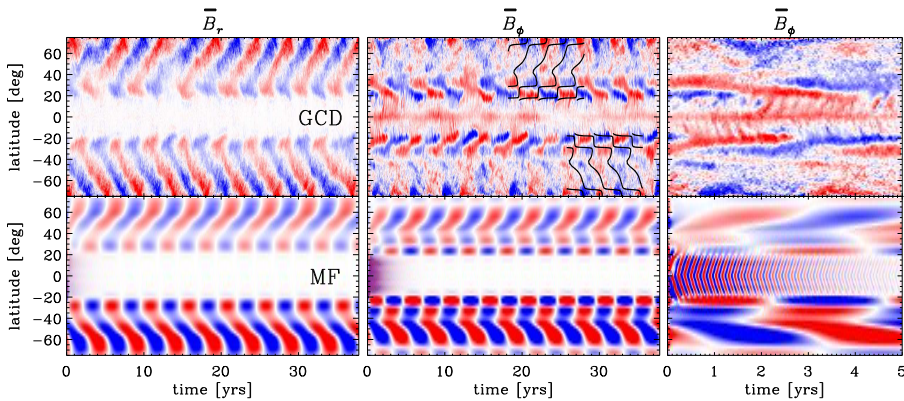


Fig. 25 Butterfly diagrams of radial (left column) and azimuthal (middle and right columns) magnetic fields from a global 3D simulation (top row), and a mean-field model using turbulent transport coefficients from the test field method (lower row). Adapted from [Warnecke et al. \(2021\)](#).

$\bar{\mathcal{E}}$ can differ by a factor of two. Furthermore, it is puzzling that the studies that use only some of the coefficients from simulations or which apply an incomplete ansatz for the electromotive force also tend to often capture the large-scale field evolution rather well (e.g. [Simard et al. 2013](#)). This can mean that the large-scale dynamo mode established in the simulations is quite insensitive to the choice of the turbulent transport coefficients. None of the studies discussed above consider non-locality or incoherent dynamo effects that have been suggested as drivers of dynamos in simpler settings (e.g. [Rheinhardt et al. 2014](#); [Brandenburg et al. 2008a](#)).

7.4 Magnetic helicity conservation and saturation of large-scale dynamos

The relation of magnetic helicity conservation to the non-linear saturation of large-scale dynamos is a topic that has been actively studied using numerical simulations. The simplest way of testing this is to change the magnetic boundary conditions of the system such that they either allow or prevent the flux of magnetic helicity across the boundary. Such experiments were conducted by [Käpylä et al. \(2010a\)](#), with local simulations of convection with shear and rotation. In such cases a shear-mediated magnetic helicity flux has been suggested to alleviate catastrophic quenching (e.g. [Vishniac and Cho 2001](#)). The results of [Käpylä et al. \(2010a\)](#) show that the dynamos in cases with open and closed boundaries show dramatically different behavior especially at high values of Re_M . The saturation amplitude of the total magnetic energy is independent of Re_M for open boundaries and proportional to Re_M^{-1} for closed (perfectly conducting) boundaries, the latter coinciding with catastrophic quenching. However, the mean magnetic field was proportional to $Re_M^{-0.25}$ ($Re_M^{-1.6}$) for open (closed) boundaries and for closed boundaries. Both of these trends are steeper

than that expected from efficient small-scale magnetic helicity fluxes out of the system and catastrophic quenching, respectively. The magnetic Reynolds numbers in this study were still very modest ($\text{Re}_M \approx 200$) compared to astrophysically relevant regimes and it is plausible that significantly higher Re_M are needed to reach a regime where asymptotic scaling manifests. A similar conclusion was drawn earlier from mean-field models applying the dynamical quenching formalism by [Brandenburg et al. \(2009\)](#) who found that an asymptotic regime is reached for Re_M of the order of 10^4 .

[Hubbard and Brandenburg \(2012\)](#) distinguished two types of catastrophic quenching which refer to low saturated field amplitude (Type I) and to slow saturation in resistive timescale (Type II). Although the magnetic Reynolds numbers were rather modest, no evidence of Type I quenching was found from helically forced α^2 dynamos. [Hubbard and Brandenburg \(2012\)](#) also concluded that if shear is present in the system, dynamo-generated large-scale fields are typically weakly helical, and that such fields can grow to be dynamically significant already in the kinematic phase of the dynamo without yet being affected by the magnetic helicity constraint. Furthermore, open boundaries help to avoid also Type II catastrophic quenching. This was explored in [Del Sordo et al. \(2013\)](#) with helically forced turbulence simulations where a wind out of the dynamo region was introduced. The top panel of Fig. 26 shows that the contribution by the wind to the negative divergence of the magnetic helicity flux ($-\nabla \cdot \bar{\mathcal{F}}_f$) becomes independent of Re_M around $\text{Re}_M = 170$ and whereas the resistive losses ($-2\eta \bar{\mathbf{j}} \cdot \bar{\mathbf{b}}$) decrease as $\text{Re}_M^{-2/3}$. Furthermore, the advective term reaches the magnitude of the resistive term around $\text{Re}_M = 10^3$ such that it alleviates otherwise catastrophic quenching.

As discussed in Sect. 4.3, catastrophic quenching can also be alleviated by internal magnetic helicity fluxes even if the domain is closed (e.g. [Mitra et al. 2010a](#)). High resolution 3D simulations by [Rincon \(2021\)](#) used a setup where the mean kinetic helicity had a sinusoidal variation with a sign change at an equator, similar to that expected in the Sun. [Rincon \(2021\)](#) found that the small-scale magnetic helicity flux overcomes the resistive contribution and compensates for the transfer term proportional to $\bar{\mathcal{E}} \cdot \bar{\mathbf{B}}$ at $\text{Re}_M \gtrsim 10^3$; see the top panel of Fig. 26. This can be attributed to a flux mediated by turbulent diffusion. These results corroborate the findings of [Brandenburg et al. \(2009\)](#) and suggest that non-diffusive internal magnetic helicity fluxes become effective only near the highest currently numerically achievable Re_M in excess of 10^3 . However, even in the cases with the highest Re_M the energy of the mean magnetic field is declining nearly proportional to Re_M^{-1} ; see the bottom panel of Fig. 26.

7.5 Active region formation via negative effective magnetic pressure

Sunspot formation in flux-transport solar dynamo models is usually attributed to flux tubes rising from deep layers of the convection zone or from the tachocline. On the other hand, if the magnetic field of the Sun is generated

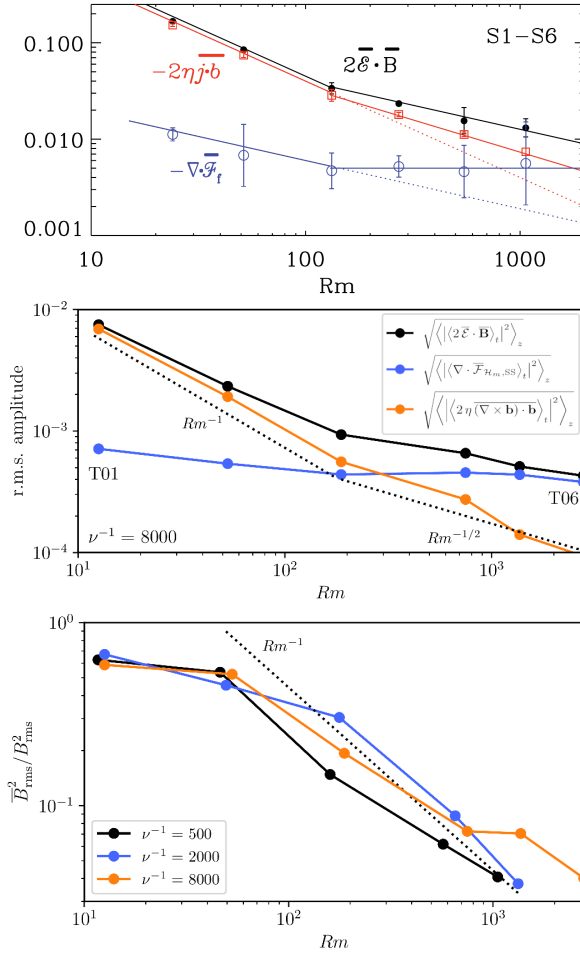


Fig. 26 Top: Terms in the conservation equation of small-scale magnetic helicity with $2\overline{\mathcal{E}} \cdot \overline{\mathbf{B}}$, $-2\overline{\eta \mathbf{j}} \cdot \overline{\mathbf{b}}$, and $-\nabla \cdot \overline{\mathcal{F}}_f$ corresponding to magnetic helicity production, resistive losses, and divergence of advective flux due to wind, respectively. Adapted from [Del Sordo et al. \(2013\)](#). Middle: Rms amplitudes of the terms in the small-scale current helicity evolution equation as functions of Rm ($= Re_M$) from a set of 3D simulations of a Galloway-Proctor-like helical flow with sinusoidal variation of kinetic helicity from [Rincon \(2021\)](#). Bottom: Mean magnetic field energy as a function of Re_M from an extended set of runs from the same study.

within the convection zone by a distributed dynamo, and consists of relatively diffuse fields, another mechanism is needed to form magnetic field concentrations. Numerical studies of sunspots operate on much smaller scales than the global dynamo and do not typically consider the origin of the magnetic field but assume an initial condition that leads to spot formation (e.g. [Rempel et al. 2009a](#); [Rempel and Cheung 2014](#); [Fang and Fan 2015](#)). In the model of [Stein and Nordlund \(2012\)](#) a bipolar spot pair forms from flux advected through the

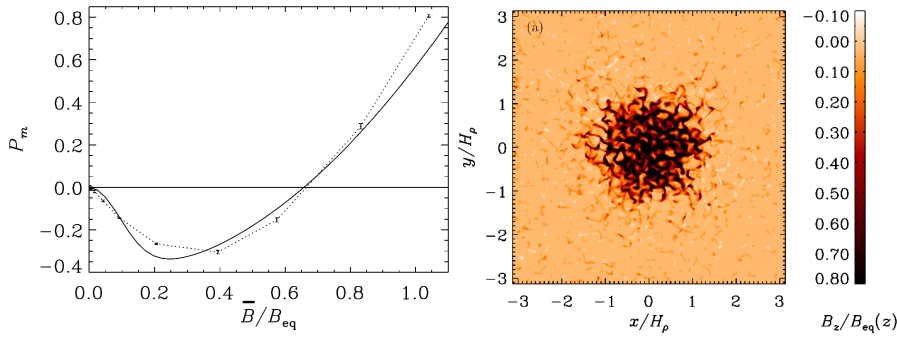


Fig. 27 Left: Effective magnetic pressure as a function of $\overline{B}/B_{\text{eq}}$ from 3D simulations of forced turbulence (dotted line) and an analytic profile (solid line). Adapted from [Brandenburg et al. \(2010\)](#). Right: Magnetic field concentration produced by NEMPI in density-stratified turbulence. Adapted from [Brandenburg et al. \(2013b\)](#).

lower boundary due to processing by convection, but again the spot-forming magnetic field was not a produced by a dynamo. A few 3D dynamo simulations have shown buoyantly rising flux tubes but these structures are on much larger scales than sunspots (e.g. [Guerrero and Käpylä 2011](#); [Nelson et al. 2013, 2014](#)).

A possible candidate arises when a large-scale magnetic field is superimposed on a turbulent background, leading to negative effective magnetic pressure (e.g. [Kleeorin et al. 1989, 1990](#); [Rogachevskii and Kleeorin 2007](#); [Brandenburg et al. 2010, 2012a](#)). This effect arises from a mean-field analysis of the momentum equation involving Reynolds and Maxwell stress tensors. This is measured by the effective magnetic pressure

$$\mathcal{P}_{\text{eff}} = \frac{1}{2}(1 - q_p)\beta^2, \quad (65)$$

where $\beta^2 = \overline{B}^2/B_{\text{eq}}^2$, and where q_p is the contribution of the mean field on the magnetic pressure. $\mathcal{P}_{\text{eff}} < 0$ is a necessary condition for the negative effective magnetic pressure instability (NEMPI), which causes initially uniform fields to form flux concentrations. This can be understood such that a large-scale (mean) magnetic field itself has a positive pressure but it suppresses turbulence and leads to decreased small-scale (turbulent) pressure. If the latter effect is larger, corresponding to $q_p > 1$, the *effective* magnetic pressure is negative leading to instability. Negative contribution to magnetic pressure and the related instability have been detected from simulations of forced turbulence given that the scale separation between the scale of the turbulence and the system size is sufficiently large (e.g. [Brandenburg et al. 2011](#); [Kemel et al. 2012](#); [Brandenburg et al. 2013b](#); [Kemel et al. 2013](#)); see Fig. 27. Furthermore, density stratification is another crucial element for NEMPI. Since the negative effective pressure effect vanishes for $|\overline{B}| \gtrsim 0.4B_{\text{eq}}$, the concentrations it produces are likely only progenitors of active regions and sunspots and that, e.g., the buoyancy instability ([Parker 1955b, 1975](#)) is still needed to produce

superequipartition fields as in sunspots. Furthermore, rotation has been shown to suppress NEMPI (e.g. [Losada et al. 2012, 2013, 2019](#)), such that it may only operate near the surface of the Sun, e.g., in the NSSL.

Convection simulations also show $\mathcal{P}_{\text{eff}} < 0$, but no instability has been detected as of yet ([Käpylä et al. 2012a, 2016b](#)). The most likely cause for this is that the scale separation in convection simulations is much poorer than in the forced turbulence models where this is an input to the model. This can also be related to the convective conundrum which is the issue that deep convection in the Sun appears to behave drastically differently than what current simulations and theoretical models predict (e.g. [Hanasoge et al. 2016; Hotta et al. 2023](#), and references therein). Nevertheless, it remains unclear whether NEMPI is possible in convection.

8 Outstanding issues

8.1 Self-consistent inclusion of large-scale flows

In practically all of the comparisons between 3D simulations and mean-field models the large-scale flows are assumed to be given, e.g., by the time-averaged flows from the original DNS. Furthermore, these are often taken from hydrodynamic runs although the dynamo coefficients are extracted from the magnetically saturated regimes. This is unsatisfactory from a rigorous theoretical point of view because the large-scale flows themselves are self-consistently generated in the DNS and affected by the dynamo-generated magnetic fields. Therefore the mean-field modeling should not only relate to magnetic field generation but also extended to the mean-field hydrodynamics (e.g. [Rüdiger 1989; Rüdiger and Hollerbach 2004](#)) that govern the large-scale flows. This complicates the mean-field models considerably because in addition to the EMF, further turbulent correlations including the Reynolds stress and turbulent heat flux need to be modeled. This is exacerbated by the fact that the Navier-Stokes equations are inherently non-linear. Some mean-field models take all of these effect into account either in parametric way (e.g. [Brandenburg et al. 1992; Rempel 2006](#)) or via detailed theoretical expressions (e.g. [Pipin 2017; Pipin and Kosovichev 2018](#)). While some efforts have been made to compare hydrodynamic 3D simulations with mean-field hydrodynamics (e.g. [Rieutord et al. 1994; Barekat et al. 2021](#)), approaches where both, the dynamo and the large-scale flow generation, would be interpreted in the mean-field framework have yet to appear. An additional complication is the convective conundrum which hinders current 3D simulations from reproducing the solar differential rotation, possibly hinting at fundamental issues in the theory of stellar convection (e.g. [Spruit 1997; Brandenburg 2016; Käpylä 2025](#)). Finally, the NSSL may play a role in shaping the solar dynamo (e.g. [Brandenburg 2005a](#)) as well as in sunspot formation, but current simulations struggle to incorporate it self-consistently due to high computational demands deriving from the large gap in spatial and temporal scales near the surface in comparison to the deep convection zone.

Thus, the current NSSL-resolving simulations cannot be run long enough for the large-scale dynamo to grow and saturate (e.g. [Hotta 2025](#)) and therefore the impact of the NSSL on the dynamo in these models is unclear.

8.2 Nonlinearity and non-locality

In a general theory of dynamos, non-linearity due to magnetic fields needs to be incorporated from the outset. This includes the back-reaction of the magnetic field on the large-scale flows such as differential rotation as well as the small-scale flows that ultimately enter $\overline{\mathcal{E}}$. This is challenging especially in cases where a small-scale dynamo is excited and changes the dynamics (e.g. [Käpylä et al. 2017a](#); [Hotta et al. 2022](#)). In the comparisons of 3D simulations and corresponding mean-field models, the large-scale flows are often assumed to be stationary. However, the large-scale flows are time-dependent especially if the large-scale dynamo is cyclic (e.g. [Käpylä et al. 2016a](#); [Strugarek et al. 2018](#)). Furthermore, the turbulent transport coefficients are typically computed from saturated regimes of dynamos with the often implicit assumption that the measured coefficients are already affected by the magnetic fields. However, such quenched coefficients are likely specific to the magnetic field configuration in the simulation from which they were extracted and their use in other settings is likely problematic.

Another aspect that is particularly important in dynamos driven by convection is non-locality. The turbulent transport coefficients from the test field method are always scale dependent, even in cases where the scale separation is assumed at least moderate from the outset (e.g. [Brandenburg et al. 2008c, 2012b](#); [Käpylä et al. 2020c](#)). For convection the situation is even worse with some coefficients changing sign as a function of the spatial scale (e.g. [Käpylä et al. 2009a](#)); see [Fig. 14](#). None of the current comparisons between 3D simulations and mean-field models take non-locality into account, yet mean-field models often capture the large-scale fields of simulations remarkably well (e.g. [Warnecke et al. 2021](#)). Even more remarkably, even if the turbulent transport coefficients in the mean-fields models are estimated using highly idealized approximations such as FOSA, the large-scale fields of the simulations are nevertheless often recovered (e.g. [Dubé and Charbonneau 2013](#); [Masada and Sano 2014](#)). This seems to suggest that the dominant dynamo modes excited in the simulations are largely insensitive to the details of the mean-field models. However, rigorous studies of this issue are currently missing.

9 Conclusions and outlook

Significant progress has been made in both the mean-field models and 3D simulations of astrophysical dynamos in the last two decades or so. Simulations corresponding to classical α^2 and $\alpha\Omega$ are the most well studied and their behavior, including aspects of non-linear evolution, are now quite well understood in the framework of mean-field dynamos including magnetic helicity

conservation. The situation is significantly less straightforward for spherical shell dynamos aiming to reproduce solar and stellar dynamos. Comparisons between such simulations and corresponding mean-field models are still challenging and often marred with issues in the computation of turbulent transport coefficients and issues related to non-linearity and non-locality. It is remarkable that the mean-field models reproduce the simulations results to the degree that they do despite the various shortcomings in the modeling approaches. However, in many cases the dynamos in simulations can be interpreted in terms of relatively simple classical $\alpha\Omega$ or $\alpha^2\Omega$ dynamos.

The main challenge in the interpretations of 3D simulations with mean-field theory and models continues to be the computation of turbulent transport coefficients. The numerical cost of computing all of the (possibly scale dependent) coefficients with, e.g., test field methods is high and increases further when non-linearity is taken into account. Furthermore, taking all of these effects into account increases the complexity of the resulting mean-field models immensely. The increasing complexity works against the main premise of mean-field modeling that the salient large-scale physics can be represented by a model with far fewer degrees of freedom than in the original simulation. While test field methods are likely to be developed further, another possibility is to use machine learning methods on numerical data that can perhaps extract the interdependencies in a more compact form in the future.

Acknowledgements I gratefully acknowledge the detailed comments from two referees that led to significant improvement of the review. I wish to thank Igor Rogachevskii and Nishant Singh for their valuable comments on the manuscript. This work was partly supported by the Deutsche Forschungsgemeinschaft Heisenberg programme (grant No. KA 4825/4-1) and by the Munich Institute for Astro-, Particle and BioPhysics (MIAPbP) which is funded by the DFG under Germany's Excellence Strategy – EXC-2094 – 390783311. I also thank the Isaac Newton Institute for Mathematical Sciences, Cambridge, for support and hospitality during the programme DYT2 where part of the work on this review was undertaken. This work was supported by EPSRC grant EP/R014604/1. This work was also partially supported by a grant from the Simons Foundation. Finally, I acknowledge the stimulating discussions with participants of the Nordita Scientific Program on “Stellar Convection: Modeling, Theory and Observations”, in August and September 2024 in Stockholm.

Conflict of interest

The author declares that he has no conflict of interest.

References

- Arlt R, Vaquero JM (2020) Historical sunspot records. *Living Rev Sol Phys* 17(1):1. <https://doi.org/10.1007/s41116-020-0023-y>
- Augustson K, Brun AS, Miesch M, Toomre J (2015) Grand Minima and Equatorward Propagation in a Cycling Stellar Convective Dynamo. *Astrophys J* 809:149. <https://doi.org/10.1088/0004-637X/809/2/149>. [arXiv:1410.6547](https://arxiv.org/abs/1410.6547) [astro-ph.SR]
- Balbus SA, Hawley JF (1991) A Powerful Local Shear Instability in Weakly Magnetized Disks. I. Linear Analysis. *Astrophys J* 376:214. <https://doi.org/10.1086/170270>

- Balsara D, Pouquet A (1999) The formation of large-scale structures in supersonic magneto-hydrodynamic flows. *Physics of Plasmas* 6(1):89–99. <https://doi.org/10.1063/1.873263>
- Barekat A, Käpylä MJ, Käpylä PJ, Gilson EP, Ji H (2021) Generation of mean flows in rotating anisotropic turbulence: The case of solar near-surface shear layer. *Astron Astrophys* 655:A79. <https://doi.org/10.1051/0004-6361/202040052>. [arXiv:2012.06343](https://arxiv.org/abs/2012.06343) [astro-ph.SR]
- Baryshnikova I, Shukurov A (1987) Oscillatory alpha-squared dynamo - Numerical investigation. *AN* 308:89–100
- Beaudoin P, Simard C, Cossette JF, Charbonneau P (2016) Double Dynamo Signatures in a Global MHD Simulation and Mean-field Dynamos. *Astrophys J* 826(2):138. <https://doi.org/10.3847/0004-637X/826/2/138>
- Bendre A, Gressel O, Elstner D (2015) Dynamo saturation in direct simulations of the multi-phase turbulent interstellar medium. *Astron Nachr* 336(10):991. <https://doi.org/10.1002/asna.201512211>. [arXiv:1510.04178](https://arxiv.org/abs/1510.04178) [astro-ph.GA]
- Berdyugina SV (2005) Starspots: A Key to the Stellar Dynamo. *Living Rev Sol Phys* 2:8. <https://doi.org/10.12942/lrsp-2005-8>
- Bhattacharjee A, Yuan Y (1995) Self-Consistency Constraints on the Dynamo Mechanism. *Astrophys J* 449:739. <https://doi.org/10.1086/176094>
- Bice CP, Toomre J (2023) Nature of Intense Magnetism and Differential Rotation in Convective Dynamos of M-dwarf Stars with Tachoclines. *Astrophys J* 947(1):36. <https://doi.org/10.3847/1538-4357/acac78>
- Biermann L (1950) Über den Ursprung der Magnetfelder auf Sternen und im interstellaren Raum (miteinem Anhang von A. Schlüter). *Z Naturforsch A* 5:65
- Birch AC, Schunker H, Braun DC, Cameron R, Gizon L, Löptien B, Rempel M (2016) A low upper limit on the subsurface rise speed of solar active regions. *Science Advances* 2:e1600557–e1600557. <https://doi.org/10.1126/sciadv.1600557>. [arXiv:1607.05250](https://arxiv.org/abs/1607.05250) [astro-ph.SR]
- Birch AC, Proxauf B, Duvall TL, Gizon L, Hanasoge S, Hindman BW, Sreenivasan KR (2024) Solar convective velocities: Updated helioseismic constraints. *Physics of Fluids* 36(11):117136. <https://doi.org/10.1063/5.0216728>
- Blackman EG, Field GB (2000) Constraints on the Magnitude of α in Dynamo Theory. *Astrophys J* 534(2):984–988. <https://doi.org/10.1086/308767>. [arXiv:astro-ph/9903384](https://arxiv.org/abs/astro-ph/9903384) [astro-ph]
- Blackman EG, Field GB (2002) New Dynamical Mean-Field Dynamo Theory and Closure Approach. *Physical Review Letters* 89(26):265007. <https://doi.org/10.1103/PhysRevLett.89.265007>. [astro-ph/0207435](https://arxiv.org/abs/astro-ph/0207435)
- Braginsky SI, Roberts PH (1995) Equations governing convection in earth's core and the geodynamo. *Geophys Astrophys Fluid Dyn* 79(1):1–97. <https://doi.org/10.1080/03091929508228992>
- Brandenburg A (2001) The Inverse Cascade and Nonlinear Alpha-Effect in Simulations of Isotropic Helical Hydromagnetic Turbulence. *Astrophys J* 550:824–840. <https://doi.org/10.1086/319783>. [arXiv:astro-ph/0006186](https://arxiv.org/abs/astro-ph/0006186)
- Brandenburg A (2005a) The case for a distributed solar dynamo shaped by near-surface shear. *Astrophys J* 625:539–547. <https://doi.org/10.1086/429584>. [arXiv:astro-ph/0502275](https://arxiv.org/abs/astro-ph/0502275)
- Brandenburg A (2005b) Turbulence and its parameterization in accretion discs. *Astron Nachr* 326(9):787–797. <https://doi.org/10.1002/asna.200510414>. [arXiv:astro-ph/0510015](https://arxiv.org/abs/astro-ph/0510015) [astro-ph]
- Brandenburg A (2008) The dual role of shear in large-scale dynamos. *Astron Nachr* 329(7):725. <https://doi.org/10.1002/asna.200811027>. [arXiv:0808.0959](https://arxiv.org/abs/0808.0959) [astro-ph]
- Brandenburg A (2016) Stellar mixing length theory with entropy rain. *Astrophys J* 832:6. <https://doi.org/10.3847/0004-637X/832/1/6>. [arXiv:1504.03189](https://arxiv.org/abs/1504.03189) [astro-ph.SR]
- Brandenburg A (2017) Analytic solution of an oscillatory migratory α^2 stellar dynamo. *Astron Astrophys* 598:A117. <https://doi.org/10.1051/0004-6361/201630033>. [arXiv:1611.02671](https://arxiv.org/abs/1611.02671) [astro-ph.SR]
- Brandenburg A (2018a) Advances in mean-field dynamo theory and applications to astrophysical turbulence. *Journal of Plasma Physics* 84(4):735840404. <https://doi.org/10.1017/S0022377818000806>. [arXiv:1801.05384](https://arxiv.org/abs/1801.05384) [physics.flu-dyn]

- Brandenburg A (2018b) Magnetic helicity and fluxes in an inhomogeneous α^2 dynamo. *Astron Nachr* 339(631):631–640. <https://doi.org/10.1002/asna.201913604>
- Brandenburg A, Chatterjee P (2018) Strong nonlocality variations in a spherical mean-field dynamo. *Astron Nachr* 339:118–126. <https://doi.org/10.1002/asna.201813472>. [arXiv:1802.04231](https://arxiv.org/abs/1802.04231) [astro-ph.SR]
- Brandenburg A, Dobler W (2001) Large scale dynamos with helicity loss through boundaries. *Astron Astrophys* 369:329–338. <https://doi.org/10.1051/0004-6361:20010123>. [astro-ph/0012472](https://arxiv.org/abs/astro-ph/0012472)
- Brandenburg A, Dobler W (2002) Solar and stellar dynamos - latest developments. *Astron Nachr* 323:411–416. [https://doi.org/10.1002/1521-3994\(200208\)323:3/4<411::AID-ASNA411>3.0.CO;2-H](https://doi.org/10.1002/1521-3994(200208)323:3/4<411::AID-ASNA411>3.0.CO;2-H). [arXiv:astro-ph/0207393](https://arxiv.org/abs/astro-ph/0207393) [astro-ph]
- Brandenburg A, Käpylä PJ (2007) Magnetic helicity effects in astrophysical and laboratory dynamos. *New Journal of Physics* 9(8):305. <https://doi.org/10.1088/1367-2630/9/8/305>. [arXiv:0705.3507](https://arxiv.org/abs/0705.3507) [astro-ph]
- Brandenburg A, Rädler KH (2013) Yoshizawa's cross-helicity effect and its quenching. *Geophys Astrophys Fluid Dyn* 107(1-2):207–217. <https://doi.org/10.1080/03091929.2012.681307>. [arXiv:1112.1237](https://arxiv.org/abs/1112.1237) [astro-ph.SR]
- Brandenburg A, Sokoloff D (2002) Local and Nonlocal Magnetic Diffusion and Alpha-Effect Tensors in Shear Flow Turbulence. *Geophys Astrophys Fluid Dynam* 96:319–344. <https://doi.org/10.1080/03091920290032974>. [astro-ph/0111568](https://arxiv.org/abs/astro-ph/0111568)
- Brandenburg A, Subramanian K (2005a) Astrophysical magnetic fields and nonlinear dynamo theory. *Phys Rep* 417:1–209. <https://doi.org/10.1016/j.physrep.2005.06.005>. [astro-ph/0405052](https://arxiv.org/abs/astro-ph/0405052)
- Brandenburg A, Subramanian K (2005b) Minimal tau approximation and simulations of the alpha effect. *Astron Astrophys* 439:835–843. <https://doi.org/10.1051/0004-6361:20053221>. [astro-ph/0504222](https://arxiv.org/abs/astro-ph/0504222)
- Brandenburg A, Subramanian K (2005c) Strong mean field dynamos require supercritical helicity fluxes. *Astron Nachr* 326(6):400–408. <https://doi.org/10.1002/asna.200510362>. [arXiv:astro-ph/0505457](https://arxiv.org/abs/astro-ph/0505457) [astro-ph]
- Brandenburg A, Nordlund Å, Pulkkinen P, Stein RF, Tuominen I (1990a) Turbulent diffusivities derived from simulations. In: Finnish Astronomical Society. pp 1–4
- Brandenburg A, Tuominen I, Nordlund A, Pulkkinen P, Stein RF (1990b) 3-D simulation of turbulent cyclonic magneto-convection. *Astron Astrophys* 232:277–291
- Brandenburg A, Moss D, Tuominen I (1992) Stratification and thermodynamics in mean-field dynamos. *Astron Astrophys* 265:328–344
- Brandenburg A, Nordlund A, Stein RF, Torkelsson U (1995) Dynamo-generated Turbulence and Large-Scale Magnetic Fields in a Keplerian Shear Flow. *Astrophys J* 446:741. <https://doi.org/10.1086/175831>
- Brandenburg A, Jennings RL, Nordlund Å, Rieutord M, Stein RF, Tuominen I (1996) Magnetic structures in a dynamo simulation. *J Fluid Mech* 306:325–352. <https://doi.org/10.1017/S0022112096001322>
- Brandenburg A, Dobler W, Subramanian K (2002) Magnetic helicity in stellar dynamos: new numerical experiments. *Astron Nachr* 323(2):99–122. [https://doi.org/10.1002/1521-3994\(200207\)323:2<99::AID-ASNA99>3.0.CO;2-B](https://doi.org/10.1002/1521-3994(200207)323:2<99::AID-ASNA99>3.0.CO;2-B). [arXiv:astro-ph/0111567](https://arxiv.org/abs/astro-ph/0111567) [astro-ph]
- Brandenburg A, Rädler KH, Rheinhardt M, Käpylä PJ (2008a) Magnetic Diffusivity Tensor and Dynamo Effects in Rotating and Shearing Turbulence. *Astrophys J* 676:740–751. <https://doi.org/10.1086/527373>. [arXiv:0710.4059](https://arxiv.org/abs/0710.4059)
- Brandenburg A, Rädler KH, Rheinhardt M, Subramanian K (2008b) Magnetic Quenching of α and Diffusivity Tensors in Helical Turbulence. *Astrophys J Lett* 687:L49. <https://doi.org/10.1086/593146>. [arXiv:0805.1287](https://arxiv.org/abs/0805.1287)
- Brandenburg A, Rädler KH, Schinner M (2008c) Scale dependence of alpha effect and turbulent diffusivity. *Astron Astrophys* 482:739–746. <https://doi.org/10.1051/0004-6361:200809365>. [arXiv:0801.1320](https://arxiv.org/abs/0801.1320)
- Brandenburg A, Candelaresi S, Chatterjee P (2009) Small-scale magnetic helicity losses from a mean-field dynamo. *Mon Not R Astron Soc* 398:1414–1422. <https://doi.org/10.1111/j.1365-2966.2009.15188.x>. [arXiv:0905.0242](https://arxiv.org/abs/0905.0242) [astro-ph.SR]
- Brandenburg A, Kleorin N, Rogachevskii I (2010) Large-scale magnetic flux concen-

- trations from turbulent stresses. AN 331:5. <https://doi.org/10.1002/asna.200911311>. [arXiv:0910.1835](https://arxiv.org/abs/0910.1835) [astro-ph.SR]
- Brandenburg A, Kemel K, Kleeorin N, Mitra D, Rogachevskii I (2011) Detection of Negative Effective Magnetic Pressure Instability in Turbulence Simulations. *Astrophys J Lett* 740:L50. <https://doi.org/10.1088/2041-8205/740/2/L50>. [arXiv:1109.1270](https://arxiv.org/abs/1109.1270) [astro-ph.SR]
- Brandenburg A, Kemel K, Kleeorin N, Rogachevskii I (2012a) The Negative Effective Magnetic Pressure in Stratified Forced Turbulence. *Astrophys J* 749:179. <https://doi.org/10.1088/0004-637X/749/2/179>. [arXiv:1005.5700](https://arxiv.org/abs/1005.5700) [astro-ph.SR]
- Brandenburg A, Rädler KH, Kemel K (2012b) Mean-field transport in stratified and/or rotating turbulence. *Astron Astrophys* 539:A35. <https://doi.org/10.1051/0004-6361/201117871>. [arXiv:1108.2264](https://arxiv.org/abs/1108.2264) [astro-ph.SR]
- Brandenburg A, Gressel O, Käpylä PJ, Kleeorin N, Mantere MJ, Rogachevskii I (2013a) New Scaling for the Alpha Effect in Slowly Rotating Turbulence. *Astrophys J* 762:127. <https://doi.org/10.1088/0004-637X/762/2/127>. [arXiv:1208.5004](https://arxiv.org/abs/1208.5004) [astro-ph.SR]
- Brandenburg A, Kleeorin N, Rogachevskii I (2013b) Self-assembly of Shallow Magnetic Spots through Strongly Stratified Turbulence. *Astrophys J Lett* 776:L23. <https://doi.org/10.1088/2041-8205/776/2/L23>. [arXiv:1306.4915](https://arxiv.org/abs/1306.4915) [astro-ph.SR]
- Brandenburg A, Mathur S, Metcalfe TS (2017a) Evolution of Co-existing Long and Short Period Stellar Activity Cycles. *Astrophys J* 845(1):79. <https://doi.org/10.3847/1538-4357/aa7cfa>. [arXiv:1704.09009](https://arxiv.org/abs/1704.09009) [astro-ph.SR]
- Brandenburg A, Schober J, Rogachevskii I (2017b) The contribution of kinetic helicity to turbulent magnetic diffusivity. *Astron Nachr* 338(7):790–793. <https://doi.org/10.1002/asna.201713384>. [arXiv:1706.03421](https://arxiv.org/abs/1706.03421) [physics.flu-dyn]
- Brandenburg A, Elstner D, Masada Y, Pipin V (2023) Turbulent Processes and Mean-Field Dynamo. *Space Sci Rev* 219(7):55. <https://doi.org/10.1007/s11214-023-00999-3>. [arXiv:2303.12425](https://arxiv.org/abs/2303.12425) [astro-ph.SR]
- Brandenburg A, Käpylä PJ, Rogachevskii I, Yokoi N (2025) Helicity Effect on Turbulent Passive and Active Scalar Diffusivities. *Astrophys J* 984(1):88. <https://doi.org/10.3847/1538-4357/adc691>. [arXiv:2501.08879](https://arxiv.org/abs/2501.08879) [physics.flu-dyn]
- Brown BP, Miesch MS, Browning MK, Brun AS, Toomre J (2011) Magnetic Cycles in a Convective Dynamo Simulation of a Young Solar-type Star. *Astrophys J* 731:69. <https://doi.org/10.1088/0004-637X/731/1/69>. [arXiv:1102.1993](https://arxiv.org/abs/1102.1993) [astro-ph.SR]
- Brun AS, Browning MK (2017) Magnetism, dynamo action and the solar-stellar connection. *Liv Rev Sol Phys* 14:4. <https://doi.org/10.1007/s41116-017-0007-8>
- Brun AS, Toomre J (2002) Turbulent Convection under the Influence of Rotation: Sustaining a Strong Differential Rotation. *Astrophys J* 570:865–885. <https://doi.org/10.1086/339228>. [astro-ph/0206196](https://arxiv.org/abs/astro-ph/0206196)
- Brun AS, Miesch MS, Toomre J (2004) Global-Scale Turbulent Convection and Magnetic Dynamo Action in the Solar Envelope. *Astrophys J* 614:1073–1098. <https://doi.org/10.1086/423835>. [arXiv:astro-ph/0610073](https://arxiv.org/abs/astro-ph/0610073)
- Brun AS, Strugarek A, Varela J, Matt SP, Augustson KC, Emeriau C, DoCao OL, Brown B, Toomre J (2017) On Differential Rotation and Overshooting in Solar-like Stars. *Astrophys J* 836:192. <https://doi.org/10.3847/1538-4357/aa5c40>. [arXiv:1702.06598](https://arxiv.org/abs/1702.06598) [astro-ph.SR]
- Brun AS, Strugarek A, Noraz Q, Perri B, Varela J, Augustson K, Charbonneau P, Toomre J (2022) Powering Stellar Magnetism: Energy Transfers in Cyclic Dynamoes of Sun-like Stars. *Astrophys J* 926(1):21. <https://doi.org/10.3847/1538-4357/ac469b>. [arXiv:2201.13218](https://arxiv.org/abs/2201.13218) [astro-ph.SR]
- Bushby PJ, Käpylä PJ, Masada Y, Brandenburg A, Favier B, Guervilly C, Käpylä MJ (2018) Large-scale dynamoes in rapidly rotating plane layer convection. *Astron Astrophys* 612:A97. <https://doi.org/10.1051/0004-6361/201732066>. [arXiv:1710.03174](https://arxiv.org/abs/1710.03174) [astro-ph.SR]
- Busse FH, Simitev RD (2006) Parameter dependences of convection-driven dynamoes in rotating spherical fluid shells. *Geophys Astrophys Fluid Dynam* 100:341–361. <https://doi.org/10.1080/03091920600784873>. [arXiv:0904.4293](https://arxiv.org/abs/0904.4293) [physics.flu-dyn]
- Candelaresi S, Brandenburg A (2013) Kinetic helicity needed to drive large-scale dynamoes. *Phys Rev E* 87(4):043104. <https://doi.org/10.1103/PhysRevE.87.043104>. [arXiv:1208.4529](https://arxiv.org/abs/1208.4529) [astro-ph.SR]

- Cattaneo F (1999) On the Origin of Magnetic Fields in the Quiet Photosphere. *Astrophys J Lett* 515:L39–L42. <https://doi.org/10.1086/311962>
- Cattaneo F, Hughes DW (1996) Nonlinear saturation of the turbulent α effect. *Phys Rev E* 54:4532. <https://doi.org/10.1103/PhysRevE.54.R4532>
- Cattaneo F, Hughes DW (2006) Dynamo action in a rotating convective layer. *J Fluid Mech* 553:401–418. <https://doi.org/10.1017/S0022112006009165>
- Cattaneo F, Tobias SM (2014) On Large-scale Dynamo Action at High Magnetic Reynolds Number. *Astrophys J* 789(1):70. <https://doi.org/10.1088/0004-637X/789/1/70>. [arXiv:1405.3071](https://arxiv.org/abs/1405.3071) [astro-ph.SR]
- Cattaneo F, Vainshtein SI (1991) Suppression of turbulent transport by a weak magnetic field. *Astrophys J Lett* 376:L21–L24. <https://doi.org/10.1086/186093>
- Chan KL (2007) Rotating convection in f-boxes: Faster rotation. *Astron Nachr* 328:1059. <https://doi.org/10.1002/asna.200710837>
- Chan KL, Mayr HG (2013) Numerical simulation of convectively generated vortices: Application to the Jovian planets. *Earth and Planetary Science Letters* 371:212–219. <https://doi.org/10.1016/j.epsl.2013.03.046>
- Charbonneau P (2020) Dynamo models of the solar cycle. *Living Rev Sol Phys* 17(1):4. <https://doi.org/10.1007/s41116-020-00025-6>
- Charbonneau P, Sokoloff D (2023) Evolution of Solar and Stellar Dynamo Theory. *Space Sci Rev* 219(5):35. <https://doi.org/10.1007/s11214-023-00980-0>. [arXiv:2305.16553](https://arxiv.org/abs/2305.16553) [astro-ph.SR]
- Chatterjee P, Nandy D, Choudhuri AR (2004) Full-sphere simulations of a circulation-dominated solar dynamo: Exploring the parity issue. *Astron Astrophys* 427:1019–1030. <https://doi.org/10.1051/0004-6361:20041199>. [arXiv:astro-ph/0405027](https://arxiv.org/abs/astro-ph/0405027)
- Chatterjee P, Mitra D, Rheinhardt M, Brandenburg A (2011) Alpha effect due to buoyancy instability of a magnetic layer. *Astron Astrophys* 534:A46. <https://doi.org/10.1051/0004-6361/201016108>. [arXiv:1011.1218](https://arxiv.org/abs/1011.1218) [astro-ph.SR]
- Christensen UR (2002) Zonal flow driven by strongly supercritical convection in rotating spherical shells. *J Fluid Mech* 470(1):115–133. <https://doi.org/10.1017/S0022112002002008>
- Christensen UR, Aubert J (2006) Scaling properties of convection-driven dynamos in rotating spherical shells and application to planetary magnetic fields. *Geophys J Int* 166:97–114. <https://doi.org/10.1111/j.1365-246X.2006.03009.x>
- Cole E, Brandenburg A, Käpylä PJ, Käpylä MJ (2016) Robustness of oscillatory α^2 dynamos in spherical wedges. *Astron Astrophys* 593:A134. <https://doi.org/10.1051/0004-6361/201628165>. [arXiv:1601.05246](https://arxiv.org/abs/1601.05246) [astro-ph.SR]
- Courvoisier A, Hughes DW, Proctor MRE (2010) A self-consistent treatment of the electromotive force in magnetohydrodynamics for large diffusivities. *Astron Nachr* 331:667. <https://doi.org/10.1002/asna.201011358>. [arXiv:1001.4398](https://arxiv.org/abs/1001.4398) [astro-ph.SR]
- Covas E, Tavakol R, Tworkowski A, Brandenburg A (1998) Axisymmetric mean field dynamos with dynamic and algebraic alpha -quenched. *Astron Astrophys* 329:350–360. <https://doi.org/10.48550/arXiv.astro-ph/9709062>. [arXiv:astro-ph/9709062](https://arxiv.org/abs/astro-ph/9709062) [astro-ph]
- Cowling TG (1933) The magnetic field of sunspots. *Mon Not R Astron Soc* 94:39–48. <https://doi.org/10.1093/mnras/94.1.39>
- Davidson PA (2001) *An Introduction to Magnetohydrodynamics*. Cambridge Texts in Applied Mathematics, Cambridge University Press. <https://doi.org/10.1017/CBO9780511626333>
- Del Sordo F, Guerrero G, Brandenburg A (2013) Turbulent dynamos with advective magnetic helicity flux. *Mon Not R Astron Soc* 429:1686–1694. <https://doi.org/10.1093/mnras/sts398>. [arXiv:1205.3502](https://arxiv.org/abs/1205.3502) [astro-ph.GA]
- Dikpati M, Charbonneau P (1999) A Babcock-Leighton Flux Transport Dynamo with Solar-like Differential Rotation. *Astrophys J* 518:508–520. <https://doi.org/10.1086/307269>
- Dobler W, Stix M, Brandenburg A (2006) Magnetic Field Generation in Fully Convective Rotating Spheres. *Astrophys J* 638:336–347. <https://doi.org/10.1086/498634>. [arXiv:astro-ph/0410645](https://arxiv.org/abs/astro-ph/0410645)
- Dorch SBF (2004) Magnetic activity in late-type giant stars: Numerical MHD simulations of non-linear dynamo action in Betelgeuse. *Astron Astrophys* 423:1101–1107. <https://doi.org/10.1051/0004-6361:20040435>. [arXiv:astro-ph/0403321](https://arxiv.org/abs/astro-ph/0403321) [astro-ph]

- Dorch SBF, Nordlund Å (2001) On the transport of magnetic fields by solar-like stratified convection. *Astron Astrophys* 365:562–570. <https://doi.org/10.1051/0004-6361:20000141>
- Duarte LDV, Wicht J, Browning MK, Gastine T (2016) Helicity inversion in spherical convection as a means for equatorward dynamo wave propagation. *Mon Not R Astron Soc* 456:1708–1722. <https://doi.org/10.1093/mnras/stv2726>. [arXiv:1511.05813](https://arxiv.org/abs/1511.05813) [astro-ph.SR]
- Dubé C, Charbonneau P (2013) Stellar Dynamos and Cycles from Numerical Simulations of Convection. *Astrophys J* 775:69. <https://doi.org/10.1088/0004-637X/775/1/69>
- Elliott JR, Miesch MS, Toomre J (2000) Turbulent Solar Convection and Its Coupling with Rotation: The Effect of Prandtl Number and Thermal Boundary Conditions on the Resulting Differential Rotation. *Astrophys J* 533(1):546–556. <https://doi.org/10.1086/308643>
- Fan Y, Fang F (2014) A Simulation of Convective Dynamo in the Solar Convective Envelope: Maintenance of the Solar-like Differential Rotation and Emerging Flux. *Astrophys J* 789:35. <https://doi.org/10.1088/0004-637X/789/1/35>. [arXiv:1405.3926](https://arxiv.org/abs/1405.3926) [astro-ph.SR]
- Fang F, Fan Y (2015) δ -Sunspot Formation in Simulation of Active-region-scale Flux Emergence. *Astrophys J* 806(1):79. <https://doi.org/10.1088/0004-637X/806/1/79>. [arXiv:1504.04393](https://arxiv.org/abs/1504.04393) [astro-ph.SR]
- Favier B, Bushby PJ (2012) Small-scale dynamo action in rotating compressible convection. *J Fluid Mech* 690:262–287. <https://doi.org/10.1017/jfm.2011.429>. [arXiv:1110.0374](https://arxiv.org/abs/1110.0374) [astro-ph.SR]
- Forgács-Dajka E, Petrovay K (2001) Tachocline Confinement by an Oscillatory Magnetic Field. *Sol Phys* 203(2):195–210. <https://doi.org/10.1023/A:1013389631585>. [arXiv:astro-ph/0106133](https://arxiv.org/abs/astro-ph/0106133) [astro-ph]
- Galloway DJ, Proctor MRE (1992) Numerical calculations of fast dynamos in smooth velocity fields with realistic diffusion. *Nature* 356(6371):691–693. <https://doi.org/10.1038/356691a0>
- Gastine T, Duarte L, Wicht J (2012) Dipolar versus multipolar dynamos: the influence of the background density stratification. *Astron Astrophys* 546:A19. <https://doi.org/10.1051/0004-6361/201219799>. [arXiv:1208.6093](https://arxiv.org/abs/1208.6093) [astro-ph.SR]
- Gastine T, Yadav RK, Morin J, Reiners A, Wicht J (2014) From solar-like to antisolar differential rotation in cool stars. *Mon Not R Astron Soc* 438:L76–L80. <https://doi.org/10.1093/mnras/slt162>. [arXiv:1311.3047](https://arxiv.org/abs/1311.3047) [astro-ph.SR]
- Gent FA, Shukurov A, Sarson GR, Fletcher A, Mantere MJ (2013) The supernova-regulated ISM - II. The mean magnetic field. *Mon Not R Astron Soc* 430:L40–L44. <https://doi.org/10.1093/mnras/sls042>. [arXiv:1206.6784](https://arxiv.org/abs/1206.6784) [astro-ph.GA]
- Ghizaru M, Charbonneau P, Smolarkiewicz PK (2010) Magnetic Cycles in Global Large-eddy Simulations of Solar Convection. *Astrophys J Lett* 715:L133–L137. <https://doi.org/10.1088/2041-8205/715/2/L133>
- Gilman PA (1983) Dynamically consistent nonlinear dynamos driven by convection in a rotating spherical shell. II - Dynamos with cycles and strong feedbacks. *Astrophys J Suppl* 53:243–268. <https://doi.org/10.1086/190891>
- Gilman PA, Miller J (1981) Dynamically consistent nonlinear dynamos driven by convection in a rotating spherical shell. *Astrophys J Suppl* 46:211–238. <https://doi.org/10.1086/190743>
- Gizon L, Cameron RH, Pourabdian M, Liang ZC, Fournier D, Birch AC, Hanson CS (2020) Meridional flow in the Sun’s convection zone is a single cell in each hemisphere. *Science* 368(6498):1469–1472. <https://doi.org/10.1126/science.aaz7119>
- Glatzmaier GA (1984) Numerical simulations of stellar convective dynamos. I. The model and method. *J Comput Phys* 55:461–484. [https://doi.org/10.1016/0021-9991\(84\)90033-0](https://doi.org/10.1016/0021-9991(84)90033-0)
- Glatzmaier GA (1985) Numerical simulations of stellar convective dynamos. II - Field propagation in the convection zone. *Astrophys J* 291:300–307. <https://doi.org/10.1086/163069>
- Gopalakrishnan K, Subramanian K (2023) Magnetic Helicity Fluxes from Triple Correlators. *Astrophys J* 943(1):66. <https://doi.org/10.3847/1538-4357/aca808>. [arXiv:2209.14810](https://arxiv.org/abs/2209.14810) [astro-ph.GA]

- Gough DO, McIntyre ME (1998) Inevitability of a magnetic field in the Sun's radiative interior. *Nature* 394(6695):755–757. <https://doi.org/10.1038/29472>
- Gressel O (2010) A mean-field approach to the propagation of field patterns in stratified magnetorotational turbulence. *Mon Not R Astron Soc* 405:41–48. <https://doi.org/10.1111/j.1365-2966.2010.16440.x>. [arXiv:1001.5250](https://arxiv.org/abs/1001.5250) [astro-ph.EP]
- Gressel O, Elstner D, Ziegler U, Rüdiger G (2008) Direct simulations of a supernova-driven galactic dynamo. *Astron Astrophys* 486(3):L35–L38. <https://doi.org/10.1051/0004-6361/200810195>. [arXiv:0805.2616](https://arxiv.org/abs/0805.2616) [astro-ph]
- Gruzinov AV, Diamond PH (1994) Self-consistent theory of mean-field electrodynamics. *Phys Rev Lett* 72(11):1651–1653. <https://doi.org/10.1103/PhysRevLett.72.1651>
- Gruzinov AV, Diamond PH (1995) Self-consistent mean field electrodynamics of turbulent dynamos. *Phys Plasmas* 2:1941–1946. <https://doi.org/10.1063/1.871495>
- Guerrero G, Käpylä PJ (2011) Dynamo action and magnetic buoyancy in convection simulations with vertical shear. *Astron Astrophys* 533:A40. <https://doi.org/10.1051/0004-6361/201116749>. [arXiv:1102.3598](https://arxiv.org/abs/1102.3598) [astro-ph.SR]
- Guerrero G, Smolarkiewicz PK, de Gouveia Dal Pino EM, Kosovichev AG, Mansour NN (2016) On the Role of Tachoclines in Solar and Stellar Dynamos. *Astrophys J* 819:104. <https://doi.org/10.3847/0004-637X/819/2/104>. [arXiv:1507.04434](https://arxiv.org/abs/1507.04434) [astro-ph.SR]
- Guerrero G, Zaire B, Smolarkiewicz PK, de Gouveia Dal Pino EM, Kosovichev AG, Mansour NN (2019) What Sets the Magnetic Field Strength and Cycle Period in Solar-type Stars? *Astrophys J* 880(1):6. <https://doi.org/10.3847/1538-4357/ab224a>. [arXiv:1810.07978](https://arxiv.org/abs/1810.07978) [astro-ph.SR]
- Guerrero G, Stejko AM, Kosovichev AG, Smolarkiewicz PK, Strugarek A (2022) Implicit Large-eddy Simulations of Global Solar Convection: Effects of Numerical Resolution in Nonrotating and Rotating Cases. *Astrophys J* 940(2):151. <https://doi.org/10.3847/1538-4357/ac9af3>. [arXiv:2208.05738](https://arxiv.org/abs/2208.05738) [astro-ph.SR]
- Guervilly C, Hughes DW, Jones CA (2014) Large-scale vortices in rapidly rotating Rayleigh-Bénard convection. *J Fluid Mech* 758:407–435. <https://doi.org/10.1017/jfm.2014.542>. [arXiv:1403.7442](https://arxiv.org/abs/1403.7442) [physics.flu-dyn]
- Guervilly C, Hughes DW, Jones CA (2015) Generation of magnetic fields by large-scale vortices in rotating convection. *Phys Rev E* 91(4):041001. <https://doi.org/10.1103/PhysRevE.91.041001>. [arXiv:1503.08599](https://arxiv.org/abs/1503.08599) [physics.flu-dyn]
- Guervilly C, Hughes DW, Jones CA (2017) Large-scale-vortex dynamos in planar rotating convection. *J Fluid Mech* 815:333–360. <https://doi.org/10.1017/jfm.2017.56>. [arXiv:1607.00824](https://arxiv.org/abs/1607.00824) [physics.flu-dyn]
- Hale GE (1908) On the Probable Existence of a Magnetic Field in Sun-Spots. *Astrophys J* 28:315. <https://doi.org/10.1086/141602>
- Hale GE, Ellerman F, Nicholson SB, Joy AH (1919) The Magnetic Polarity of Sun-Spots. *Astrophys J* 49:153. <https://doi.org/10.1086/142452>
- Hanasoge S, Gizon L, Sreenivasan KR (2016) Seismic Sounding of Convection in the Sun. *Annu Rev Fluid Mech* 48:191–217. <https://doi.org/10.1146/annurev-fluid-122414-034534>. [arXiv:1503.07961](https://arxiv.org/abs/1503.07961) [astro-ph.SR]
- Hanasoge SM (2022) Surface and interior meridional circulation in the Sun. *Living Rev Sol Phys* 19(1):3. <https://doi.org/10.1007/s41116-022-00034-7>
- Hanasoge SM, Duvall TL, Sreenivasan KR (2012) Anomalously weak solar convection. *Proc Natl Acad Sci* 109:11928–11932. <https://doi.org/10.1073/pnas.1206570109>. [arXiv:1206.3173](https://arxiv.org/abs/1206.3173) [astro-ph.SR]
- Hanasoge SM, Hotta H, Sreenivasan KR (2020) Turbulence in the Sun is suppressed on large scales and confined to equatorial regions. *Science Advances* 6(30):eaba9639. <https://doi.org/10.1126/sciadv.aba9639>
- Hathaway DH (2015) The Solar Cycle. *Living Rev Sol Phys* 12:4. <https://doi.org/10.1007/lrsp-2015-4>. [arXiv:1502.07020](https://arxiv.org/abs/1502.07020) [astro-ph.SR]
- Haugen NEL, Brandenburg A, Dobler W (2004) Simulations of nonhelical hydromagnetic turbulence. *Phys Rev E* 70(1):016308. <https://doi.org/10.1103/PhysRevE.70.016308>. [astro-ph/0307059](https://arxiv.org/abs/astro-ph/0307059)
- Hidalgo JP, Käpylä PJ, Schleicher DRG, Ortiz-Rodríguez CA, Navarrete FH (2024) Magnetohydrodynamic simulations of A-type stars: Long-term evolution of core dynamo cycles. *Astron Astrophys* 691:A326. <https://doi.org/10.1051/0004-6361/202449977>.

- [arXiv:2409.18066](#) [astro-ph.SR]
- Hotta H (2017) Solar Overshoot Region and Small-scale Dynamo with Realistic Energy Flux. *Astrophys J* 843:52. <https://doi.org/10.3847/1538-4357/aa784b>. [arXiv:1706.06413](#) [astro-ph.SR]
- Hotta H (2025) Simultaneous Construction of Fast Equator, Poleward Meridional Flow, and Near-surface Shear Layer in Solar Magnetohydrodynamic Calculation. *Astrophys J* 985(2):163. <https://doi.org/10.3847/1538-4357/adca3b>. [arXiv:2504.05680](#) [astro-ph.SR]
- Hotta H, Kusano K (2021) Solar differential rotation reproduced with high-resolution simulation. *Nature Astronomy* 5:1100–1102. <https://doi.org/10.1038/s41550-021-01459-0>. [arXiv:2109.06280](#) [astro-ph.SR]
- Hotta H, Rempel M, Yokoyama T, Iida Y, Fan Y (2012) Numerical calculation of convection with reduced speed of sound technique. *Astron Astrophys* 539:A30. <https://doi.org/10.1051/0004-6361/201118268>. [arXiv:1201.1061](#) [astro-ph.SR]
- Hotta H, Rempel M, Yokoyama T (2015) High-resolution Calculation of the Solar Global Convection with the Reduced Speed of Sound Technique. II. Near Surface Shear Layer with the Rotation. *Astrophys J* 798:51. <https://doi.org/10.1088/0004-637X/798/1/51>. [arXiv:1410.7093](#) [astro-ph.SR]
- Hotta H, Rempel M, Yokoyama T (2016) Large-scale magnetic fields at high reynolds numbers in magnetohydrodynamic simulations. *Science* 351(6280):1427–1430. <https://doi.org/10.1126/science.aad1893>
- Hotta H, Kusano K, Shimada R (2022) Generation of Solar-like Differential Rotation. *Astrophys J* 933(2):199. <https://doi.org/10.3847/1538-4357/ac7395>. [arXiv:2202.04183](#) [astro-ph.SR]
- Hotta H, Bekki Y, Gizon L, Noraz Q, Rast M (2023) Dynamics of Large-Scale Solar Flows. *Space Sci Rev* 219(8):77. <https://doi.org/10.1007/s11214-023-01021-6>. [arXiv:2307.06481](#) [astro-ph.SR]
- Howe R (2009) Solar Interior Rotation and its Variation. *Living Rev Sol Phys* 6(1):1. <https://doi.org/10.12942/lrsp-2009-1>. [arXiv:0902.2406](#) [astro-ph.SR]
- Hubbard A, Brandenburg A (2009) Memory Effects in Turbulent Transport. *Astrophys J* 706:712–726. <https://doi.org/10.1088/0004-637X/706/1/712>. [arXiv:0811.2561](#)
- Hubbard A, Brandenburg A (2012) Catastrophic Quenching in $\alpha\Omega$ Dynamos Revisited. *Astrophys J* 748(1):51. <https://doi.org/10.1088/0004-637X/748/1/51>. [arXiv:1107.0238](#) [astro-ph.SR]
- Hubbard A, Del Sordo F, Käpylä PJ, Brandenburg A (2009) The α effect with imposed and dynamo-generated magnetic fields. *Mon Not R Astron Soc* 398(4):1891–1899. <https://doi.org/10.1111/j.1365-2966.2009.15108.x>. [arXiv:0904.2773](#) [astro-ph.SR]
- Hubbard A, Rheinhardt M, Brandenburg A (2011) The fratricide of $\alpha\Omega$ dynamos by their α^2 siblings. *Astron Astrophys* 535:A48. <https://doi.org/10.1051/0004-6361/201116705>. [arXiv:1102.2617](#) [astro-ph.SR]
- Hughes DW, Cattaneo F (2008) The alpha-effect in rotating convection: size matters. *J Fluid Mech* 594:445–461. <https://doi.org/10.1017/S0022112007009214>
- Hughes DW, Proctor MRE (2009) Large-Scale Dynamo Action Driven by Velocity Shear and Rotating Convection. *Phys Rev Lett* 102(4):044501. <https://doi.org/10.1103/PhysRevLett.102.044501>. [arXiv:0810.1586](#)
- Hughes DW, Proctor MRE (2013) The effect of velocity shear on dynamo action due to rotating convection. *J Fluid Mech* 717:395–416. <https://doi.org/10.1017/jfm.2012.584>. [arXiv:1211.5339](#) [astro-ph.SR]
- Iskakov AB, Schekochihin AA, Cowley SC, McWilliams JC, Proctor MRE (2007) Numerical Demonstration of Fluctuation Dynamo at Low Magnetic Prandtl Numbers. *Phys Rev Lett* 98(20):208501. <https://doi.org/10.1103/PhysRevLett.98.208501>. [arXiv:astro-ph/0702291](#)
- Jabbari S, Brandenburg A, Kleorin N, Mitra D, Rogachevskii I (2015) Bipolar Magnetic Spots from Dynamos in Stratified Spherical Shell Turbulence. *Astrophys J* 805:166. <https://doi.org/10.1088/0004-637X/805/2/166>. [arXiv:1411.4912](#) [astro-ph.SR]
- Jermyn AS, Anders EH, Lecoanet D, Cantiello M (2022) An Atlas of Convection in Main-sequence Stars. *Astrophys J Suppl* 262(1):19. <https://doi.org/10.3847/1538-4365/ac7cee>. [arXiv:2206.00011](#) [astro-ph.SR]

- Jiang J, Hathaway DH, Cameron RH, Solanki SK, Gizon L, Upton L (2014) Magnetic Flux Transport at the Solar Surface. *Space Sci Rev* 186(1-4):491–523. <https://doi.org/10.1007/s11214-014-0083-1>. arXiv:1408.3186 [astro-ph.SR]
- Jingade N, Singh NK (2021) Mean field dynamo action in shearing flows - II. Fluctuating kinetic helicity with zero mean. *Mon Not R Astron Soc* 508(4):5163–5175. <https://doi.org/10.1093/mnras/stab2854>. arXiv:2103.12599 [physics.flu-dyn]
- Jones CA, Kuzanyan KM (2009) Compressible convection in the deep atmospheres of giant planets. *Icarus* 204(1):227–238. <https://doi.org/10.1016/j.icarus.2009.05.022>
- Jones CA, Roberts PH (2000) Convection-driven dynamos in a rotating plane layer. *J Fluid Mech* 404(1):311–343. <https://doi.org/10.1017/S0022112099007363>
- Käpylä MJ, Käpylä PJ, Olsper N, Brandenburg A, Warnecke J, Karak BB, Pelt J (2016a) Multiple dynamo modes as a mechanism for long-term solar activity variations. *Astron Astrophys* 589:A56. <https://doi.org/10.1051/0004-6361/201527002>. arXiv:1507.05417 [astro-ph.SR]
- Käpylä MJ, Vizoso JÁ, Rheinhardt M, Brandenburg A, Singh NK (2020a) On the Existence of Shear-current Effects in Magnetized Burgulence. *Astrophys J* 905(2):179. <https://doi.org/10.3847/1538-4357/abc1e8>. arXiv:2006.05661 [physics.flu-dyn]
- Käpylä MJ, Rheinhardt M, Brandenburg A (2022) Compressible Test-field Method and Its Application to Shear Dynamos. *Astrophys J* 932(1):8. <https://doi.org/10.3847/1538-4357/ac5b78>. arXiv:2106.01107 [physics.flu-dyn]
- Käpylä PJ (2021) Star-in-a-box simulations of fully convective stars. *Astron Astrophys* 651:A66. <https://doi.org/10.1051/0004-6361/202040049>. arXiv:2012.01259 [astro-ph.SR]
- Käpylä PJ (2022) Solar-like dynamos and rotational scaling of cycles from star-in-a-box simulations. *Astrophys J Lett* 931(2):L17. <https://doi.org/10.3847/2041-8213/ac6e6b>. arXiv:2202.04329 [astro-ph.SR]
- Käpylä PJ (2023) Transition from anti-solar to solar-like differential rotation: Dependence on Prandtl number. *Astron Astrophys* 669:A98. <https://doi.org/10.1051/0004-6361/202244395>. arXiv:2207.00302 [astro-ph.SR]
- Käpylä PJ (2024) Convective scale and subadiabatic layers in simulations of rotating compressible convection. *Astron Astrophys* 683:A221. <https://doi.org/10.1051/0004-6361/202348325>. arXiv:2310.12855 [astro-ph.SR]
- Käpylä PJ (2025) Simulations of entropy rain-driven convection. *Astron Astrophys* 698:L13. <https://doi.org/10.1051/0004-6361/202554952>. arXiv:2504.00738 [astro-ph.SR]
- Käpylä PJ, Brandenburg A (2009) Turbulent Dynamos with Shear and Fractional Helicity. *Astrophys J* 699:1059–1066. <https://doi.org/10.1088/0004-637X/699/2/1059>. arXiv:0810.2298
- Käpylä PJ, Korpi MJ, Ossendrijver M, Stix M (2006a) Magnetoconvection and dynamo coefficients. III. α -effect and magnetic pumping in the rapid rotation regime. *Astron Astrophys* 455:401–412. <https://doi.org/10.1051/0004-6361/20064972>. arXiv:astro-ph/0602111
- Käpylä PJ, Korpi MJ, Tuominen I (2006b) Solar dynamo models with α -effect and turbulent pumping from local 3D convection calculations. *Astron Nachr* 327:884. <https://doi.org/10.1002/asna.200610636>. arXiv:astro-ph/0606089
- Käpylä PJ, Korpi MJ, Brandenburg A (2008) Large-scale dynamos in turbulent convection with shear. *Astron Astrophys* 491:353–362. <https://doi.org/10.1051/0004-6361/200810307>. arXiv:0806.0375
- Käpylä PJ, Korpi MJ, Brandenburg A (2009a) Alpha effect and turbulent diffusion from convection. *Astron Astrophys* 500:633–646. <https://doi.org/10.1051/0004-6361/200811498>. arXiv:0812.1792
- Käpylä PJ, Korpi MJ, Brandenburg A (2009b) Large-scale Dynamos in Rigidly Rotating Turbulent Convection. *Astrophys J* 697:1153–1163. <https://doi.org/10.1088/0004-637X/697/2/1153>. arXiv:0812.3958
- Käpylä PJ, Korpi MJ, Brandenburg A (2010a) Open and closed boundaries in large-scale convective dynamos. *Astron Astrophys* 518:A22. <https://doi.org/10.1051/0004-6361/200913722>. arXiv:0911.4120 [astro-ph.SR]

- Käpylä PJ, Korpi MJ, Brandenburg A (2010b) The α effect in rotating convection with sinusoidal shear. *Mon Not R Astron Soc* 402:1458–1466. <https://doi.org/10.1111/j.1365-2966.2009.16004.x>. arXiv:0908.2423 [astro-ph.SR]
- Käpylä PJ, Korpi MJ, Brandenburg A, Mitra D, Tavakol R (2010c) Convective dynamos in spherical wedge geometry. *Astron Nachr* 331:73. <https://doi.org/10.1002/asna.200911252>. arXiv:0909.1330 [astro-ph.SR]
- Käpylä PJ, Mantere MJ, Hackman T (2011) Starspots due to Large-scale Vortices in Rotating Turbulent Convection. *Astrophys J* 742:34. <https://doi.org/10.1088/0004-637X/742/1/34>. arXiv:1106.6029 [astro-ph.SR]
- Käpylä PJ, Brandenburg A, Kleeorin N, Mantere MJ, Rogachevskii I (2012a) Negative effective magnetic pressure in turbulent convection. *Mon Not R Astron Soc* 422:2465–2473. <https://doi.org/10.1111/j.1365-2966.2012.20801.x>. arXiv:1104.4541 [astro-ph.SR]
- Käpylä PJ, Mantere MJ, Brandenburg A (2012b) Cyclic Magnetic Activity due to Turbulent Convection in Spherical Wedge Geometry. *Astrophys J Lett* 755:L22. <https://doi.org/10.1088/2041-8205/755/1/L22>. arXiv:1205.4719 [astro-ph.SR]
- Käpylä PJ, Mantere MJ, Brandenburg A (2013a) Oscillatory large-scale dynamos from Cartesian convection simulations. *Geophys Astrophys Fluid Dynam* 107:244–257. <https://doi.org/10.1080/03091929.2012.715158>
- Käpylä PJ, Mantere MJ, Cole E, Warnecke J, Brandenburg A (2013b) Effects of Enhanced Stratification on Equatorward Dynamo Wave Propagation. *Astrophys J* 778:41. <https://doi.org/10.1088/0004-637X/778/1/41>. arXiv:1301.2595 [astro-ph.SR]
- Käpylä PJ, Käpylä MJ, Brandenburg A (2014) Confirmation of bistable stellar differential rotation profiles. *Astron Astrophys* 570:A43. arXiv:1401.2981 [astro-ph.SR]
- Käpylä PJ, Brandenburg A, Kleeorin N, Käpylä MJ, Rogachevskii I (2016b) Magnetic flux concentrations from turbulent stratified convection. *Astron Astrophys* 588:A150. <https://doi.org/10.1051/0004-6361/201527731>. arXiv:1511.03718 [astro-ph.SR]
- Käpylä PJ, Käpylä MJ, Olsper N, Warnecke J, Brandenburg A (2017a) Convection-driven spherical shell dynamos at varying Prandtl numbers. *Astron Astrophys* 599:A4. <https://doi.org/10.1051/0004-6361/201628973>. arXiv:1605.05885 [astro-ph.SR]
- Käpylä PJ, Rheinhardt M, Brandenburg A, Arlt R, Käpylä MJ, Lagg A, Olsper N, Warnecke J (2017b) Extended Subadiabatic Layer in Simulations of Overshooting Convection. *Astrophys J Lett* 845:L23. <https://doi.org/10.3847/2041-8213/aa83ab>. arXiv:1703.06845 [astro-ph.SR]
- Käpylä PJ, Viviani M, Käpylä MJ, Brandenburg A, Spada F (2019) Effects of a subadiabatic layer on convection and dynamos in spherical wedge simulations. *Geophys Astrophys Fluid Dyn* 113:149–183. <https://doi.org/10.1080/03091929.2019.1571584>. arXiv:1803.05898 [astro-ph.SR]
- Käpylä PJ, Gent FA, Olsper N, Käpylä MJ, Brandenburg A (2020b) Sensitivity to luminosity, centrifugal force, and boundary conditions in spherical shell convection. *Geophys Astrophys Fluid Dyn* 114(1-2):8–34. <https://doi.org/10.1080/03091929.2019.1571586>
- Käpylä PJ, Rheinhardt M, Brandenburg A, Käpylä MJ (2020c) Turbulent viscosity and magnetic Prandtl number from simulations of isotropically forced turbulence. *Astron Astrophys* 636:A93. <https://doi.org/10.1051/0004-6361/201935012>. arXiv:1901.00787 [astro-ph.SR]
- Käpylä PJ, Browning MK, Brun AS, Guerrero G, Warnecke J (2023) Simulations of Solar and Stellar Dynamos and Their Theoretical Interpretation. *Space Sci Rev* 219(7):58. <https://doi.org/10.1007/s11214-023-01005-6>. arXiv:2305.16790 [astro-ph.SR]
- Karak BB (2023) Models for the long-term variations of solar activity. *Living Reviews in Solar Physics* 20(1):3. <https://doi.org/10.1007/s41116-023-00037-y>. arXiv:2305.17188 [astro-ph.SR]
- Karak BB, Brandenburg A (2016) Is the Small-scale Magnetic Field Correlated with the Dynamo Cycle? *Astrophys J* 816:28. <https://doi.org/10.3847/0004-637X/816/1/28>. arXiv:1505.06632 [astro-ph.SR]
- Karak BB, Choudhuri AR (2011) The Waldmeier effect and the flux transport solar dynamo. *Mon Not R Astron Soc* 410(3):1503–1512. <https://doi.org/10.1111/j.1365-2966.2010.17531.x>. arXiv:1008.0824 [astro-ph.SR]
- Karak BB, Rheinhardt M, Brandenburg A, Käpylä PJ, Käpylä MJ (2014) Quenching and Anisotropy of Hydromagnetic Turbulent Transport. *Astrophys J* 795:16. <https://doi.org/10.1088/0004-637X/795/1/16>

- [org/10.1088/0004-637X/795/1/16](https://doi.org/10.1088/0004-637X/795/1/16). [arXiv:1406.4521](https://arxiv.org/abs/1406.4521) [astro-ph.SR]
- Kemel K, Brandenburg A, Kleeorin N, Mitra D, Rogachevskii I (2012) Spontaneous Formation of Magnetic Flux Concentrations in Stratified Turbulence. *Sol Phys* 280:321–333. <https://doi.org/10.1007/s11207-012-9949-0>. [arXiv:1112.0279](https://arxiv.org/abs/1112.0279) [astro-ph.SR]
- Kemel K, Brandenburg A, Kleeorin N, Mitra D, Rogachevskii I (2013) Active Region Formation through the Negative Effective Magnetic Pressure Instability. *Sol Phys* 287:293–313. <https://doi.org/10.1007/s11207-012-0031-8>. [arXiv:1203.1232](https://arxiv.org/abs/1203.1232) [astro-ph.SR]
- Kichatinov LL (1991) Turbulent transport of magnetic fields in a highly conducting rotating fluid and the solar cycle. *Astron Astrophys* 243(2):483–491
- Kitchatinov LL, Rüdiger G (1995) Differential rotation in solar-type stars: revisiting the Taylor-number puzzle. *Astron Astrophys* 299:446
- Kitchatinov LL, Pipin VV, Rüdiger G (1994) Turbulent viscosity, magnetic diffusivity, and heat conductivity under the influence of rotation and magnetic field. *Astron Nachr* 315:157–170
- Kleeorin N, Rogachevskii I (2003) Effect of rotation on a developed turbulent stratified convection: The hydrodynamic helicity, the α effect, and the effective drift velocity. *Phys Rev E* 67(2):026321. <https://doi.org/10.1103/PhysRevE.67.026321>. [arXiv:astro-ph/0209530](https://arxiv.org/abs/astro-ph/0209530) [astro-ph]
- Kleeorin N, Rogachevskii I (2008) Mean-field dynamo in a turbulence with shear and kinetic helicity fluctuations. *Phys Rev E* 77(3):036307. <https://doi.org/10.1103/PhysRevE.77.036307>. [arXiv:0711.4726](https://arxiv.org/abs/0711.4726) [astro-ph]
- Kleeorin N, Rogachevskii I (2012) Growth rate of small-scale dynamo at low magnetic Prandtl numbers. *Phys. Scr* 86(1):018404. <https://doi.org/10.1088/0031-8949/86/01/018404>. [arXiv:1112.3926](https://arxiv.org/abs/1112.3926) [astro-ph.SR]
- Kleeorin N, Rogachevskii I (2022) Turbulent magnetic helicity fluxes in solar convective zone. *Mon Not R Astron Soc* 515(4):5437–5448. <https://doi.org/10.1093/mnras/stac2141>. [arXiv:2206.14152](https://arxiv.org/abs/2206.14152) [astro-ph.SR]
- Kleeorin N, Moss D, Rogachevskii I, Sokoloff D (2000) Helicity balance and steady-state strength of the dynamo generated galactic magnetic field. *Astron Astrophys* 361:L5–L8. <https://doi.org/10.48550/arXiv.astro-ph/0205266>. [arXiv:astro-ph/0205266](https://arxiv.org/abs/astro-ph/0205266) [astro-ph]
- Kleeorin NI, Rogachevskii IV, Ruzmaikin AA (1989) Negative Magnetic Pressure as a Trigger of Large-scale Magnetic Instability in the Solar Convective Zone. *Sov Astron Lett* 15:274
- Kleeorin NI, Rogachevskii IV, Ruzmaikin AA (1990) Magnetic force reversal and instability in a plasma with advanced magnetohydrodynamic turbulence. *Sov Phys JETP* 70:878–883
- Kraichnan RH (1976) Diffusion of passive-scalar and magnetic fields by helical turbulence. *J Fluid Mech* 77:753–768. <https://doi.org/10.1017/S0022112076002875>
- Krause F, Rädler KH (1980) Mean-field Magnetohydrodynamics and Dynamo Theory. Pergamon Press, Oxford
- Krause F, Steenbeck M (1967) Untersuchung der Dynamowirkung enier nichtspiegelsymmetrischen Turbulenz an einfachen Modellen. *Z Naturforsch A* 22:671. <https://doi.org/10.1515/zna-1967-0512>
- Kupka F, Muthsam HJ (2017) Modelling of stellar convection. *Liv Rev Comp Astrophys* 3:1. <https://doi.org/10.1007/s41115-017-0001-9>
- Larmor J (1919) How could a rotating body such as the sun become a magnet. *Rep Brit Adv Sci* pp 159–160. URL <https://ci.nii.ac.jp/naid/10029017512/en/>
- Larson TP, Schou J (2018) Global-Mode Analysis of Full-Disk Data from the Michelson Doppler Imager and the Helioseismic and Magnetic Imager. *Sol Phys* 293(2):29. <https://doi.org/10.1007/s11207-017-1201-5>
- Losada IR, Brandenburg A, Kleeorin N, Mitra D, Rogachevskii I (2012) Rotational effects on the negative magnetic pressure instability. *Astron Astrophys* 548:A49. <https://doi.org/10.1051/0004-6361/201220078>. [arXiv:1207.5392](https://arxiv.org/abs/1207.5392) [astro-ph.SR]
- Losada IR, Brandenburg A, Kleeorin N, Rogachevskii I (2013) Competition of rotation and stratification in flux concentrations. *Astron Astrophys* 556:A83. <https://doi.org/10.1051/0004-6361/201220939>. [arXiv:1212.4077](https://arxiv.org/abs/1212.4077) [astro-ph.SR]
- Losada IR, Warnecke J, Brandenburg A, Kleeorin N, Rogachevskii I (2019) Magnetic bipoles in rotating turbulence with coronal envelope. *Astron Astrophys* 621:A61. <https://doi.org/10.1051/0004-6361/201833400>

- [org/10.1051/0004-6361/201833018](https://doi.org/10.1051/0004-6361/201833018). [arXiv:1803.04446](https://arxiv.org/abs/1803.04446) [astro-ph.SR]
- Mabuchi J, Masada Y, Kageyama A (2015) Differential Rotation in Magnetized and Non-magnetized Stars. *Astrophys J* 806:10. <https://doi.org/10.1088/0004-637X/806/1/10>. [arXiv:1504.01129](https://arxiv.org/abs/1504.01129) [astro-ph.SR]
- Malkus WVR, Proctor MRE (1975) The macrodynamics of alpha-effect dynamos in rotating fluids. *J Fluid Mech* 67:417–443. <https://doi.org/10.1017/S0022112075000390>
- Masada Y, Sano T (2014) Mean-Field Modeling of an α^2 Dynamo Coupled with Direct Numerical Simulations of Rigidly Rotating Convection. *Astrophys J Lett* 794(1):L6. <https://doi.org/10.1088/2041-8205/794/1/L6>. [arXiv:1409.3256](https://arxiv.org/abs/1409.3256) [astro-ph.SR]
- Masada Y, Sano T (2016) Spontaneous Formation of Surface Magnetic Structure from Large-scale Dynamo in Strongly Stratified Convection. *Astrophys J Lett* 822:L22. <https://doi.org/10.3847/2041-8205/822/2/L22>. [arXiv:1604.05374](https://arxiv.org/abs/1604.05374) [astro-ph.SR]
- Masada Y, Sano T (2022) Rotational Dependence of Large-scale Dynamo in Strongly-stratified Convection: What Causes It? *arXiv e-prints arXiv:2206.06566*. [arXiv:2206.06566](https://arxiv.org/abs/2206.06566) [astro-ph.SR]
- Masada Y, Takiwaki T, Kotake K (2022) Convection and Dynamo in Newly Born Neutron Stars. *Astrophys J* 924(2):75. <https://doi.org/10.3847/1538-4357/ac34f6>. [arXiv:2001.08452](https://arxiv.org/abs/2001.08452) [astro-ph.HE]
- Matilsky LI, Toomre J (2020) Exploring Bistability in the Cycles of the Solar Dynamo through Global Simulations. *Astrophys J* 892(2):106. <https://doi.org/10.3847/1538-4357/ab791c>. [arXiv:1912.08158](https://arxiv.org/abs/1912.08158) [astro-ph.SR]
- Matilsky LI, Hindman BW, Toomre J (2019) The Role of Downflows in Establishing Solar Near-surface Shear. *Astrophys J* 871:217. <https://doi.org/10.3847/1538-4357/aaf647>. [arXiv:1810.00115](https://arxiv.org/abs/1810.00115) [astro-ph.SR]
- Matilsky LI, Hindman BW, Featherstone NA, Blume CC, Toomre J (2022) Confinement of the Solar Tachocline by Dynamo Action in the Radiative Interior. *Astrophys J Lett* 940(2):L50. <https://doi.org/10.3847/2041-8213/ac93ef>. [arXiv:2206.12920](https://arxiv.org/abs/2206.12920) [astro-ph.SR]
- Meneguzzi M, Pouquet A (1989) Turbulent dynamos driven by convection. *J Fluid Mech* 205:297–318. <https://doi.org/10.1017/S0022112089002041>
- Meneguzzi M, Frisch U, Pouquet A (1981) Helical and nonhelical turbulent dynamos. *Phys Rev Lett* 47(15):1060–1064. <https://doi.org/10.1103/PhysRevLett.47.1060>
- Miesch M, Matthaeus W, Brandenburg A, Petrosyan A, Pouquet A, Cambon C, Jenko F, Uzdensky D, Stone J, Tobias S, Toomre J, Velli M (2015) Large-Eddy Simulations of Magnetohydrodynamic Turbulence in Heliophysics and Astrophysics. *Space Sci Rev* 194:97–137. <https://doi.org/10.1007/s11214-015-0190-7>. [arXiv:1505.01808](https://arxiv.org/abs/1505.01808) [astro-ph.SR]
- Miesch MS, Toomre J (2009) Turbulence, Magnetism, and Shear in Stellar Interiors. *Ann Rev Fluid Mech* 41:317–345. <https://doi.org/10.1146/annurev.fluid.010908.165215>
- Miesch MS, Elliott JR, Toomre J, Clune TL, Glatzmaier GA, Gilman PA (2000) Three-dimensional Spherical Simulations of Solar Convection. I. Differential Rotation and Pattern Evolution Achieved with Laminar and Turbulent States. *Astrophys J* 532:593–615. <https://doi.org/10.1086/308555>
- Mitra D, Käpylä PJ, Tavakol R, Brandenburg A (2009a) Alpha effect and diffusivity in helical turbulence with shear. *Astron Astrophys* 495:1–8. <https://doi.org/10.1051/0004-6361/200810359>. [arXiv:0806.1608](https://arxiv.org/abs/0806.1608)
- Mitra D, Tavakol R, Brandenburg A, Moss D (2009b) Turbulent Dynamos in Spherical Shell Segments of Varying Geometrical Extent. *Astrophys J* 697:923–933. <https://doi.org/10.1088/0004-637X/697/1/923>. [arXiv:0812.3106](https://arxiv.org/abs/0812.3106)
- Mitra D, Candelaresi S, Chatterjee P, Tavakol R, Brandenburg A (2010a) Equatorial magnetic helicity flux in simulations with different gauges. *Astron Nachr* 331:130. <https://doi.org/10.1002/asna.200911308>. [arXiv:0911.0969](https://arxiv.org/abs/0911.0969) [astro-ph.SR]
- Mitra D, Tavakol R, Käpylä PJ, Brandenburg A (2010b) Oscillatory Migrating Magnetic Fields in Helical Turbulence in Spherical Domains. *Astrophys J Lett* 719:L1–L4. <https://doi.org/10.1088/2041-8205/719/1/L1>. [arXiv:0901.2364](https://arxiv.org/abs/0901.2364) [astro-ph.SR]
- Mizerski KA (2023) Helical correction to turbulent magnetic diffusivity. *Phys Rev E* 107(5):055205. <https://doi.org/10.1103/PhysRevE.107.055205>
- Moffatt HK (1974) The mean electromotive force generated by turbulence in the limit of perfect conductivity. *J Fluid Mech* 65:1–10. <https://doi.org/10.1017/S0022112074001200>

- Moffatt HK (1978) *Magnetic Field Generation in Electrically Conducting Fluids*. Cambridge University Press, Cambridge
- Moffatt K, Dormy E (2019) *Self-Exciting Fluid Dynamos*. Cambridge Texts in Applied Mathematics, Cambridge University Press. <https://doi.org/10.1017/9781107588691>
- Moss D, Brandenburg A (1995) The generation of nonaxisymmetric magnetic fields in the giant planets. *Geophys Astrophys Fluid Dyn* 80:229–240. <https://doi.org/10.1080/03091929508228956>
- Nelson NJ, Brown BP, Brun AS, Miesch MS, Toomre J (2013) Magnetic Wreaths and Cycles in Convective Dynamos. *Astrophys J* 762:73. <https://doi.org/10.1088/0004-637X/762/2/73>. [arXiv:1211.3129](https://arxiv.org/abs/1211.3129) [astro-ph.SR]
- Nelson NJ, Brown BP, Sacha Brun A, Miesch MS, Toomre J (2014) Buoyant Magnetic Loops Generated by Global Convective Dynamo Action. *Sol Phys* 289:441–458. <https://doi.org/10.1007/s11207-012-0221-4>. [arXiv:1212.5612](https://arxiv.org/abs/1212.5612) [astro-ph.SR]
- Nicklaus B, Stix M (1988) Corrections to first order smoothing in mean-field electrodynamics. *Geophys Astrophys Fluid Dyn* 43(2):149–166. <https://doi.org/10.1080/03091928808213623>
- Nordlund A, Brandenburg A, Jennings RL, Rieutord M, Ruokolainen J, Stein RF, Tuominen I (1992) Dynamo action in stratified convection with overshoot. *Astrophys J* 392:647–652. <https://doi.org/10.1086/171465>
- O’Mara B, Miesch MS, Featherstone NA, Augustson KC (2016) Velocity amplitudes in global convection simulations: The role of the Prandtl number and near-surface driving. *Adv Space Res* 58:1475–1489. <https://doi.org/10.1016/j.asr.2016.03.038>. [arXiv:1603.06107](https://arxiv.org/abs/1603.06107) [astro-ph.SR]
- Ortiz-Rodríguez CA, Käpylä PJ, Navarrete FH, Schleicher DRG, Mennickent RE, Hidalgo JP, Toro-Velásquez B (2023) Simulations of dynamo action in slowly rotating M dwarfs: Dependence on dimensionless parameters. *Astron Astrophys* 678:A82. <https://doi.org/10.1051/0004-6361/202244666>. [arXiv:2305.16447](https://arxiv.org/abs/2305.16447) [astro-ph.SR]
- Orvedahl RJ, Calkins MA, Featherstone NA, Hindman BW (2018) Prandtl-number Effects in High-Rayleigh-number Spherical Convection. *Astrophys J* 856(1):L13. <https://doi.org/10.3847/1538-4357/aaeb5>. [arXiv:1803.07035](https://arxiv.org/abs/1803.07035) [astro-ph.SR]
- Ossendrijver M (2003) The solar dynamo. *Astron Astrophys Rev* 11:287–367. <https://doi.org/10.1007/s00159-003-0019-3>
- Ossendrijver M, Stix M, Brandenburg A (2001) Magnetoconvection and dynamo coefficients: Dependence of the alpha effect on rotation and magnetic field. *Astron Astrophys* 376:713–726. <https://doi.org/10.1051/0004-6361:20011041>. [astro-ph/0108274](https://arxiv.org/abs/astro-ph/0108274)
- Ossendrijver M, Stix M, Brandenburg A, Rüdiger G (2002) Magnetoconvection and dynamo coefficients. II. Field-direction dependent pumping of magnetic field. *Astron Astrophys* 394:735–745. <https://doi.org/10.1051/0004-6361:20021224>. [astro-ph/0202299](https://arxiv.org/abs/astro-ph/0202299)
- Parker EN (1955a) Hydromagnetic Dynamo Models. *Astrophys J* 122:293. <https://doi.org/10.1086/146087>
- Parker EN (1955b) The Formation of Sunspots from the Solar Toroidal Field. *Astrophys J* 121:491. <https://doi.org/10.1086/146010>
- Parker EN (1971) The Generation of Magnetic Fields in Astrophysical Bodies. III. Turbulent Diffusion of Fields and Efficient Dynamos. *Astrophys J* 163:279. <https://doi.org/10.1086/150766>
- Parker EN (1975) The generation of magnetic fields in astrophysical bodies. X. Magnetic buoyancy and the solar dynamo. *Astrophys J* 198:205–209. <https://doi.org/10.1086/153593>
- Parker EN (1979) *Cosmical magnetic fields: Their origin and their activity*. Oxford, Clarendon Press; New York, Oxford University Press
- Passos D, Charbonneau P (2014) Characteristics of magnetic solar-like cycles in a 3D MHD simulation of solar convection. *Astron Astrophys* 568:A113. <https://doi.org/10.1051/0004-6361/201423700>
- Passos D, Charbonneau P, Miesch M (2015) Meridional Circulation Dynamics from 3D Magnetohydrodynamic Global Simulations of Solar Convection. *Astrophys J Lett* 800:L18. <https://doi.org/10.1088/2041-8205/800/1/L18>. [arXiv:1502.01154](https://arxiv.org/abs/1502.01154) [astro-ph.SR]
- Petitdemange L, Marcotte F, Gissinger C (2023) Spin-down by dynamo action in simulated radiative stellar layers. *Science* 379(6629):300–303. <https://doi.org/10.1126/>

- science.abk2169. arXiv:2206.13819 [astro-ph.SR]
- Pipin VV (2008) The mean electro-motive force and current helicity under the influence of rotation, magnetic field and shear. *Geophys Astrophys Fluid Dyn* 102(1):21–49. <https://doi.org/10.1080/03091920701374772>. arXiv:astro-ph/0606265 [astro-ph]
- Pipin VV (2017) Non-linear regimes in mean-field full-sphere dynamo. *Mon Not R Astron Soc* 466:3007–3020. <https://doi.org/10.1093/mnras/stw3182>. arXiv:1609.00906 [astro-ph.SR]
- Pipin VV (2023) Spatio-temporal non-localities in a solar-like mean-field dynamo. *Mon Not R Astron Soc* 522(2):2919–2927. <https://doi.org/10.1093/mnras/stad1150>. arXiv:2302.11176 [astro-ph.SR]
- Pipin VV, Kosovichev AG (2018) On the Origin of the Double-cell Meridional Circulation in the Solar Convection Zone. *Astrophys J* 854:67. <https://doi.org/10.3847/1538-4357/aaa759>. arXiv:1708.03073 [astro-ph.SR]
- Plunian F, Alboussière T (2020) Axisymmetric dynamo action is possible with anisotropic conductivity. *Physical Review Research* 2(1):013321. <https://doi.org/10.1103/PhysRevResearch.2.013321>. arXiv:2004.08157 [physics.flu-dyn]
- Pongkitiwanchakul P, Nigro G, Cattaneo F, Tobias SM (2016) Shear-driven Dynamo Waves in the Fully Nonlinear Regime. *Astrophys J* 825(1):23. <https://doi.org/10.3847/0004-637X/825/1/23>
- Pouquet A, Frisch U, Léorat J (1976) Strong MHD helical turbulence and the nonlinear dynamo effect. *J Fluid Mech* 77:321–354. <https://doi.org/10.1017/S0022112076002140>
- Proctor MRE (2007) Effects of fluctuation on $\alpha\Omega$ dynamo models. *Mon Not R Astron Soc* 382(1):L39–L42. <https://doi.org/10.1111/j.1745-3933.2007.00385.x>. arXiv:0708.3210 [astro-ph]
- Proxauf B (2021) Observations of large-scale solar flows. PhD thesis, Georg August University of Göttingen, Germany
- Pulkkinen P, Tuominen I (1998) Velocity structures from sunspot statistics in cycles 10 to 22. I. Rotational velocity. *Astron Astrophys* 332:748–754
- Racine É, Charbonneau P, Ghizaru M, Bouchat A, Smolarkiewicz PK (2011) On the Mode of Dynamo Action in a Global Large-eddy Simulation of Solar Convection. *Astrophys J* 735:46. <https://doi.org/10.1088/0004-637X/735/1/46>
- Rädler KH (1969) On some electromagnetic phenomena in electrically conducting turbulently moving matter, especially in the presence of Coriolis forces. *Veroeffentlichungen der Geod Geophys* 13:131–135
- Rädler KH (1976) Mean-Field Magnetohydrodynamics as a Basis of Solar Dynamo Theory. In: Bumba V, Kleczek J (eds) *Basic Mechanisms of Solar Activity*. vol 71. p 323
- Rädler KH (1980) Mean-field approach to spherical dynamo models. *Astron Nachr* 301(3):101–129. <https://doi.org/10.1002/asna.2103010302>
- Rädler KH (2014) Mean-field dynamos: The old concept and some recent developments. Karl Schwarzschild Award Lecture 2013. *Astron Nachr* 335(5):459. <https://doi.org/10.1002/asna.201412055>
- Rädler KH, Brandenburg A (2009) Mean-field effects in the Galloway-Proctor flow. *Mon Not R Astron Soc* 393(1):113–125. <https://doi.org/10.1111/j.1365-2966.2008.14173.x>. arXiv:0809.0851 [astro-ph]
- Rädler KH, Bräuer HJ (1987) On the oscillatory behaviour of kinematic mean-field dynamos. *Astron Nachr* 308:101–109
- Rädler KH, Rheinhardt M (2007) Mean-field electrodynamics: critical analysis of various analytical approaches to the mean electromotive force. *Geophys Astrophys Fluid Dyn* 101(2):117–154. <https://doi.org/10.1080/03091920601111068>. arXiv:astro-ph/0606267 [astro-ph]
- Rädler KH, Stepanov R (2006) Mean electromotive force due to turbulence of a conducting fluid in the presence of mean flow. *Phys Rev E* 73(5):056311. <https://doi.org/10.1103/PhysRevE.73.056311>. arXiv:physics/0512120 [physics.flu-dyn]
- Rempel M (2005) Solar Differential Rotation and Meridional Flow: The Role of a Subadiabatic Tachocline for the Taylor-Proudman Balance. *Astrophys J* 622:1320–1332. <https://doi.org/10.1086/428282>. arXiv:astro-ph/0604451
- Rempel M (2006) Flux-Transport Dynamos with Lorentz Force Feedback on Differential Rotation and Meridional Flow: Saturation Mechanism and Torsional Oscillations. As-

- trophys J 647:662–675. <https://doi.org/10.1086/505170>. arXiv:astro-ph/0604446
- Rempel M, Cheung MCM (2014) Numerical Simulations of Active Region Scale Flux Emergence: From Spot Formation to Decay. *Astrophys J* 785:90. <https://doi.org/10.1088/0004-637X/785/2/90>. arXiv:1402.4703 [astro-ph.SR]
- Rempel M, Schüssler M, Cameron RH, Knölker M (2009a) Penumbral Structure and Outflows in Simulated Sunspots. *Science* 325:171–. <https://doi.org/10.1126/science.1173798>. arXiv:0907.2259 [astro-ph.SR]
- Rempel M, Schüssler M, Knölker M (2009b) Radiative Magnetohydrodynamic Simulation of Sunspot Structure. *Astrophys J* 691:640–649. <https://doi.org/10.1088/0004-637X/691/1/640>. arXiv:0808.3294
- Rempel M, Bhatia T, Bellot Rubio L, Korpi-Lagg MJ (2023) Small-Scale Dynamos: From Idealized Models to Solar and Stellar Applications. *Space Sci Rev* 219(5):36. <https://doi.org/10.1007/s11214-023-00981-z>. arXiv:2305.02787 [astro-ph.SR]
- Rheinhardt M, Brandenburg A (2010) Test-field method for mean-field coefficients with MHD background. *Astron Astrophys* 520:A28. <https://doi.org/10.1051/0004-6361/201014700>. arXiv:1004.0689 [astro-ph.SR]
- Rheinhardt M, Brandenburg A (2012) Modeling spatio-temporal nonlocality in mean-field dynamos. *Astron Nachr* 333:71–77. <https://doi.org/10.1002/asna.201111625>. arXiv:1110.2891 [astro-ph.SR]
- Rheinhardt M, Devlen E, Rädler KH, Brandenburg A (2014) Mean-field dynamo action from delayed transport. *Mon Not R Astron Soc* 441(1):116–126. <https://doi.org/10.1093/mnras/stu438>. arXiv:1401.5026 [astro-ph.SR]
- Rieutord M, Brandenburg A, Mangeney A, Drossart P (1994) Reynolds stresses and differential rotation in Boussinesq convection in a rotating spherical shell. *Astron Astrophys* 286:471–480
- Rincon F (2019) Dynamo theories. *Journal of Plasma Physics* 85(4):205850401. <https://doi.org/10.1017/S0022377819000539>. arXiv:1903.07829 [physics.plasm-ph]
- Rincon F (2021) Helical turbulent nonlinear dynamo at large magnetic Reynolds numbers. *Physical Review Fluids* 6(12):L121701. <https://doi.org/10.1103/PhysRevFluids.6.L121701>. arXiv:2108.12037 [physics.flu-dyn]
- Roberts GO (1972) Dynamo Action of Fluid Motions with Two-Dimensional Periodicity. *Philosophical Transactions of the Royal Society of London Series A* 271(1216):411–454. <https://doi.org/10.1098/rsta.1972.0015>
- Roberts PH, Stix M (1972) Ac-Effect Dynamos, by the Buliard-Gefman Formalism. *Astron Astrophys* 18:453
- Rogachevskii I (2021) Introduction to Turbulent Transport of Particles, Temperature and Magnetic Fields: Analytical Methods for Physicists and Engineers. Cambridge University Press
- Rogachevskii I, Kleeorin N (2003) Electromotive force and large-scale magnetic dynamo in a turbulent flow with a mean shear. *Phys Rev E* 68(3):036301. <https://doi.org/10.1103/PhysRevE.68.036301>. astro-ph/0209309
- Rogachevskii I, Kleeorin N (2004) Nonlinear theory of a “shear-current” effect and mean-field magnetic dynamos. *Phys Rev E* 70(4):046310. <https://doi.org/10.1103/PhysRevE.70.046310>. astro-ph/0406328
- Rogachevskii I, Kleeorin N (2007) Magnetic fluctuations and formation of large-scale inhomogeneous magnetic structures in a turbulent convection. *Phys Rev E* 76(5):056307. <https://doi.org/10.1103/PhysRevE.76.056307>. arXiv:0710.5052
- Rogachevskii I, Kleeorin N (2015) Turbulent fluxes of entropy and internal energy in temperature stratified flows. *Journal of Plasma Physics* 81(5):395810504. <https://doi.org/10.1017/S0022377815000963>. arXiv:1508.04109 [physics.flu-dyn]
- Rogachevskii I, Kleeorin N (2024) Budget equations and astrophysical non-linear mean-field dynamos. *Mon Not R Astron Soc* 530(1):382–392. <https://doi.org/10.1093/mnras/stae660>. arXiv:2308.05590 [astro-ph.SR]
- Rogachevskii I, Kleeorin N, Brandenburg A (2025) Theory of the Kinetic Helicity Effect on Turbulent Diffusion of Magnetic and Scalar Fields. *Astrophys J* 985(1):18. <https://doi.org/10.3847/1538-4357/adcec0>. arXiv:2501.13807 [physics.flu-dyn]
- Roxburgh LW, Simmons J (1993) Numerical studies of convective penetration in plane parallel layers and the integral constraint. *Astron Astrophys* 277:93

- Rüdiger G (1989) *Differential Rotation and Stellar Convection*. Sun and Solar-type Stars. Akademie Verlag, Berlin
- Rüdiger G, Hollerbach R (2004) *The Magnetic Universe: Geophysical and Astrophysical Dynamo Theory*. Wiley-VCH, Weinheim
- Rüdiger G, Kichatinov LL (1993) Alpha-effect and alpha-quenching. *Astron Astrophys* 269(1-2):581–588
- Rüdiger G, Kitchatinov LL (1997) The slender solar tachocline: a magnetic model. *Astron Nachr* 318(5):273. <https://doi.org/10.1002/asna.2113180504>
- Rüdiger G, Kitchatinov LL, Hollerbach R (2013) *Magnetic Processes in Astrophysics: theory, simulations, experiments*. Wiley-VCH
- Schad A, Timmer J, Roth M (2013) Global Helioseismic Evidence for a Deeply Penetrating Solar Meridional Flow Consisting of Multiple Flow Cells. *Astrophys J Lett* 778:L38. <https://doi.org/10.1088/2041-8205/778/2/L38>. [arXiv:1311.7623](https://arxiv.org/abs/1311.7623) [astro-ph.SR]
- Schou J, Antia HM, Basu S, Bogart RS, Bush RI, Chitre SM, Christensen-Dalsgaard J, di Mauro MP, Dziembowski WA, Eff-Darwich A, Gough DO, Haber DA, Hoeksema JT, Howe R, Korzenik SG, Kosovichev AG, Larsen RM, Pijpers FP, Scherrer PH, Sekii T, Tarbell TD, Title AM, Thompson MJ, Toomre J (1998) Helioseismic Studies of Differential Rotation in the Solar Envelope by the Solar Oscillations Investigation Using the Michelson Doppler Imager. *Astrophys J* 505:390–417. <https://doi.org/10.1086/306146>
- Schrinner M (2011) Global dynamo models from direct numerical simulations and their mean-field counterparts. *Astron Astrophys* 533:A108. <https://doi.org/10.1051/0004-6361/201116642>. [arXiv:1105.2912](https://arxiv.org/abs/1105.2912) [astro-ph.SR]
- Schrinner M (2013) Rotational threshold in global numerical dynamo simulations. *Mon Not R Astron Soc* 431:L78–L82. <https://doi.org/10.1093/mnras/slt012>. [arXiv:1212.6910](https://arxiv.org/abs/1212.6910) [astro-ph.SR]
- Schrinner M, Rädler KH, Schmitt D, Rheinhardt M, Christensen U (2005) Mean-field view on rotating magnetoconvection and a geodynamo model. *Astron Nachr* 326:245–249. <https://doi.org/10.1002/asna.200410384>
- Schrinner M, Rädler KH, Schmitt D, Rheinhardt M, Christensen UR (2007) Mean-field concept and direct numerical simulations of rotating magnetoconvection and the geodynamo. *Geophys Astrophys Fluid Dynam* 101:81–116. <https://doi.org/10.1080/03091920701345707>. [astro-ph/0609752](https://arxiv.org/abs/0609752)
- Schrinner M, Petitdemange L, Dormy E (2011) Oscillatory dynamos and their induction mechanisms. *Astron Astrophys* 530:A140. <https://doi.org/10.1051/0004-6361/201016372>. [arXiv:1101.1837](https://arxiv.org/abs/1101.1837) [astro-ph.SR]
- Schrinner M, Petitdemange L, Dormy E (2012) Dipole Collapse and Dynamo Waves in Global Direct Numerical Simulations. *Astrophys J* 752:121. <https://doi.org/10.1088/0004-637X/752/2/121>. [arXiv:1202.4666](https://arxiv.org/abs/1202.4666) [astro-ph.SR]
- Schumacher J, Sreenivasan KR (2020) Colloquium: Unusual dynamics of convection in the Sun. *Reviews of Modern Physics* 92(4):041001. <https://doi.org/10.1103/RevModPhys.92.041001>
- Schwabe H (1844) *Sonnenbeobachtungen im Jahre 1843*. Von Herrn Hofrath Schwabe in Dessau. *Astron Nachr* 21(15):233. <https://doi.org/10.1002/asna.18440211505>
- Shimada R, Hotta H, Yokoyama T (2022) Mean-field Analysis on Large-scale Magnetic Fields at High Reynolds Numbers. *Astrophys J* 935(1):55. <https://doi.org/10.3847/1538-4357/ac7e43>. [arXiv:2207.01639](https://arxiv.org/abs/2207.01639) [astro-ph.SR]
- Simard C, Charbonneau P (2020) Grand Minima in a spherical non-kinematic $\alpha^2\Omega$ mean-field dynamo model. *Journal of Space Weather and Space Climate* 10:9. <https://doi.org/10.1051/swsc/2020006>
- Simard C, Charbonneau P, Bouchat A (2013) Magnetohydrodynamic Simulation-driven Kinematic Mean Field Model of the Solar Cycle. *Astrophys J* 768:16. <https://doi.org/10.1088/0004-637X/768/1/16>
- Simard C, Charbonneau P, Dubé C (2016) Characterisation of the turbulent electromotive force and its magnetically-mediated quenching in a global EULAG-MHD simulation of solar convection. *Adv Space Res* 58:1522–1537. <https://doi.org/10.1016/j.asr.2016.03.041>. [arXiv:1604.01533](https://arxiv.org/abs/1604.01533) [astro-ph.SR]
- Simitev RD, Kosovichev AG, Busse FH (2015) Dynamo Effects Near the Transition from Solar to Anti-Solar Differential Rotation. *Astrophys J* 810:80. <https://doi.org/10.1088/0004-637X/810/1/80>

- 0004-637X/810/1/80. [arXiv:1504.07835](https://arxiv.org/abs/1504.07835) [astro-ph.SR]
- Singh NK, Brandenburg A, Rheinhardt M (2014) Fanning Out of the Solar f-mode in the Presence of Non-uniform Magnetic Fields? *Astrophys J Lett* 795(1):L8. <https://doi.org/10.1088/2041-8205/795/1/L8>. [arXiv:1407.0356](https://arxiv.org/abs/1407.0356) [astro-ph.SR]
- Singh NK, Brandenburg A, Chitre SM, Rheinhardt M (2015) Properties of p and f modes in hydromagnetic turbulence. *Mon Not R Astron Soc* 447:3708–3722. <https://doi.org/10.1093/mnras/stu2540>. [arXiv:1404.3246](https://arxiv.org/abs/1404.3246) [astro-ph.SR]
- Singh NK, Raichur H, Brandenburg A (2016) High-wavenumber Solar f-mode Strengthening Prior to Active Region Formation. *Astrophys J* 832(2):120. <https://doi.org/10.3847/0004-637X/832/2/120>. [arXiv:1601.00629](https://arxiv.org/abs/1601.00629) [astro-ph.SR]
- Singh NK, Raichur H, Käpylä MJ, Rheinhardt M, Brandenburg A, Käpylä PJ (2020) f-mode strengthening from a localised bipolar subsurface magnetic field. *Geophys Astrophys Fluid Dyn* 114(1-2):196–212. <https://doi.org/10.1080/03091929.2019.1653461>
- Sokolov DD (1997) The disk dynamo with fluctuating spirality. *Astronomy Reports* 41(1):68–72
- Solanki SK (2003) Sunspots: An overview. *Astron Astrophys Rev* 11:153–286. <https://doi.org/10.1007/s00159-003-0018-4>
- Solanki SK, Usoskin IG, Kromer B, Schüssler M, Beer J (2004) Unusual activity of the Sun during recent decades compared to the previous 11,000 years. *Nature* 431(7012):1084–1087. <https://doi.org/10.1038/nature02995>
- Speziale CG (1991) Analytical methods for the development of reynolds-stress closures in turbulence. *Annu Rev Fluid Mech* 23:107–157. <https://doi.org/10.1146/annurev.fl.23.010191.000543>
- Spitzer L (1962) *Physics of Fully Ionized Gases*, 2nd edn. Interscience, New York
- Spruit H (1997) Convection in stellar envelopes: a changing paradigm. *Mem. Soc. Astron. Ital* 68:397. [astro-ph/9605020](https://arxiv.org/abs/astro-ph/9605020)
- Squire J, Bhattacharjee A (2015a) Coherent Nonhelical Shear Dynamos Driven by Magnetic Fluctuations at Low Reynolds Numbers. *Astrophys J* 813(1):52. <https://doi.org/10.1088/0004-637X/813/1/52>. [arXiv:1507.03154](https://arxiv.org/abs/1507.03154) [astro-ph.HE]
- Squire J, Bhattacharjee A (2015b) Electromotive force due to magnetohydrodynamic fluctuations in sheared rotating turbulence. *Phys Rev E* 92(5):053101. <https://doi.org/10.1103/PhysRevE.92.053101>. [arXiv:1508.01566](https://arxiv.org/abs/1508.01566) [astro-ph.HE]
- Squire J, Bhattacharjee A (2016) The magnetic shear-current effect: generation of large-scale magnetic fields by the small-scale dynamo. *Journal of Plasma Physics* 82(2):535820201. <https://doi.org/10.1017/S0022377816000258>. [arXiv:1512.04511](https://arxiv.org/abs/1512.04511) [astro-ph.HE]
- Sridhar S, Singh NK (2010) The shear dynamo problem for small magnetic Reynolds numbers. *J Fluid Mech* 664:265–285. <https://doi.org/10.1017/S0022112010003745>. [arXiv:0910.2141](https://arxiv.org/abs/0910.2141) [astro-ph.GA]
- Steenbeck M, Krause F (1969a) On the Dynamo Theory of Stellar and Planetary Magnetic Fields. I. AC Dynamos of Solar Type. *Astron Nachr* 291:49–84. <https://doi.org/10.1002/asna.19692910201>
- Steenbeck M, Krause F (1969b) On the Dynamo Theory of Stellar and Planetary Magnetic Fields. II. DC Dynamos of Planetary Type. *Astron Nachr* 291:271–286
- Steenbeck M, Krause F, Rädler KH (1966) Berechnung der mittleren Lorentz-Feldstärke $\overline{\mathbf{v} \times \mathbf{B}}$ für ein elektrisch leitendes Medium in turbulenter, durch Coriolis-Kräfte beeinflusster Bewegung. *Z Naturforsch A* 21:369. <https://doi.org/10.1515/zna-1966-0401>
- Stein RF, Nordlund Å (2012) On the Formation of Active Regions. *Astrophys J Lett* 753:L13. <https://doi.org/10.1088/2041-8205/753/1/L13>. [arXiv:1207.4248](https://arxiv.org/abs/1207.4248) [astro-ph.SR]
- Stix M (1971) A Non-Axisymmetric α -Effect Dynamo. *Astron Astrophys* 13:203
- Stix M (1976) Differential rotation and the solar dynamo. *Astron Astrophys* 47:243–254
- Strugarek A, Beaudoin P, Charbonneau P, Brun AS, do Nascimento JD (2017) Reconciling solar and stellar magnetic cycles with nonlinear dynamo simulations. *Science* 357:185–187. <https://doi.org/10.1126/science.aal3999>. [arXiv:1707.04335](https://arxiv.org/abs/1707.04335) [astro-ph.SR]
- Strugarek A, Beaudoin P, Charbonneau P, Brun AS (2018) On the Sensitivity of Magnetic Cycles in Global Simulations of Solar-like Stars. *Astrophys J* 863:35. <https://doi.org/10.3847/1538-4357/aac9e>. [arXiv:1806.09484](https://arxiv.org/abs/1806.09484) [astro-ph.SR]
- Subramanian K, Brandenburg A (2014) Traces of large-scale dynamo action in the kinematic stage. *Mon Not R Astron Soc* 445:2930–2940. <https://doi.org/10.1093/mnras/stu1954>.

- [arXiv:1408.4416](https://arxiv.org/abs/1408.4416)
- Sur S, Shukurov A, Subramanian K (2007) Galactic dynamos supported by magnetic helicity fluxes. *Mon Not R Astron Soc* 377:874–882. <https://doi.org/10.1111/j.1365-2966.2007.11662.x>. [astro-ph/0612756](https://arxiv.org/abs/0612756)
- Sur S, Brandenburg A, Subramanian K (2008) Kinematic α -effect in isotropic turbulence simulations. *Mon Not R Astron Soc* 385:L15–L19. <https://doi.org/10.1111/j.1745-3933.2008.00423.x>. [arXiv:0711.3789](https://arxiv.org/abs/0711.3789)
- Taylor RJ (1973) The adiabatic stability of stars containing magnetic fields-I. Toroidal fields. *Mon Not R Astron Soc* 161:365. <https://doi.org/10.1093/mnras/161.4.365>
- Taylor GI (1922) Diffusion by Continuous Movements. *Proceedings of the London Mathematical Society* s2-20(1):196–212. <https://doi.org/10.1112/plms/s2-20.1.196>
- Teed RJ, Proctor MRE (2016) Destruction of large-scale magnetic field in non-linear simulations of the shear dynamo. *Mon Not R Astron Soc* 458(3):2885–2889. <https://doi.org/10.1093/mnras/stw490>
- Teed RJ, Proctor MRE (2017) Quasi-cyclic behaviour in non-linear simulations of the shear dynamo. *Mon Not R Astron Soc* 467(4):4858–4864. <https://doi.org/10.1093/mnras/stx421>
- Tobias SM (2021) The turbulent dynamo. *J Fluid Mech* 912:P1. <https://doi.org/10.1017/jfm.2020.1055>. [arXiv:1907.03685](https://arxiv.org/abs/1907.03685) [physics.flu-dyn]
- Tobias SM, Cattaneo F (2013) Shear-driven dynamo waves at high magnetic Reynolds number. *Nature* 497(7450):463–465. <https://doi.org/10.1038/nature12177>
- Tobias SM, Brummell NH, Clune TL, Toomre J (1998) Pumping of Magnetic Fields by Turbulent Penetrative Convection. *Astrophys J Lett* 502:L177–L180. <https://doi.org/10.1086/311501>
- Tobias SM, Brummell NH, Clune TL, Toomre J (2001) Transport and Storage of Magnetic Field by Overshooting Turbulent Compressible Convection. *Astrophys J* 549:1183–1203. <https://doi.org/10.1086/319448>
- Tobias SM, Cattaneo F, Brummell NH (2008) Convective Dynamos with Penetration, Rotation, and Shear. *Astrophys J* 685(1):596–605. <https://doi.org/10.1086/590422>
- Tremblay PE, Ludwig HG, Freytag B, Fontaine G, Steffen M, Brassard P (2015) Calibration of the Mixing-length Theory for Convective White Dwarf Envelopes. *Astrophys J* 799:142. <https://doi.org/10.1088/0004-637X/799/2/142>. [arXiv:1412.1789](https://arxiv.org/abs/1412.1789) [astro-ph.SR]
- Usoskin IG (2017) A history of solar activity over millennia. *Living Rev Sol Phys* 14(1):3. <https://doi.org/10.1007/s41116-017-0006-9>
- Vainshtein SI, Cattaneo F (1992) Nonlinear restrictions on dynamo action. *Astrophys J* 393:165–171. <https://doi.org/10.1086/171494>
- Velikhov E (1959) Stability of an ideally conducting liquid flowing between rotating cylinders in a magnetic field. *J Exptl Theoret Phys* 36:1398–1404
- Vishniac ET, Brandenburg A (1997) An Incoherent α - Ω Dynamo in Accretion Disks. *Astrophys J* 475:263–274. <https://doi.org/10.1086/303504>. [astro-ph/9510038](https://arxiv.org/abs/astro-ph/9510038)
- Vishniac ET, Cho J (2001) Magnetic Helicity Conservation and Astrophysical Dynamos. *Astrophys J* 550(2):752–760. <https://doi.org/10.1086/319817>. [arXiv:astro-ph/0010373](https://arxiv.org/abs/astro-ph/0010373) [astro-ph]
- Vishniac ET, Shapovalov D (2014) Properties of Magnetic Helicity Flux in Turbulent Dynamos. *Astrophys J* 780(2):144. <https://doi.org/10.1088/0004-637X/780/2/144>
- Viviani M, Käpylä MJ (2021) Physically motivated heat-conduction treatment in simulations of solar-like stars: effects on dynamo transitions. *Astron Astrophys* 645:A141. <https://doi.org/10.1051/0004-6361/202038603>. [arXiv:2006.04426](https://arxiv.org/abs/2006.04426) [astro-ph.SR]
- Viviani M, Warnecke J, Käpylä MJ, Käpylä PJ, Olsper N, Cole-Kodikara EM, Lehtinen JJ, Brandenburg A (2018) Transition from axi- to nonaxisymmetric dynamo modes in spherical convection models of solar-like stars. *Astron Astrophys* 616:A160. <https://doi.org/10.1051/0004-6361/201732191>. [arXiv:1710.10222](https://arxiv.org/abs/1710.10222) [astro-ph.SR]
- Viviani M, Käpylä MJ, Warnecke J, Käpylä PJ, Rheinhardt M (2019) Stellar Dynamos in the Transition Regime: Multiple Dynamo Modes and Antisolar Differential Rotation. *Astrophys J* 886(1):21. <https://doi.org/10.3847/1538-4357/ab3e07>. [arXiv:1902.04019](https://arxiv.org/abs/1902.04019) [astro-ph.SR]
- Waidele M, Roth M, Singh NK, Käpylä PJ (2023) On Strengthening of the Solar f-Mode Prior to Active Region Emergence Using the Fourier-Hankel Analysis. *Sol Phys*

- 298(2):30. <https://doi.org/10.1007/s11207-023-02124-7>. arXiv:2202.11236 [astro-ph.SR]
- Warnecke J (2018) Dynamo cycles in global convection simulations of solar-like stars. *Astron Astrophys* 616:A72. <https://doi.org/10.1051/0004-6361/201732413>. arXiv:1712.01248 [astro-ph.SR]
- Warnecke J, Käpylä MJ (2020) Rotational dependence of turbulent transport coefficients in global convective dynamo simulations of solar-like stars. *Astron Astrophys* 642:A66. <https://doi.org/10.1051/0004-6361/201936922>. arXiv:1910.06776 [astro-ph.SR]
- Warnecke J, Käpylä PJ, Käpylä MJ, Brandenburg A (2014) On The Cause of Solar-like Equatorward Migration in Global Convective Dynamo Simulations. *Astrophys J Lett* 796:L12. <https://doi.org/10.1088/2041-8205/796/1/L12>. arXiv:1409.3213 [astro-ph.SR]
- Warnecke J, Käpylä PJ, Käpylä MJ, Brandenburg A (2016) Influence of a coronal envelope as a free boundary to global convective dynamo simulations. *Astron Astrophys* 596:A115. <https://doi.org/10.1051/0004-6361/201526131>. arXiv:1503.05251 [astro-ph.SR]
- Warnecke J, Rheinhardt M, Tuomisto S, Käpylä PJ, Käpylä MJ, Brandenburg A (2018) Turbulent transport coefficients in spherical wedge dynamo simulations of solar-like stars. *Astron Astrophys* 609:A51. <https://doi.org/10.1051/0004-6361/201628136>. arXiv:1601.03730 [astro-ph.SR]
- Warnecke J, Rheinhardt M, Viviani M, Gent FA, Tuomisto S, Käpylä MJ (2021) Investigating Global Convective Dynamos with Mean-field Models: Full Spectrum of Turbulent Effects Required. *Astrophys J Lett* 919(2):L13. <https://doi.org/10.3847/2041-8213/ac1db5>. arXiv:2105.07708 [astro-ph.SR]
- Warnecke J, Korpi-Lagg MJ, Gent FA, Rheinhardt M (2023) Numerical evidence for a small-scale dynamo approaching solar magnetic Prandtl numbers. *Nature Astronomy* 7:662–668. <https://doi.org/10.1038/s41550-023-01975-1>. arXiv:2306.03991 [astro-ph.SR]
- Warnecke J, Korpi-Lagg MJ, Rheinhardt M, Viviani M, Prabhu A (2025) Small-scale and large-scale dynamos in global convection simulations of solar-like stars. *Astron Astrophys* 696:A93. <https://doi.org/10.1051/0004-6361/202451085>. arXiv:2406.08967 [astro-ph.SR]
- Yoshimura H (1975) Solar-cycle dynamo wave propagation. *Astrophys J* 201:740–748. <https://doi.org/10.1086/153940>
- Yoshizawa A (1990) Self-consistent turbulent dynamo modeling of reversed field pinches and planetary magnetic fields. *Physics of Fluids B* 2(7):1589–1600. <https://doi.org/10.1063/1.859484>
- Yoshizawa A, Yokoi N (1993) Turbulent Magnetohydrodynamic Dynamo for Accretion Disks Using the Cross-Helicity Effect. *Astrophys J* 407:540. <https://doi.org/10.1086/172535>
- Yousef TA, Heinemann T, Rincon F, Schekochihin AA, Kleeorin N, Rogachevskii I, Cowley SC, McWilliams JC (2008a) Numerical experiments on dynamo action in sheared and rotating turbulence. *Astron Nachr* 329:737. <https://doi.org/10.1002/asna.200811018>. arXiv:0807.1122
- Yousef TA, Heinemann T, Schekochihin AA, Kleeorin N, Rogachevskii I, Iskakov AB, Cowley SC, McWilliams JC (2008b) Generation of Magnetic Field by Combined Action of Turbulence and Shear. *Phys Rev Lett* 100(18):184501. <https://doi.org/10.1103/PhysRevLett.100.184501>. arXiv:0710.3359
- Zeldovich IB, Ruzmaikin AA, Sokolov DD (eds) (1983) Magnetic fields in astrophysics. vol 3
- Zeldovich YB (1957) The magnetic field in the two-dimensional motion of a conducting turbulent fluid. *Sov Phys JETP* 4:460–462. <https://doi.org/10.1093/mnras/stac2769>
- Zhao J, Bogart RS, Kosovichev AG, Duvall TL Jr, Hartlep T (2013) Detection of Equatorward Meridional Flow and Evidence of Double-cell Meridional Circulation inside the Sun. *Astrophys J Lett* 774:L29. <https://doi.org/10.1088/2041-8205/774/2/L29>. arXiv:1307.8422 [astro-ph.SR]